

# Inventory of Supporting Information

Manuscript #: [NATMETAB-A20083350A](#)

Corresponding author name(s): [Stefan Trapp](#)

## 1. Extended Data

Figure #	Figure title	Filename	Figure Legend
	One sentence only	This should be the name the file is saved as when it is uploaded to our system. Please include the file extension. i.e.: <i>Smith_ED_Fig1.jpg</i>	If you are citing a reference for the first time in these legends, please include all new references in the Online Methods References section, and carry on the numbering from the main References section of the paper.
Extended Data Fig. 1	PPG <sup>NTS</sup> neurons selectively encode large meal satiation	ED_Fig1_Rev2.jpg	(a) Experimental model and paradigm for metabolic phenotyping of PPG <sup>NTS</sup> -DTA mice (DTA, n=8) or mCherry-transduced controls (mCh, n=7). n=8 (DTA) / 7 (mCh) animals for analyses presented in b-o.  (b) Cumulative hourly food intake over 1 day, 2-way mixed-model ANOVA: Virus $F_{(1,13)}=0.015$ , $p=0.904$ .  (c) Daily food intake by sex, 2-way mixed-model ANOVA: Virus $F_{(1,11)}=0.012$ , $p=0.914$ ; Sex $F_{(1,11)}=0.683$ , $p=0.426$ .  (d) Directed ambulatory locomotion (excluding fine movements) over 1 day, 2-way mixed-model ANOVA: Virus $F_{(1,11)}=0.493$ , $p=0.497$ .  (e-i) Meal pattern and metabolic parameters over 1 day, unpaired 2-tailed t-test or Mann-Whitney U test: e) $U=25$ ,

			<p><math>p=0.779</math>; f) <math>t_{(13)}=0.997</math>, <math>p=0.337</math>; g) <math>t_{(13)}=0.565</math>, <math>p=0.582</math>; h) <math>t_{(13)}=0.797</math>, <math>p=0.440</math>; i) <math>t_{(13)}=0.323</math>, <math>p=0.752</math>.</p> <p>(j) Mean bodyweight over the 24h test period, unpaired 2-tailed t-test: <math>t_{(13)}=0.883</math>, <math>p=0.393</math>.</p> <p>(k-l) Food intake during dark and light phases, unpaired 2-tailed t-test: k) <math>t_{(13)}=0.668</math>, <math>p=0.516</math>; l) <math>t_{(13)}=1.251</math>, <math>p=0.233</math>.</p> <p>(m) 24h water intake, unpaired 2-tailed t-test: <math>t_{(13)}=0.205</math>, <math>p=0.841</math>.</p> <p>(n) Ensure liquid diet preload intake, unpaired 2-tailed t-test: <math>t_{(8)}=0.219</math>, <math>p=0.832</math>; and post-Ensure chow intake, Mann-Whitney U test: <math>U=2</math>, <math>p=0.038</math>.</p> <p>(o) Post-fast refeed intake, unpaired 2-tailed t-test: <math>t_{(12)}=2.501</math>, <math>p=0.028</math>.</p> <p>(p-q) Hourly and cumulative intakes over 1 day from <i>ad libitum</i> eating PPG<sup>NTS</sup>-hM4Di mice (n=8 animals), 2-way within-subjects ANOVA: p) Drug <math>F_{(1,7)}=0.241</math>, <math>p=0.639</math>; q) Drug <math>F_{(1,7)}=0.411</math>, <math>p=0.542</math>.</p> <p>(r) Raster plot of chow pellet retrievals during the dark phase. Plots from the same mouse after saline and CNO injections presented adjacently.</p> <p>All data presented as mean <math>\pm</math> SEM.</p>
Extended Data Fig. 2	PPG <sup>NTS</sup> neurons suppress eating without behavioural disruption	ED_Fig2_Rev2.jpg	(a) Non-cumulative hourly food intake over the circadian cycle from <i>ad libitum</i> eating PPG <sup>NTS</sup> -hM3Dq mice (n=7 animals for analyses presented in a-b), 2-way within-subjects ANOVA:

			<p>Drug x Time <math>F_{(23,138)}=4.599, p&lt;0.0001</math>.</p> <p>(b) Dark phase food intake by sex, 2-way mixed-model ANOVA: Drug <math>F_{(1,5)}=19.97, p=0.0066</math>; Sex <math>F_{(1,5)}=3.854, p=0.107</math>.</p> <p>(c-d) Photomicrographs of co-localised cFos immunoreactivity and DIO-hM3Dq-mCherry in NTS of PPG-Cre:tdRFP mice perfused 3 hours after injection of saline or CNO (photomicrographs representative of independent experiments from 4/3 animals), cc: central canal. Scale=100<math>\mu</math>m (inset 50<math>\mu</math>m).</p> <p>(e) Proportion of mCherry-expressing neurons co-localised with cFos-ir in mice perfused after administration of saline or CNO (n=4 (SAL) / 3 (CNO) animals), unpaired 1-tailed t-test: <math>t_{(5)}=13.94, p&lt;0.0001</math>.</p> <p>(f) Non-cumulative hourly food intake over 1 day from 18h fasted PPG<sup>NTS</sup>-hM3Dq mice (n=7 animals for analyses presented in f-h), 2-way within-subjects ANOVA: Drug x Time <math>F_{(23,138)}=3.745, p&lt;0.0001</math>. The behavioural satiety sequence (BSS) was analysed during the first 40 minutes of the dark phase.</p> <p>(g-h) Food intake and eating rate over 40 minute BSS test, paired 2-tailed t-test and Wilcoxon matched pairs test: g) <math>t_{(6)}=4.088, p=0.0064</math>; h) <math>W=18, p=0.156</math>.</p> <p>All data presented as mean <math>\pm</math> SEM.</p>
Extended Data Fig. 3	<i>Glp1r</i> -expressing VANs suppress eating and condition flavour	ED_Fig3_Rev2.jpg	(a-c) Light phase food intake and metabolic parameters from <i>ad libitum</i> eating GLP-1R <sup>Nodose</sup> -hM3Dq mice (n=7 animals for analyses presented in a-c), paired 2-tailed t-test: a) $t_{(6)}=0.0141$ ,

	avoidance		<p><math>p=0.989</math>; b) <math>t_{(6)}=0.952</math>, <math>p=0.378</math>; c) <math>t_{(6)}=0.0406</math>, <math>p=0.969</math>.</p> <p>(d) Photomicrographs of cFos immunoreactivity (cFos-ir) in coronal NTS sections from GLP-1R-Cre x PPG-YFP mice bilaterally injected in nodose ganglia with dye (Control) or AAV9-DIO-hM3Dq-mCherry (hM3Dq) and administered saline or CNO (photomicrographs representative of independent experiments from 3/3 animals). Distance in mm posterior to Bregma in bottom left, cc: central canal. Scale=100<math>\mu</math>m.</p> <p>(e) cFos immunoreactive cells in the NTS (mean per section) of control) and hM3Dq mice (n=3 animals per group for analyses in e-f), unpaired 2-tailed t-test: <math>t_{(4)}=2.981</math>, <math>p=0.0407</math>.</p> <p>(f) PPG<sup>NTS</sup> neurons co-localised with cFos immunoreactivity in the NTS. Mann-Whitney 2-tailed U-test: <math>U=0</math>, <math>p=0.100</math>.</p> <p>(g) Photomicrograph of nodose ganglion section from GLP-1R-Cre:tdRFP mouse injected with AAV encoding Cre-dependent channelrhodopsin and eYFP fluorescent reporter (DIO-CHR2-eYFP), and co-localisation of the tdRFP and eYFP reporters (photomicrographs representative of independent experiments from 4 animals). Scale=100<math>\mu</math>m.</p> <p>(h-i) Quantification of viral transduction specificity (h; co-localised cells as % (<math>\pm</math>SEM) of all eYFP+ cells) and efficiency (i; co-localised cells as % (<math>\pm</math>SEM) of all tdRFP+ cells), from a total of 374 tdRFP+ cells and 366 eYFP+ cells from the nodose ganglia of 3 mice.</p> <p>All data presented as mean <math>\pm</math> SEM.</p>
Extended Data Fig. 4	<i>Oxtr</i> rather than <i>Glp1r</i>	ED_Fig4_Rev2.jpg	(a) Photomicrograph of coronal NTS section from PPG-

	<p>VANs are the major vagal input to PPG<sup>NTS</sup> neurons</p>		<p>Cre:tdRFP mouse transduced with DIO-TVA-mCherry + DIO-RabiesG, and subsequently with rabies virus-ΔG-GFP (RABV). Bilateral NTS injection of TVA+RabiesG and counterbalanced unilateral injection of RABV (4 mice / side) resulted in 40.5% (±5.5) of all PPG<sup>NTS</sup> neurons being successfully transduced 'starter' neurons, identified by co-localization of mCherry (and/or tdRFP) and GFP (photomicrographs in a-h representative of independent experiments from 8 animals). Despite unilateral RABV injection, starter neurons were observed in left and right NTS in all mice, indicating significant viral spread and bilateral transduction. Scale=100μm.</p> <p>(b) Total RABV+ cells in left and right nodose ganglia (LNG / RNG; n=6 / 7 biologically independent samples), unpaired 2-tailed t-test: <math>t_{(11)}=0.214</math>, <math>p=0.834</math>.</p> <p>(c-d) Quantification of <i>Glp1r</i> and <i>Oxtr</i> co-localization in nodose ganglia (c), and proportions of dual-expressing <i>Glp1r</i> / <i>Oxtr</i> cells co-localised with RABV (d). This dual population comprises 24.7% of all <i>Glp1r</i> cells and 19.7% of all <i>Oxtr</i> cells. 9% of RABV+ vagal inputs to PPG<sup>NTS</sup> neurons express both <i>Glp1r</i> and <i>Oxtr</i>, and 26.1% of dual-expressing <i>Glp1r</i> / <i>Oxtr</i> cells are RABV+ vagal inputs to PPG<sup>NTS</sup> neurons.</p> <p>(e) Quantification of RABV and <i>Glp1r</i> co-localization in NG as proportions of all RABV+ cells and all <i>Glp1r</i>+ cells, including those <i>Glp1r</i> cells that also express <i>Oxtr</i>.</p> <p>(f) Quantification of RABV and <i>Oxtr</i> co-localization in NG as proportions of all RABV+ cells and all <i>Oxtr</i>+ cells, including those <i>Oxtr</i> cells that also express <i>Glp1r</i>.</p>
--	--	--	---

			<p>(g-h) Photomicrographs of left and right nodose ganglion sections showing rabies virus GFP expression (RABV) and <i>Glp1r</i> and <i>Oxtr</i> FISH. RABV+<i>Glp1r</i> co-localization shown by white arrows, RABV+<i>Oxtr</i> by green arrows and RABV+<i>Glp1r</i>+<i>Oxtr</i> by white-edged green arrow. Scale=100µm.</p> <p>All data presented as mean ± SEM.</p>
Extended Data Fig. 5	PPG <sup>NTS</sup> neurons are necessary for oxytocin-induced eating suppression	ED_Fig5_Rev2.jpg	<p>(a-b) Food intake and bodyweight change over 1 day in eGFP and DTA mice (n=5 (DTA) / 7 (eGFP) animals) administered oxytocin (0.4 mg/kg, i.p.), 2-way mixed-model ANOVA: a) Drug <math>F_{(1,10)}=0.00474</math>, <math>p=0.947</math>; b) Drug <math>F_{(1,10)}=0.0989</math>, <math>p=0.760</math>.</p> <p>(c-d) Photomicrographs of coronal NTS sections from PPG-Cre:GCaMP3 mice injected with eGFP control virus (c) or DTA virus (d). Note the complete absence of green (GCaMP3-expressing, amplified by immunostaining against the GFP antigen) PPG<sup>NTS</sup> neurons in DTA-ablated tissue, and the extent of viral spread as demonstrated by constitutive expression of mCherry (photomicrographs representative of independent experiments from 7/5 animals). Distance in mm posterior to Bregma in bottom left, cc: central canal. Scale=100µm.</p> <p>All data presented as mean ± SEM.</p>
Extended Data Fig. 6	PPG <sup>NTS</sup> neurons are not a major synaptic target of area postrema <i>Glp1r</i> neurons	ED_Fig6_Rev2.jpg	<p>(a) Photomicrographs of coronal NTS section showing RABV expression, <i>Glp1r</i> FISH and TH-ir. RABV+<i>Glp1r</i>+TH-ir co-localization shown by white-edged green arrows (photomicrographs representative of independent experiments from 4 animals). Scale=100µm (inset 20µm).</p> <p>(b-c) Quantification of <i>Glp1r</i> and TH-ir co-localization in area</p>

			<p>postrema (b), and proportions of dual <i>Glp1r</i> / TH-ir cells co-localised with RABV (c). This dual population comprises 49.4% of all TH-ir cells and 31.2% of all <i>Glp1r</i> cells. 9.7% of RABV+ AP inputs to PPG<sup>NTS</sup> neurons express <i>Glp1r</i> and are TH-ir, and 2.7% of dual <i>Glp1r</i> / TH-ir cells are RABV+ AP inputs to PPG<sup>NTS</sup> neurons.</p> <p>All data presented as mean ± SEM.</p>
Extended Data Fig. 7	Liraglutide and semaglutide suppress eating independently of PPG <sup>NTS</sup> neurons	ED_Fig7_Rev2.jpg	<p>(a-e) Cumulative food intake by virus at 1,2,4,6 and 21hr in eGFP and DTA mice (n=8 (DTA) / 7 (eGFP) animals for analyses presented in a-j) administered liraglutide (200 µg/kg, s.c.), 2-way mixed-model ANOVA: a) Drug <math>F_{(1,13)}=0.246</math>, <math>p=0.628</math>; b) Drug <math>F_{(1,13)}=2.108</math>, <math>p=0.170</math>; c) Drug <math>F_{(1,13)}=37.44</math>, <math>p&lt;0.0001</math>, Virus <math>F_{(1,13)}=0.836</math>, <math>p=0.377</math>; d) Drug <math>F_{(1,13)}=75.09</math>, <math>p&lt;0.0001</math>, Virus <math>F_{(1,13)}=1.877</math>, <math>p=0.194</math>; e) Drug <math>F_{(1,13)}=154.9</math>, <math>p&lt;0.0001</math>, Virus <math>F_{(1,13)}=1.272</math>, <math>p=0.280</math>.</p> <p>(f-j) Cumulative food intake by virus at 1,2,4,6 and 21hr in eGFP and DTA mice administered semaglutide (60 µg/kg, s.c.), 2-way mixed-model ANOVA: f) Drug <math>F_{(1,13)}=1.965</math>, <math>p=0.184</math>; g) Drug <math>F_{(1,13)}=17.1</math>, <math>p=0.0012</math>; Virus <math>F_{(1,13)}=0.630</math>, <math>p=0.442</math>; h) Drug <math>F_{(1,13)}=82.49</math>, <math>p&lt;0.0001</math>, Virus <math>F_{(1,13)}=0.332</math>, <math>p=0.574</math>; i) Drug <math>F_{(1,13)}=98.21</math>, <math>p&lt;0.0001</math>, Virus <math>F_{(1,13)}=0.840</math>, <math>p=0.376</math>; j) Drug <math>F_{(1,13)}=126.1</math>, <math>p&lt;0.0001</math>, Virus <math>F_{(1,13)}=3.42</math>, <math>p=0.0873</math>.</p> <p>(k-m) Representative photomicrographs of cFos immunoreactivity (cFos-ir) in arcuate nucleus of the hypothalamus (ARC) 4 hours after vehicle (VEH, n=4 animals) or semaglutide (SEMA, 60 µg/kg, s.c., n=4 animals) administration, and total cFos count, unpaired 1-tailed t-test:</p>

			<p>m) <math>t_{(6)}=2.614, p=0.020</math>. Scale=100<math>\mu</math>m.</p> <p>(n-p) Representative photomicrographs of cFos-ir in paraventricular nucleus of the hypothalamus (PVN) 4 hours after vehicle or semaglutide administration (n=4 / 4 animals), and total cFos count, unpaired 1-tailed t-test: p) <math>t_{(6)}=5.109, p=0.0011</math>. Scale=100<math>\mu</math>m.</p> <p>(q-t) Representative photomicrographs of cFos-ir in dorsal lateral and external lateral subdivisions of the parabrachial nucleus (dlPBN / elPBN) 4 hours after vehicle or semaglutide administration (n=3 / 4 animals), and total cFos count, unpaired 1-tailed t-tests: s) <math>t_{(5)}=1.693, p=0.0756</math>; t) <math>t_{(5)}=3.57, p=0.0080</math>. Semaglutide did not increase cFos-ir in the medial PBN, <math>t_{(5)}=0.435, p=0.341</math>. Scale=100<math>\mu</math>m.</p> <p>All data presented as mean <math>\pm</math> SEM.</p>
Extended Data Fig. 8	PPG <sup>NTS</sup> neuron activation augments semaglutide-induced eating suppression	ED_Fig8_Rev2.jpg	<p>(a-d) Bodyweight change at 24 and 48 hours, and cumulative food intake at 48 and 72 hours (n=6 animals), 1-way within-subjects ANOVA: a) Drug <math>F_{(2.1,10.5)}=61.61, p&lt;0.0001</math>; b) Drug <math>F_{(2.3,11.3)}=102.7, p&lt;0.0001</math>; c) Drug <math>F_{(2.1,10.6)}=24.38, p&lt;0.0001</math>; d) Drug <math>F_{(1.9,9.3)}=40.35, p&lt;0.0001</math>. 72hr BW data not shown: Drug <math>F_{(2.0,10.2)}=4.22, p=0.0454</math>, no significant pairwise comparisons.</p> <p>(e) Photomicrographs of coronal NTS sections from PPG-Cre:GCaMP3 mice injected with AAV encoding Cre-dependent hM3Dq and mCherry fluorescent reporter (DIO-hM3Dq-mCherry), and co-localisation of the GCaMP3 (amplified by immunostaining against GFP antigen) and mCherry reporters (photomicrographs representative of independent experiments from 4 animals). Distance in mm from Bregma in</p>

			<p>bottom left, cc: central canal. Scale=100µm.</p> <p>(f-g) Quantification of viral transduction specificity (f; co-localised cells as % (<math>\pm</math>SEM) of all mCherry+ cells) and efficiency (g; co-localised cells as % (<math>\pm</math>SEM) of all GCaMP3+ cells), from a total of 410 mCherry+ cells and 391 GCaMP3+ cells from 4 mice.</p> <p>All data presented as mean <math>\pm</math> SEM.</p>
--	--	--	--

7 **Delete rows as needed to accommodate the number of figures (10 is the maximum allowed).**

8  
9  
10  
11  
12  
13  
14  
15  
16  
17

18 **2. Supplementary Information:**

19

20 **A. Flat Files**

21  
22

Item	Present?	Filename	A brief, numerical description of file contents.
		This should be the name the	i.e.: <i>Supplementary Figures 1-4, Supplementary Discussion, and</i>

		file is saved as when it is uploaded to our system, and should include the file extension. The extension must be .pdf	<i>Supplementary Tables 1-4.</i>
Supplementary Information	No		
Reporting Summary	Yes	3479_1_supp_0_qlhw66_Author_completed	

23

24

25 **Title:**

26

27 **Central and peripheral GLP-1 systems independently suppress eating**

28

29 **Authors:**

30 Daniel I. Brierley<sup>1</sup>, Marie K. Holt<sup>2</sup>, Arashdeep Singh<sup>3,7</sup>, Alan de Araujo<sup>3,7</sup>, Molly McDougale<sup>3,7</sup>,  
31 Macarena Vergara<sup>3,7</sup>, Majd H. Afaghani<sup>3,7</sup>, Shin Jae Lee<sup>4</sup>, Karen Scott<sup>3</sup>, Calyn Maske<sup>3,7</sup>,  
32 Wolfgang Langhans<sup>4</sup>, Eric Krause<sup>3,7</sup>, Annette de Kloet<sup>5,7</sup>, Fiona M. Gribble<sup>6</sup>, Frank Reimann<sup>6</sup>,  
33 Linda Rinaman<sup>2</sup>, Guillaume de Lartigue<sup>3,7\*</sup>, Stefan Trapp<sup>1,\*</sup>.

34

35 **Affiliations:**

- 36 1. Centre for Cardiovascular and Metabolic Neuroscience, Department of Neuroscience,  
37 Physiology and Pharmacology, University College London, UK.  
38 2. Department of Psychology, Program in Neuroscience, Florida State University, USA.  
39 3. Department of Pharmacodynamics, University of Florida, USA.  
40 4. Department of Health Sciences and Technology, ETH Zurich, Switzerland.  
41 5. Department of Physiology and Functional Genomics, University of Florida, USA.  
42 6. Institute of Metabolic Science, University of Cambridge, UK.  
43 7. Center for Integrative Cardiovascular and Metabolic Disease, University of Florida, USA

44 \* Correspondence: s.trapp@ucl.ac.uk, GdeLartigue@cop.ufl.edu

45

46

47 **Keywords:**

48 Glucagon-like peptide-1; preproglucagon; oxytocin; nucleus tractus solitarius, vagal afferent  
49 neurons; eating; feeding; satiation; behavioural satiety sequence; semaglutide.

50 **Abstract:**

51 The anorexigenic peptide glucagon-like peptide-1 (GLP-1) is secreted from gut enteroendocrine  
52 cells and brain preproglucagon (PPG) neurons, which respectively define the peripheral and  
53 central GLP-1 systems. PPG neurons in the nucleus tractus solitarii (NTS) are widely assumed  
54 to link the peripheral and central GLP-1 systems in a unified gut-brain satiation circuit. However,  
55 direct evidence for this hypothesis is lacking, and the necessary circuitry remains to be  
56 demonstrated. Here we show that PPG<sup>NTS</sup> neurons encode satiation in mice, consistent with  
57 vagal signalling of gastrointestinal distension. However, PPG<sup>NTS</sup> neurons predominantly receive  
58 vagal input from oxytocin receptor-expressing vagal neurons, rather than those expressing  
59 GLP-1 receptors. PPG<sup>NTS</sup> neurons are not necessary for eating suppression by GLP-1 receptor  
60 agonists, and concurrent PPG<sup>NTS</sup> neuron activation suppresses eating more potently than  
61 semaglutide alone. We conclude that central and peripheral GLP-1 systems suppress eating via  
62 independent gut-brain circuits, providing a rationale for pharmacological activation of PPG<sup>NTS</sup>  
63 neurons in combination with GLP-1 receptor agonists as an obesity treatment strategy.

64

65

66

67 Glucagon-like peptide 1 (GLP-1) acts as an incretin hormone and anorexigenic neuropeptide,  
68 prompting the successful and ongoing development of GLP-1-based therapies for type 2  
69 diabetes and obesity<sup>1,2</sup>. Endogenous GLP-1 is produced both by enteroendocrine cells in the  
70 gut, and proglucagon (PPG) neurons in the brain, which are the defining populations of the  
71 peripheral and central GLP-1 systems, respectively<sup>3,4</sup>. PPG neurons in the nucleus tractus  
72 solitarius (PPG<sup>NTS</sup> neurons) suppress eating when chemogenetically or optogenetically  
73 activated<sup>5-7</sup>, consistent with substantial pharmacological evidence for anorexigenic GLP-1  
74 signalling in the brain (reviewed by Muller et al<sup>4</sup>). Physiologically, PPG<sup>NTS</sup> neurons are the major  
75 source of GLP-1 in the brain, are necessary for stress-induced hypophagia, and their inhibition  
76 or ablation elicits transient hyperphagia during large intakes<sup>7</sup>. Although glutamate is a co-  
77 transmitter in these neurons<sup>8,9</sup>, selective *Ppg* knockdown has confirmed the necessity of  
78 proglucagon-derived peptides for their anorexigenic role<sup>10</sup>. PPG<sup>NTS</sup> neurons are thus the crucial  
79 component of the central GLP-1 system, which they comprise along with numerous populations  
80 of GLP-1 receptor (GLP-1R)-expressing neurons found throughout the brain<sup>11,12</sup>. PPG<sup>NTS</sup>  
81 neurons do not express GLP-1R mRNA, or directly respond to exogenous GLP-1 in *ex vivo* slice  
82 preparations<sup>13,14</sup>, therefore *direct* activation of the central GLP-1 system by peripheral GLP-1 is  
83 implausible. However, it is widely assumed that endogenous peripheral GLP-1 *indirectly*  
84 interacts with the central GLP-1 system (via vagal and/or endocrine routes) to control eating  
85 under physiological conditions, although this link is controversial and the necessary gut-brain  
86 circuitry has not been demonstrated empirically<sup>4,15-17</sup>. Indeed, experiments which could provide  
87 indirect evidence for this hypothesis suggest that functional connectivity between the two  
88 systems may in fact be very limited<sup>18,19</sup>. The difficulty in testing this link partly arises from the  
89 inherent complexity of interrogating these widely-distributed systems using pharmacological  
90 approaches, compounded by observations that native GLP-1 and pharmacokinetically-optimised  
91 therapeutic GLP-1 receptor agonists (GLP-1RAs) suppress eating via apparently divergent  
92 signalling pathways<sup>19-25</sup>.

93 Numerous studies have demonstrated the value of selective transgenic manipulations to  
94 determine the neuroanatomical organization and physiological functions of specific cell  
95 populations involved in eating control, including those comprising parts of the peripheral and  
96 central GLP-1 systems<sup>7,26-29</sup>. Here we utilized similar transgenic and viral approaches to  
97 address whether PPG<sup>NTS</sup> neurons have a role in physiological satiation, and determined their  
98 anatomical and functional connectivity to molecularly defined neuronal populations mediating  
99 gut-brain satiation signalling. Specifically, we tested the prevalent but unsubstantiated  
100 hypothesis that peripheral GLP-1 signals to the brain to suppress eating via vagal and/or

101 endocrine activation of central GLP-1-producing preproglucagon (PPG) neurons, i.e. that  
102 peripheral and central GLP-1 systems comprise a unified, directly connected gut-brain satiation  
103 circuit. We furthermore tested the role of PPG<sup>NTS</sup> neurons in eating suppression induced by the  
104 anti-obesity GLP-1RAs liraglutide and semaglutide, to establish whether this neuronal  
105 population has translational importance as a distinct therapeutic target for obesity treatment.

106 **Results:**

107 **PPG<sup>NTS</sup> neurons selectively encode large meal satiation**

108 PPG<sup>NTS</sup> neurons are not necessary for control of daily or long term food intake or bodyweight in  
109 *ad libitum* eating mice<sup>7</sup>. However, it is unknown whether they regulate within- or between-meal  
110 parameters, or whether the absence of an ablation-induced bodyweight phenotype masks more  
111 subtle alterations in energy expenditure or physical activity. We addressed these questions by  
112 metabolic phenotyping of *ad libitum* eating mice following viral ablation of PPG<sup>NTS</sup> neurons,  
113 using AAV-mediated selective expression of diphtheria toxin subunit A (DTA; Extended Data 1a).  
114 Food intake over the circadian cycle was unaffected by neuronal ablation in either sex  
115 (Extended Data 1b-c, k-l), and there was no effect on meal size, frequency or duration  
116 (Extended Data 1e-g). Similarly, ablation did not affect locomotion, energy expenditure,  
117 bodyweight or water intake (Extended Data 1d,h-j,m). As a positive control in this model we did,  
118 however, successfully replicate a previous report<sup>7</sup> that ablation induces hyperphagia both during  
119 post-fast refeeding, and after a short liquid diet preload (Extended Data 1n-o).

120 The replicable observation that ablation of PPG<sup>NTS</sup> neurons elicits transient hyperphagia only  
121 under conditions manipulated to induce large intakes<sup>7</sup> is consistent with results in rats indicating  
122 that these neurons are activated during ingestion of unusually large meals<sup>30</sup>. We thus tested the  
123 hypothesis that hyperphagic responses observed after PPG<sup>NTS</sup> neuronal ablation are specifically  
124 due to a delay in meal termination, to establish a *bona fide* role for PPG<sup>NTS</sup> neurons in the  
125 process of satiation. We conducted high resolution meal pattern analysis using home cage FED  
126 pellet dispensers (Feeding Experimentation Device<sup>28</sup>), and observational analysis of liquid diet  
127 intake, to test the effects of chemogenetic inhibition of PPG<sup>NTS</sup> neurons on termination of large  
128 solid and liquid meals, using the inhibitory hM4Di Designer Receptor Exclusively Activated by  
129 Designer Drugs (DREADD; Fig. 1a,g). PPG<sup>NTS</sup> neuron inhibition increased fasting-induced pellet  
130 refeeding during hour 1 in a sex-independent manner, and this effect was driven by increased  
131 meal size, rather than frequency (Fig. 1b-f). The hyperphagic effect in this model was also  
132 confirmed to be specific to large meals, as inhibition had no effect under *ad libitum* eating  
133 conditions (Extended Data 1p-r). We then modified a previously used Ensure liquid diet preload  
134 paradigm<sup>7</sup> to test whether PPG<sup>NTS</sup> neurons are necessary for satiation during consumption of  
135 large liquid meals (Fig. 1g), as suggested by a previous cFos expression study in rats<sup>32</sup>. Under  
136 these conditions, Ensure intake was increased by PPG<sup>NTS</sup> neuron inhibition, and, consistent with  
137 effects on pellet intake in the FED system, this increase was driven by increased duration of  
138 Ensure eating (Fig. 1h-k). While the modest but non-significant increases in eating frequency

139 mean we cannot rule out an additional role in satiety, our data unequivocally demonstrate that  
140 both under conditions of normal and negative energy balance, PPG<sup>NTS</sup> neurons are recruited to  
141 encode physiological satiation, specifically by ingestion of large meals.

142

### 143 **PPG<sup>NTS</sup> neurons suppress eating without behavioural disruption**

144 The observation that PPG<sup>NTS</sup> neurons selectively encode satiation during large meals, but  
145 apparently do not control intake under *ad libitum* eating conditions, suggests they have capacity  
146 to suppress eating when stimulated. Evidence for such capacity has been reported previously<sup>5-</sup>  
147 <sup>7</sup>, and could indicate translational potential for PPG<sup>NTS</sup> neurons as a target for therapeutic  
148 suppression of eating, provided that the eating suppression is robust, is not compensated for,  
149 and is not associated with nausea/malaise. We therefore extended these studies by testing  
150 whether hypophagia induced by chemogenetic activation of PPG<sup>NTS</sup> neurons was followed by  
151 compensatory rebound hyperphagia, or elicited significant disruption to the behavioural satiety  
152 sequence, using the excitatory hM3Dq DREADD (Fig. 2a,e). In *ad libitum* eating mice, PPG<sup>NTS</sup>  
153 activation reduced intake by ~40% in the first 24 hours (Fig. 2b) in a sex-independent manner  
154 (Extended Data 2b), predominantly driven by reductions in the first 5 hours of the dark phase  
155 (Extended Data 2a). No compensatory hyperphagia occurred, hence cumulative intake and  
156 bodyweight were still reduced 48 hours after acute CNO administration (Fig. 2c-d). This robust  
157 suppression of eating with sustained reduction in intake was also observed when PPG<sup>NTS</sup>  
158 neurons were activated immediately prior to dark onset refeeding after a prolonged (18hr) fast  
159 (Fig. 2e, Extended Data 2f). We thus combined the FED system with infrared video in this  
160 paradigm to investigate changes to the behavioural satiety sequence under relatively naturalistic  
161 home cage conditions. Following a period of eating (Extended Data 2g), PPG<sup>NTS</sup> neuron  
162 activation advanced the point of satiation by ~15 minutes (shift from time bin 4 to 1; Fig. 2f-g),  
163 and the stochastic sequence of satiety behaviours (eating → grooming → inactive) was not  
164 disrupted. Quantitative analyses revealed that PPG<sup>NTS</sup> neuron activation did not significantly  
165 alter eating rate (Extended Data 2h), but reduced eating duration during the first 15 minutes  
166 (Fig. 2h), as expected from the left-shifted satiation point. Time inactive was modestly  
167 increased, and grooming and active behaviours appeared to be correspondingly decreased,  
168 however the temporal patterns of these behaviours were maintained (Fig. 2i-k).

169 We have previously argued that chemogenetic activation of PPG<sup>NTS</sup> neurons is a  
170 supraphysiological stimulus, based on the extent of cFos expression in this population in

171 comparison to physiological stimuli<sup>7</sup>. Here we report that chemogenetic activation of PPG<sup>NTS</sup>  
172 neurons activated 82% of transduced neurons (Extended Data 2e), comparable to a previous  
173 study using another PPG-Cre mouse line which reported 98% activation<sup>5</sup>. These levels are  
174 similar to the ~80% activation reported following acute restraint stress in mice<sup>33</sup>, but  
175 substantially higher than the <50% we previously observed following the physiological stimulus  
176 of a large liquid diet meal<sup>7</sup>. That the robust suppression of intake elicited by supraphysiological  
177 activation of PPG<sup>NTS</sup> neurons is not associated with significant alteration to the behavioural  
178 satiety sequence supports the idea that PPG<sup>NTS</sup> neurons have translational potential as a  
179 pharmacological target for obesity treatment.

180 Our observations following chemogenetic activation of PPG<sup>NTS</sup> neurons contrast with previously  
181 reported effects in the BSS assay of the emesis/nausea-inducing agent lithium chloride and the  
182 GLP-1RA Exendin-4, which reduce eating rate and almost completely suppress grooming and  
183 other active behaviours<sup>34,35</sup>. Instead, and consistent with prior evidence that PPG<sup>NTS</sup> activation  
184 does not condition flavour avoidance<sup>5</sup>, the absence of behavioural satiety sequence disruption  
185 reported here supports the view that PPG<sup>NTS</sup> neuronal activation suppresses eating without  
186 inducing nausea/malaise, in contrast to the effects of peripherally administered GLP-1RAs.

187

### 188 ***Glp1r*-expressing VANs suppress eating and condition flavour avoidance**

189 Direct synaptic input from undefined population(s) of vagal afferent neurons (VANs) to PPG<sup>NTS</sup>  
190 neurons<sup>14,29</sup> presumably underlies the ability of gastrointestinal distension and large liquid  
191 intakes to induce cFos expression in this NTS population<sup>32,36</sup>, and to drive their role in large  
192 meal satiation reported here. However, the molecular identities of VAN inputs to PPG<sup>NTS</sup>  
193 neurons remain to be characterized. VANs defined by their expression of the GLP-1 receptor  
194 gene (*Glp1r*) innervate the gut and have been identified as a predominantly mechanosensory  
195 population which encode gastrointestinal distension, detected by intraganglionic laminar  
196 endings in the myenteric plexus and intramuscular arrays in the smooth muscle layers of the  
197 stomach and intestine<sup>27,28</sup>. These findings challenged the classical view that *Glp1r* VANs are  
198 chemosensory neurons which receive nutrient detection information in a paracrine manner, via  
199 binding of GLP-1 released locally from enteroendocrine cells<sup>17,25</sup>. However, it is well-established  
200 that gastrointestinal distension and the gut hormone CCK are able to synergistically activate  
201 mechanosensory VANs (original studies reviewed in<sup>37</sup>) and this has now also been  
202 demonstrated with GLP-1<sup>38</sup>. Furthermore, recent transcriptomic analyses suggest that *Glp1r*

203 VANs may be segregated into distinct mechanosensory and chemosensory subpopulations<sup>16,28</sup>.  
204 Crucially, it is unknown whether PPG<sup>NTS</sup> neurons are a major synaptic target of any *Glp1r* VAN  
205 populations, and thus to what extent direct vagal communication between peripheral and central  
206 GLP-1 systems is neuroanatomically plausible. To address this question, we developed  
207 approaches for viral targeting and activation of *Glp1r* VANs with chemogenetic and optogenetic  
208 effectors (Fig. 3a,f), and determined whether these manipulations produced effects on eating  
209 consistent with *Glp1r* VANs being part of a unified gut-brain satiation circuit with PPG<sup>NTS</sup>  
210 neurons. Chemogenetic activation of *Glp1r* VANs using the excitatory hM3Dq DREADD in *ad*  
211 *libitum* eating mice suppressed eating during the dark but not subsequent light phase (Fig. 3b,  
212 Extended Data 3a). Notably, however, the magnitude of this hypophagic effect appeared less  
213 robust than that following chemogenetic activation of PPG<sup>NTS</sup> neurons. Bodyweight was also  
214 transiently decreased, driven by suppressed eating rather than increased energy expenditure  
215 (Fig. 3c-e, Extended Data 3b-c). To functionally validate chemogenetic activation of *Glp1r*  
216 VANs, and explore their direct and/or indirect connectivity to PPG<sup>NTS</sup> neurons, we quantified  
217 neuronal activation in the NTS by cFos immunoreactivity (Extended Data 3d). Chemogenetic  
218 activation induced cFos expression in the NTS *per se*, however expression was not significantly  
219 increased in PPG<sup>NTS</sup> neurons (Extended Data 3e-f).

220 The modest anorexigenic effect of chemogenetic activation of *Glp1r* VANs in *ad libitum* eating  
221 mice precluded use of the 18hr fasted BSS paradigm in this model. We therefore instead tested  
222 whether optogenetic activation of the central axon terminals of *Glp1r* VANs with the excitatory  
223 opsin ChR2 was able to condition avoidance of, or a preference for, a paired novel flavour of  
224 Kool-Aid (Fig. 3f-g). Optogenetic activation of *Glp1r* terminals within the NTS conditioned  
225 avoidance of the paired flavour (Fig. 3h), and also modestly suppressed eating in a  
226 subsequently conducted acute eating test (Fig. 3i). Optogenetic activation of this vagal  
227 population induced robust cFos expression throughout the NTS (Fig. 3j), consistent with the  
228 effects of chemogenetic activation, and activation was similarly not significantly increased in  
229 PPG<sup>NTS</sup> neurons (Fig. 3k-j).

230 The behavioural responses to *Glp1r* VAN activation contrast both with the lack of disruption to  
231 the BSS we observed following activation of PPG<sup>NTS</sup> neurons, and a previous report that  
232 chemogenetic activation of PPG<sup>NTS</sup> neurons does not condition flavour avoidance<sup>5</sup>. They are  
233 however consistent with several reports that GLP-1RAs condition flavour avoidance and reduce  
234 reward-related behaviours<sup>39-41</sup>. These results thus support prior evidence that *Glp1r* VANs at  
235 least partly mediate endogenous or exogenous peripheral GLP-1 satiation signalling<sup>23,25</sup>.

236 However, the modest anorexigenic effects and conditioning of avoidance produced by activation  
237 of *Glp1r* VANs, and the absence of cFos induction in PPG<sup>NTS</sup> neurons by these manipulations,  
238 argue against the hypothesis that *Glp1r* VANs are the primary driver of eating suppression by  
239 PPG<sup>NTS</sup> neurons.

240

### 241 ***Oxtr* rather than *Glp1r* VANs are the major vagal input to PPG<sup>NTS</sup> neurons**

242 We next tested the neuroanatomical connectivity between PPG<sup>NTS</sup> neurons and *Glp1r* VANs,  
243 using two complementary circuit mapping approaches. Utilizing a cross of GLP-1R-Cre and  
244 PPG-YFP mouse strains<sup>13</sup> combined with unilateral viral targeting of nodose ganglia, we  
245 selectively labelled the NTS terminal fields of *Glp1r* VANs with the bright cell-filling fluorescent  
246 reporter tdTomato, allowing their simultaneous visualization with YFP-expressing PPG somata  
247 and dendrites in the NTS (Fig. 4a). While extensive innervation by both right and left branch  
248 *Glp1r* VANs was observed throughout the rostro-caudal extent of the NTS, there was little  
249 regional overlap with PPG<sup>NTS</sup> neurons. In the caudal NTS, *Glp1r* vagal afferents predominantly  
250 terminated dorsomedial to PPG<sup>NTS</sup> somata, and their terminal fields extended considerably  
251 beyond the rostral extent of the PPG<sup>NTS</sup> population (Fig. 4b-c).

252 The absence of overlap between *Glp1r* VAN terminals and PPG<sup>NTS</sup> somata does not preclude  
253 some vagal input via their distal dendrites in the dorsomedial NTS. We therefore quantified  
254 direct synaptic connectivity between *Glp1r* VANs and PPG<sup>NTS</sup> neurons by Cre-dependent  
255 monosynaptic retrograde rabies virus tracing in combination with RNAscope fluorescence *in situ*  
256 hybridisation in nodose ganglia for *Glp1r* and oxytocin receptor gene (*Oxtr*) expression (Fig. 4d).  
257 Expression of *Oxtr* was investigated based on reports of target-based scRNAseq analysis of  
258 VANs (target-scSeq), which suggest that mechanosensation of gastric and intestinal distension  
259 are predominantly encoded by VANs defined by *Glp1r* and *Oxtr* expression, respectively<sup>28</sup>. As  
260 previously reported<sup>29</sup>, we observed that rabies virus-GFP was expressed extensively in nodose  
261 ganglia, confirming substantial monosynaptic vagal innervation of PPG<sup>NTS</sup> neurons. Surprisingly,  
262 however, we found that <5% of PPG<sup>NTS</sup> neuron-innervating VANs express *Glp1r* alone, and  
263 similarly <5% of VANs expressing *Glp1r* alone synapse onto PPG<sup>NTS</sup> neurons (Fig. 4e-f).  
264 Conversely, 33% of all PPG<sup>NTS</sup> neuron-innervating VANs express *Oxtr* alone, and 21% of VANs  
265 which express *Oxtr* alone synapse onto PPG<sup>NTS</sup> neurons (Fig. 4g-h). VANs expressing both *Oxtr*  
266 and *Glp1r* (which are likely mechanosensory rather than chemosensory *Glp1r* VANs) comprise  
267 20-25% of these populations (Extended Data 4c), and 26% of these *Oxtr* / *Glp1r* VANs synapse

268 onto PPG<sup>NTS</sup> neurons, comprising an additional 9% of vagal input to this population (Extended  
269 Data 4d-h). We thus identified PPG<sup>NTS</sup> neurons as an important synaptic target of *Oxtr* VANs, in  
270 addition to the catecholaminergic target population previously identified<sup>28</sup>. Our findings strongly  
271 suggest that *Oxtr*- rather than *Glp1r*-expressing VANs are the primary source of gastrointestinal  
272 distension signals driving PPG<sup>NTS</sup> neuron-mediated satiation. Furthermore, as the overwhelming  
273 majority of VANs expressing *Glp1r* but not *Oxtr* (which presumably includes the chemosensory  
274 population) do not synapse onto PPG<sup>NTS</sup> neurons, they are highly unlikely to be a functionally  
275 relevant target of vagal-dependent paracrine signalling from the peripheral GLP-1 system.

276

### 277 **PPG<sup>NTS</sup> neurons are necessary for oxytocin-induced eating suppression**

278 Having identified *Oxtr*-expressing VAN input to PPG<sup>NTS</sup> neurons, we next characterized the  
279 effects of oxytocin itself on this population. We first performed *ex vivo* calcium imaging using  
280 coronal brainstem slices from transgenic mice expressing GCaMP3 in PPG<sup>NTS</sup> neurons<sup>42,43</sup>.  
281 Slices were taken at a rostro-caudal level containing the majority of PPG<sup>NTS</sup> neurons, and which  
282 is reported to contain substantial *Oxtr* VAN terminal fields<sup>28</sup>. Superfusion of oxytocin activated  
283 84% of glutamate-responsive PPG<sup>NTS</sup> neurons, as determined by increased calcium-dependent  
284 fluorescence (Fig. 5a-e). Notably, superfusion of GLP-1 has no effect on PPG<sup>NTS</sup> neurons in the  
285 same preparation<sup>13</sup>.

286 Peripherally administered oxytocin is reported to suppress eating in a vagal-dependent  
287 manner<sup>44,45</sup>, so we subsequently tested whether PPG<sup>NTS</sup> neurons were necessary for this effect,  
288 given their direct synaptic inputs from *Oxtr* VANs. While oxytocin acutely suppressed eating in  
289 *ad libitum* eating control mice, this effect was completely abolished in mice in which PPG<sup>NTS</sup>  
290 neurons had been virally ablated by DTA expression (Fig. 5f-i, Extended Data 5a-b), confirming  
291 these neurons as a necessary component of the gut-brain circuit recruited by peripheral  
292 oxytocin to suppress eating.

293

### 294 **PPG<sup>NTS</sup> neurons are not a major synaptic target of area postrema *Glp1r* neurons**

295 Having determined the neuroanatomical implausibility of vagal transmission of peripheral GLP-1  
296 signals to PPG<sup>NTS</sup> neurons, we next investigated a potential route for endocrine GLP-1  
297 signalling to these NTS neurons via *Glp1r* neurons in the area postrema (AP), which lacks a  
298 blood-brain barrier and has been implicated as a site where circulating GLP-1 and GLP-1RAs

299 may act to suppress eating<sup>20,23,46,47</sup>. We therefore used brainstem tissue from the same mice  
300 used for rabies virus-mediated retrograde tracing of vagal inputs to PPG<sup>NTS</sup> neurons, to also  
301 quantify monosynaptic input from AP neurons which express *Glp1r* mRNA (Fig. 6a). In contrast  
302 to robust synaptic input from VANs, synaptic inputs to PPG<sup>NTS</sup> neurons from the AP were  
303 relatively sparse (Fig. 6b). Of these sparse inputs from the AP, 25% expressed *Glp1r*, however  
304 these represented <3% of all *Glp1r* AP neurons (Fig. 6c). As catecholaminergic AP neurons  
305 express GLP-1R and have been proposed to link peripheral GLP-1 signalling to central nuclei  
306 (including the NTS) involved in eating control<sup>47</sup>, we further characterized PPG<sup>NTS</sup> neuronal input  
307 from tyrosine hydroxylase immunoreactive AP neurons using the same tissue (Fig. 6d-e,  
308 Extended Data 6a-c). ~20% of the sparse AP inputs to PPG<sup>NTS</sup> neurons are catecholaminergic,  
309 consistent with a report that PPG<sup>NTS</sup> neurons are indirectly activated by noradrenaline<sup>48</sup>.  
310 However, these presynaptic AP neurons comprised only 3% of all catecholaminergic AP  
311 neurons (Fig. 6e). Therefore, PPG<sup>NTS</sup> neurons are unlikely to be a functionally relevant target for  
312 peripheral GLP-1 and/or GLP-1RAs acting via the AP to suppress eating.

313

#### 314 **Liraglutide and semaglutide suppress eating independently of PPG<sup>NTS</sup> neurons**

315 Limitations to rabies virus propagation efficiency inevitably result in an underestimate of the total  
316 number of neurons (including *Glp1r* VANs and AP neurons) providing direct synaptic input to  
317 PPG<sup>NTS</sup> neurons. Nevertheless, it is apparent that the majority of *Glp1r* VANs and AP neurons  
318 are not directly presynaptic to the central GLP-1 system. However, one or both of these *Glp1r*  
319 populations may be polysynaptically connected to PPG<sup>NTS</sup> neurons, in which case vagal and/or  
320 endocrine peripheral GLP-1 could still provide substantial input to the central GLP-1 system.  
321 PPG<sup>NTS</sup> neurons may alternatively (or additionally) receive input from other *Glp1r*-expressing  
322 neuronal populations which are accessible to peripheral GLP-1/GLP-1RAs and are reportedly  
323 necessary for their hypophagic effects, such as glutamatergic neurons<sup>49</sup> or GABAergic NTS  
324 neurons<sup>50</sup>. We therefore investigated whether PPG<sup>NTS</sup> neurons are a necessary component of  
325 *any* neurocircuits recruited by peripheral GLP-1RAs to suppress eating, by testing whether  
326 PPG<sup>NTS</sup> neuronal ablation attenuates the anorexigenic effects of two long-acting anti-obesity  
327 GLP-1RAs, liraglutide and semaglutide (Fig. 7a). Liraglutide robustly suppressed intake and  
328 bodyweight over 24 hours in *ad libitum* eating eGFP-transduced control mice, however DTA  
329 ablation of PPG<sup>NTS</sup> neurons had no effect on the magnitude of eating suppression at any  
330 timepoint, or on 24h bodyweight loss (Fig. 7b-d, Extended Data 7a-e). Semaglutide suppressed  
331 eating to an even greater extent than liraglutide, and similarly PPG<sup>NTS</sup> neuron ablation had no

332 impact on acute or delayed eating suppression, or on bodyweight loss (Fig. 7e-g, Extended  
333 Data 7f-j).

334 These findings demonstrate that PPG<sup>NTS</sup> neurons are not necessary for GLP-1RA-induced  
335 suppression of eating. While access to the brain by GLP-1RAs is limited, they are able to  
336 access several circumventricular *Glp1r*-expressing nuclei (in addition to the AP), which may be  
337 upstream of PPG<sup>NTS</sup> neurons, or part of a subset of the *downstream* targets of these  
338 neurons<sup>12,20,24,51</sup>. Relevant GLP-1RA-accessible downstream *Glp1r* populations likely include  
339 neurons in the hypothalamic arcuate nucleus, which are at least partly necessary for liraglutide-  
340 induced suppression<sup>19</sup>. Administration of GLP-1RAs to PPG<sup>NTS</sup> neuron-ablated mice cannot  
341 differentiate between whether there are any *Glp1r* populations *upstream* of PPG<sup>NTS</sup> neurons that  
342 are functionally dispensable for eating suppression, or if GLP-1RAs only recruit circuits  
343 downstream or entirely independent of PPG<sup>NTS</sup> neurons. We therefore investigated whether the  
344 same highly anorexigenic dose of semaglutide used in the ablation experiment was able to  
345 induce neuronal activation of PPG<sup>NTS</sup> neurons, by quantifying cFos expression in the PPG-YFP  
346 mouse line<sup>51,52</sup>. Semaglutide induced robust cFos expression within the AP and throughout the  
347 rostro-caudal extent of the NTS (Fig. 7h-j), and additionally in hypothalamic and parabrachial  
348 nuclei (Extended Data 7k-t). However, consistent with a report that the GLP-1RA Exendin-4  
349 does not increase cFos expression in PPG<sup>NTS</sup> neurons<sup>18</sup>, and that these neurons themselves do  
350 not express *Glp1r*<sup>13,14</sup>, we found that <3% of PPG<sup>NTS</sup> neurons were activated by semaglutide  
351 (Fig. 7k). This finding demonstrates that systemically-administered GLP-1RAs act centrally via  
352 ascending circuits parallel to, but independent of, PPG<sup>NTS</sup> neurons, and/or by partially bypassing  
353 them to activate a subset of their downstream targets.

354

### 355 **PPG<sup>NTS</sup> neuron activation augments semaglutide-induced eating suppression**

356 The convergent lines of neuroanatomical and functional evidence reported here suggest that,  
357 rather than comprising part of a unified GLP-1 gut-brain circuit, PPG<sup>NTS</sup> neurons suppress  
358 eating via circuits which are anatomically and functionally distinct from those recruited by  
359 peripheral endogenous GLP-1 and peripherally administered GLP-1RAs. To support the  
360 hypothesis that the circuits mediating eating suppression by peripheral GLP-1RAs and PPG<sup>NTS</sup>  
361 neurons are indeed entirely independent, or at least only converge at limited peripherally-  
362 accessible downstream population(s), it is a necessary to demonstrate that their concurrent  
363 activation suppresses eating to a greater extent than either circuit alone. We therefore tested

364 this hypothesis by administering the same dose of semaglutide that elicited robust eating  
365 suppression and neuronal activation in earlier experiments, in combination with chemogenetic  
366 activation of PPG<sup>NTS</sup> neurons with hM3Dq, and assessed intake and bodyweight over 72 hours  
367 (Fig. 8a). As expected, either manipulation alone suppressed eating over the first 24 hours, with  
368 semaglutide eliciting the stronger effect. Crucially, their combined effect was significantly greater  
369 than that of semaglutide alone throughout the duration of acute chemogenetic activation (Fig.  
370 8b-e). Consistent with our observation that PPG<sup>NTS</sup> neuron activation suppresses eating without  
371 compensatory rebound hyperphagia, both cumulative intake and bodyweight were reduced at  
372 24 and 48 hours in both of the semaglutide-treated groups. The apparent floor effect on eating  
373 suppression at 24 hours confirmed that an appropriately high dose of semaglutide was used,  
374 but this likely precluded the ability to detect significantly augmented intake suppression and  
375 weight loss at these later timepoints (Fig. 8f, Extended Data 8a-d). The observed augmentation  
376 of the semaglutide effect could theoretically be explained by incomplete GLP-1R saturation by  
377 semaglutide within a peripherally-accessible subset of *Glp1r*-expressing nuclei downstream of  
378 PPG<sup>NTS</sup> neurons. However, as we deliberately used a high dose of semaglutide to overcome  
379 this possibility, and chemogenetic activation is itself a potent supraphysiological stimulus, this  
380 explanation is unlikely. Rather, as GLP-1RAs do not suppress eating via PPG<sup>NTS</sup> neurons, and  
381 since these neurons project to numerous central nuclei involved in eating control which are not  
382 accessible to GLP-1RAs, the most parsimonious explanation is that the observed augmentation  
383 derives from concurrent activation of distinct anorexigenic neurocircuits (summarised in Fig. 8g).

384

### 385 **Discussion:**

386 Here we report that PPG<sup>NTS</sup> neurons encode satiation specifically during large meals, and have  
387 capacity for pharmacological activation to suppress eating without compensatory rebound  
388 hyperphagia or behavioural disruption. Activation of *Glp1r* VANs similarly suppressed intake, but  
389 did condition flavour avoidance, and complementary circuit mapping approaches demonstrated  
390 that PPG<sup>NTS</sup> neurons are not a major synaptic target of this vagal population. We report that  
391 PPG<sup>NTS</sup> neurons instead predominantly receive vagal input from *Oxtr* VANs, and are required  
392 for peripheral oxytocin-induced eating suppression. Similarly, PPG<sup>NTS</sup> neurons are at most a  
393 minor synaptic target of *Glp1r* neurons in the area postrema, suggesting that endocrine GLP-1  
394 signalling from the periphery by this route does not require PPG<sup>NTS</sup> neurons. Consistent with this  
395 observation, PPG<sup>NTS</sup> neurons are not recruited by peripherally administered semaglutide, or  
396 required for the anorexigenic effects of liraglutide or semaglutide, and concurrent activation of

397 PPG<sup>NTS</sup> neurons augments semaglutide-induced eating suppression. We therefore conclude  
398 that the unified peripheral to central GLP-1 satiation circuit hypothesis cannot be supported, but  
399 that the peripheral and central GLP-1 systems are rather components of functionally and  
400 anatomically independent eating control circuits. Furthermore, while pharmacokinetically-  
401 optimised GLP-1RAs may access a limited subset of *Glp1r* neuron populations downstream of  
402 PPG<sup>NTS</sup> neurons, such partial convergence of recruited circuits does not preclude the ability of  
403 PPG<sup>NTS</sup> neurons to augment GLP-1RA-induced eating suppression. Activation of PPG<sup>NTS</sup>  
404 neurons, either alone or in combination with GLP-1RAs, thus represents a rational strategy for  
405 obesity treatment. Given the unmet clinical need for effective and well-tolerated  
406 pharmacotherapies for obesity, an urgent research effort is warranted to identify and validate  
407 pharmacological targets for activation of PPG<sup>NTS</sup> neurons.

408

409

410

411

412

413 **Acknowledgements:**

414 We would like to thank Lotte Bjerre Knudsen at Novo Nordisk for valuable discussions and  
415 provision of liraglutide and semaglutide. We would also like to thank Myrtha Arnold at ETH  
416 Zurich and Yalun Tan at the University of Florida for their expert technical assistance, and Kevin  
417 Beier at UC Irvine for providing rabies virus for retrograde tracing. This study was supported by  
418 MRC project grant MR/N02589X/1 to ST. The initial collaboration between the Trapp, de  
419 Lartigue and Langhans labs which generated this work was made possible thanks to a UCL  
420 Global Engagement Fund award to DB, and a UCL Neuroscience ZNZ Collaboration award to  
421 ST and WL. Research in the de Lartigue lab was funded by the NIH (NIDDK grant R01  
422 DK116004) and with institutional support from the University of Florida College of Pharmacy.  
423 Research in the Reimann/Gribble laboratories was funded by the Wellcome Trust  
424 (106262/Z/14/Z and 106263/Z/14/Z) and the MRC (MRC\_MC\_UU\_12012/3). Research in the  
425 Rinaman laboratory was funded by the U.S. National Institutes of Health (MH059911 and  
426 DK100685).

427

428 **Author Contributions:**

429 *Conceptualisation:* DB, MH, WL, GL, ST; *Methodology:* DB, MH, FG, FR, GL, ST; *Formal*  
430 *analysis:* DB, AS, MM; *Investigation:* DB, MH, AS, AA, MM, MV, MA, SL, CM, KS, GL, ST;  
431 *Resources:* DB, KS, WL, EK, AK, FG, FR, LR, GL, ST; *Data Curation:* DB; *Writing – Original*  
432 *Draft:* DB, GL, ST; *Writing – Review & Editing:* All authors; *Visualisation:* DB, MH, ST;  
433 *Supervision:* DB, KS, WL, EK, AK, LR, GL, ST; *Project Administration:* DB, GL, ST; *Funding*  
434 *Acquisition:* DB, WL, FG, FR, LR, GL, ST. (Contributions defined according to the CRediT  
435 taxonomy.)

436

437 **Competing Interests Statement:**

438 The FR + FMG laboratory receives funding from AstraZeneca, Eli Lilly and LGM for unrelated  
439 research and FMG consults for Kallyope (New York). All other authors have nothing to declare.

440 **Methods:**

441 ***Animals***

442 We used 136 mice of both sexes (10-32 weeks old) from five previously-reported transgenic  
443 strains on C57BL/6NJ backgrounds. All experimental mice were from in-house colonies derived  
444 from breeding pairs supplied by Frank Reimann. For selective Cre-dependent viral targeting and  
445 *ex vivo* Ca<sup>2+</sup> imaging of PPG neurons, we used mGlu-Cre/tdRFP<sup>53</sup> and mGlu-Cre/GCaMP3  
446 strains<sup>42</sup>, referred to herein as PPG-Cre:tdRFP and PPG-Cre:GCaMP3, respectively. For  
447 visualization of PPG neuron somata, axons and dendrites, we used the mGlu-YFP strain<sup>52</sup>,  
448 referred to herein as PPG-YFP. For selective Cre-dependent viral targeting of GLP-1 receptor-  
449 expressing neurons we used the *Glp1r*-Cre/tdRFP strain<sup>54</sup>, or a cross with the PPG-YFP strain  
450<sup>13</sup>, referred to herein as GLP-1R-Cre:tdRFP and GLP-1R-Cre x PPG-YFP respectively. All mice  
451 were kept on a 12h light/dark cycle at 20-24°C and 45-65% relative humidity (typically 21°C and  
452 55%). Normal rodent chow (Teklad 2018 or 7912, Envigo) and tap water were available *ad*  
453 *libitum*, and animals were group housed until surgery and/or behavioural experiments. Within-  
454 subjects design experiments were conducted using sex-balanced cohorts of appropriate  
455 genotype littermates as far as possible. Similarly, for between-subjects and mixed model design  
456 experiments, littermates were semi-randomly allocated to virus groups to ensure groups were  
457 balanced for sex and age as far as possible. All data are from biologically independent samples,  
458 i.e. technical repeats were not performed on any animals. Sample size calculations were not  
459 performed, appropriate group sizes (detailed in figure legends) were determined from pilot  
460 experiments and our previously published studies using these models and behavioural  
461 paradigms<sup>7,18,55</sup>.

462 Experiments conducted in the UK were performed in accordance with the U.K. Animals  
463 (Scientific Procedures) Act 1986, and experimental protocols were approved by the UCL Animal  
464 Welfare and Ethical Review Body (Bloomsbury Campus). Experiments conducted in the U.S.  
465 were performed in accordance with the U.S. Public Health Service's Policy on the Humane Care  
466 and Use of Laboratory Animals, and experimental protocols were approved by the Institutional  
467 Animal Care and Use Committees of Florida State University and the University of Florida.  
468 Experiments conducted in Switzerland were performed in accordance with the Basel  
469 Declaration and the ethical guidelines of the Ethics Committee for Animal Experimentation of  
470 the Swiss Academy of Medical Sciences (SAMS) and the Swiss Academy of Sciences  
471 (SCNAT), and experimental protocols were approved by the Canton of Zurich's Veterinary  
472 Office (ETH Zurich).

473

## 474 **Stereotaxic Surgery**

### 475 **NTS Virus Injections**

476 Mice were anaesthetized with intramuscular medetomidine (1 mg/ kg) + ketamine hydrochloride  
477 (50 mg/kg) or 1.5-2.5% isoflurane, and given carprofen analgesia (5mg/kg, s.c.). Core  
478 temperature was maintained using a homeothermic monitoring system, and appropriate depth  
479 of surgical anaesthesia was determined by absence of pedal reflex. The skull was restrained in  
480 a stereotaxic frame, and the head flexed downwards such that the nose and neck were at a  
481 right angle. The scalp was incised from the occipital crest to first vertebrae, and muscle layers  
482 parted to expose the atlanto-occipital membrane. The membrane was bisected horizontally with  
483 a 30G needle to expose the brainstem surface with obex used as an anatomical landmark. Viral  
484 vectors (as detailed in figures and Methods Table 1) were injected via pulled glass micropipettes  
485 at the following coordinates from obex: +0.1mm rostral,  $\pm$ 0.5mm lateral and -0.35mm ventral.  
486 Viruses encoding chemogenetic effectors, diphtheria toxin subunit A (DTA) and control reporters  
487 were all bilaterally injected in volumes of 200-250nl. Mice were allowed to recover for a  
488 minimum of 3 weeks before behavioural experiments began. For monosynaptic retrograde  
489 tracing from PPG neurons in the caudal NTS, 300nl of a 1:1 mix of AAV5-EF1a- FLEX-  
490 TVA:mCherry and AAV8/733-CAG-FLEX-RabiesG were bilaterally injected +0.1mm rostral,  
491  $\pm$ 0.4mm lateral and 0.35mm ventral to obex. 21 days later, 400nl in total of (EnvA)-RABV- $\Delta$ G-  
492 GFP was unilaterally injected at two injection sites: +0.1mm rostral, +0.25mm lateral and 0.35-  
493 0.45mm ventral to obex; and +0.1mm rostral, +0.4mm lateral and 0.35-0.45mm ventral to obex.  
494 Mice were transcardially perfused for histological processing and *in situ* hybridisation 7 days  
495 later.

496

### 497 **Nodose Ganglia Virus Injections**

498 Mice were anaesthetized with 1.5-2.5% isoflurane and given carprofen analgesia (5mg/kg, s.c.),  
499 then the ventral surface of the neck was incised, and muscles parted to expose the trachea. The  
500 vagus nerve was separated from the carotid artery to allow access to the nodose ganglia. In  
501 each nodose ganglia, a total volume of 500nl of viral vector (AAV5 / 9 -hSyn1-DIO-  
502 hM3Dq:mCherry, AAV5-EF1a-DIO-hChR2(H134R):mCherry, AAV9-EF1a-DIO-  
503 hChR2(H134R):eYFP, or AAV-PHP.S-CAG-DIO-tdTomato, as detailed in figures and resources  
504 table) was injected into sites rostral and caudal to the laryngeal nerve branch, using a bevelled  
505 tip pulled glass micropipette and pneumatic microinjector. Viruses encoding chemogenetic and

506 optogenetic effectors were injected bilaterally, and the virus for tdTomato-visualized projection  
507 tracing was injected unilaterally into left or right nodose ganglia. Mice were allowed to recover  
508 for a minimum of 2 weeks before behavioural experiments or transcardial perfusion.

509

## 510 **Viral Targeting Validation**

511 We have previously histologically and functionally validated all viral targeting and neuronal  
512 manipulation strategies used in the present study. These include those for chemogenetic  
513 activation, inhibition, ablation, and input mapping of PPG<sup>NTS</sup> neurons<sup>7,18,29</sup>, and for chemogenetic  
514 and optogenetic activation of vagal afferent neurons<sup>55</sup>. The same validated mouse lines and  
515 viruses were used in the present studies, and additional confirmatory validations of viral  
516 transduction efficiency / specificity and the functional efficacy of manipulations were performed  
517 as detailed below. Post-mortem tissue sections were processed from all mice used in  
518 behavioural studies and verified for appropriate expression of fluorescent reporters. Mice in  
519 which viral injection targeting was inaccurate, or transduction efficiency below expected levels,  
520 were omitted from analyses (<10% of mice across all experiments). Our individual results are  
521 therefore unlikely to be confounded by type 1 errors arising from non-specific manipulations of  
522 neuronal populations other than those targeted, nor by type 2 errors arising from failing to detect  
523 effects of our manipulations due to specific but inefficient transduction of our target populations.  
524 Sample sizes were derived from prior experiments using the same or similar viral targeting and  
525 manipulation strategies, and crucially the overall study was designed to provide convergent  
526 lines of anatomical, functional and behavioural data, thereby minimising the risk of type 1 or 2  
527 errors arising from conclusions based on a single line of evidence. The strength of this approach  
528 and reliability of strategies used is demonstrated by the internal consistency of the lines of  
529 evidence presented here, and their external consistency with prior findings our experiments  
530 have replicated and extended.

531

### 532 *PPG<sup>NTS</sup> Neuron Targeting Validation*

533 The efficiency and specificity of viral targeting of PPG<sup>NTS</sup> neurons was validated using the PPG-  
534 Cre:GCaMP3 mouse line, by quantifying co-localisation of GFP-immunoreactivity (in GCaMP3-  
535 expressing PPG<sup>NTS</sup> neurons) and mCherry expression following NTS injection of AAV encoding  
536 hM3Dq-mCherry (Extended Data 8e-g). We have previously demonstrated that neither hM3Dq

537 nor hM4Di chemogenetic effectors have constitutive activity in PPGs, and that the DREADD  
538 ligand CNO does not affect feeding behaviours in our hands at the doses used here. We have  
539 also confirmed the respective excitatory and inhibitory actions of these effectors on PPG<sup>NTS</sup>  
540 neurons using *ex vivo* patch-clamp electrophysiology and Ca<sup>2+</sup> imaging<sup>7</sup>. Further functional  
541 validation of PPG<sup>NTS</sup> neuron activation was conducted by quantification of cFos expression in  
542 these neurons following administration of CNO to mice transduced with AAV encoding hM3Dq  
543 (Extended Data 2c-e). Specifically, PPG-Cre:tdRFP mice were bilaterally injected in the NTS  
544 with AAV8-DIO-hM3Dq-mCherry and allowed to recover for ≥3 weeks as per standard surgical  
545 protocol for NTS viral injection. They were habituated to handling and the standard *ad libitum*  
546 eating protocol in which they were fasted for 3 hours and administered saline/CNO 30 mins prior  
547 to dark onset. On the test day, mice were administered saline (n=4) or 2 mg/kg CNO (n=3) and  
548 transcardially perfused 3 hours later. Tissue was subsequently processed for cFos  
549 immunofluorescence as detailed in *Immunohistochemistry & In Situ Hybridization*.

550

#### 551 *Glp1r* Vagal Afferent Neuron Targeting Validation

552 The efficiency and specificity of viral targeting of *Glp1r* VANs was validated using the GLP-1R-  
553 Cre:tdRFP mouse line by quantifying co-localisation of RFP-immunoreactivity (in tdRFP-  
554 expressing GLP-1R vagal afferent neurons) and eYFP expression, following nodose ganglia  
555 injection of AAV encoding ChR2-eYFP (Extended Data 3g-i). cFos expression in nodose ganglia  
556 is not a reliable marker of vagal afferent neuron activation, but vagal stimulation robustly  
557 induces cFos expression in downstream NTS neurons<sup>28,55</sup>. We therefore functionally validated  
558 our strategies for chemogenetic and optogenetic activation of *Glp1r* VANs by quantification of  
559 cFos expression in the NTS. Specifically, GLP-1R-Cre:tdRFP x PPG-YFP mice were injected  
560 bilaterally in nodose ganglia with either AAV9-DIO-hM3Dq-mCherry, AAV9-DIO-ChR2-eYFP or  
561 control injections (dye or control virus) as per standard surgical protocol for viral transduction of  
562 vagal afferent neurons. For validation of optogenetic activation, mice were fasted for 2 hours  
563 then anesthetized with isoflurane, nodose ganglia were surgically exposed and bilaterally  
564 stimulated with blue light from a laser fib (10mW for 1 minute). Mice were euthanized by  
565 isoflurane overdose and transcardially perfused 90 minutes later. For validation of  
566 chemogenetic activation, mice were injected with saline or 2 mg/kg CNO then euthanized by  
567 isoflurane overdose and transcardially perfused 90 minutes later. Tissue from both experiments  
568 were processed for cFos immunofluorescence as detailed in *Immunohistochemistry & In Situ*  
569 *Hybridization*.

570

### 571 **Optical Fibre Implantation**

572 Optical fibres were implanted two weeks after bilateral injection of AAV5-EF1a-DIO-  
573 hChR2(H134R)-mCherry in nodose ganglia. Optical fibres (CFLC230–10 ceramic ferrules with  
574 FT200UMT fibre, Thorlabs) were unilaterally implanted above the right caudal NTS, 7.5mm  
575 caudal, 0.25mm lateral and 4.0mm ventral to Bregma. Skull screws, superglue and dental  
576 cement were used to secure the fibre, and mice were allowed to recover for an additional 2  
577 weeks prior to behavioural testing.

578

### 579 ***Behavioural Studies***

#### 580 **Drug Administration**

581 Clozapine *N*-oxide (CNO; Hello Bio / Enzo) was administered intraperitoneally at 2 mg/kg in 2  
582 ml/kg dose volume for all experiments, typically 15 minutes prior to dark onset. We have  
583 previously determined that in our hands CNO at this dose does not affect eating behaviours in  
584 control virus transduced mice, and similarly that the chemogenetic effectors used do not have  
585 any constitutive activity which affects eating behaviours<sup>7,55</sup>. To minimize animal use and  
586 maximize statistical power, all chemogenetic experiments in the present study were therefore  
587 conducted in DREADD-expressing mice using a within-subjects design. All mice received both  
588 CNO and saline vehicle in a counterbalanced manner, and hence acted as their own controls.  
589 Similarly, when assessing the effect of PPG<sup>NTS</sup> neuron ablation on the anorexigenic actions of  
590 oxytocin, liraglutide and semaglutide, we used a mixed model design, whereby mice in DTA-  
591 ablated and control cohorts all received drug and vehicle in a counterbalanced manner.  
592 Oxytocin (Tocris) was administered intraperitoneally 15 minutes prior to dark onset at 0.4 mg/kg,  
593 based on reports that this dose and route of administration elicits vagal-dependent eating  
594 suppression in mice<sup>44,45</sup>. Liraglutide and semaglutide (gift from Lotte Bjerre Knudsen, Novo  
595 Nordisk) were administered subcutaneously 30 minutes prior to dark onset at 0.2 mg/kg and  
596 0.06 mg/kg, respectively, in 5 ml/kg dose volume, based on recommendations from LBJ and  
597 previous reports of the anorexigenic effects of these drugs in mice<sup>19,20,56</sup>.

598

#### 599 **Eating Behaviour Paradigms**

600 Drug- or neuronal manipulation-induced changes to eating behaviour were assessed from dark  
601 onset in *ad libitum* eating or fasted mice. In the *ad libitum* eating paradigm, mice were  
602 habituated ( $\geq 5$  sessions) to being fasted for the final 3 hours of the light phase and receiving  
603 saline/vehicle injections 5-30 mins prior to return of food at dark onset. This protocol minimized  
604 hypophagia from handling and injection stress, and entrained mice to eat consistently from dark  
605 onset, without needing to induce negative energy balance. All experiments using either manual  
606 or automated measurement of food intake used this protocol for assessment of *ad libitum*  
607 eating, except for metabolic phenotyping of PPG<sup>NTS</sup> ablated mice experiment, in which mice  
608 were not handled or injected and were already habituated to test cages. To assess the effect of  
609 chemogenetic manipulations on the behavioural satiety sequence, and large meals driven by  
610 refeeding after a prolonged fast, mice were fasted for 18 hours prior to dark onset. To assess  
611 the effect of optogenetic activation of *Glp1r*-expressing vagal afferent neurons on acute feeding,  
612 mice were fasted for the entire light phase and intake measured during the first 30 minutes of  
613 the dark phase. The effect of optogenetic activation was also assessed using a within-subjects  
614 design, with all mice tested for 30 minute intake under 'laser on' (20ms blue light pulse every 3  
615 seconds,  $\sim 5$ mW intensity) and 'laser off' (tethered but no light pulses) conditions in a  
616 counterbalanced manner.

617

## 618 **Food Intake Measurement**

619 Food intake was measured manually, using open source FED pellet dispensers (Feeding  
620 Experimentation Device; Nguyen et al., 2016), or using commercially-available Phenomaster  
621 (TSE Systems) or Promethion (Sable Systems) systems. For manual measurement of intake in  
622 the *ad libitum* eating paradigm, mice were weighed at the start of the 3 hour fast, then a pre-  
623 weighed amount of food was returned at dark onset. Food was again weighed at 1, 2, 4, 6  
624 (GLP-1RA experiments only), and 21 hours, at which point 24 hour bodyweight change was  
625 also determined. FED dispensers were used for all experiments involving chemogenetic  
626 manipulations of PPG<sup>NTS</sup> neurons, the Phenomaster system for chemogenetic activation of  
627 *Glp1r*-expressing vagal afferent neurons, and the Promethion system for metabolic phenotyping  
628 of PPG<sup>NTS</sup> ablated mice. For all food intake measurement systems and eating behaviour  
629 paradigms, mice were habituated to the test equipment and all aspects of the paradigm  
630 (including vehicle dosing where appropriate) prior to the start of testing. Mice were considered  
631 habituated after their intakes during  $\geq 3$  consecutive habituation sessions were not significantly  
632 different, and no directional trend was apparent. Meal pattern analysis was conducted on

633 automated food intake data from experiments testing the effect of inhibition or ablation of  
634 PPG<sup>NTS</sup> neurons. A meal was defined as the sum of all bouts  $\geq 0.02\text{g}$  with intra-meal intervals  
635  $< 10$  minutes, based on the standard operating procedure of the UC Davis Mouse Metabolic  
636 Phenotyping Centre <sup>57</sup>. Food intake and metabolic data were collected from the TSE  
637 Phenomaster system using the Phenomaster software package, and from the Sable Promethion  
638 system using ExpeData and MacroInterpreter software packages. Consumption of Ensure liquid  
639 diet was measured manually, and the temporal pattern of Ensure drinking was measured by  
640 offline video coding of licking duration (blinded to drug treatment), using the BORIS open source  
641 video coding software package <sup>58</sup>.

642

### 643 **Behavioural Satiety Sequence Analysis**

644 Alterations to the behavioural satiety sequence (BSS) following chemogenetic activation of  
645 PPG<sup>NTS</sup> neurons were determined using the continuous monitoring BSS protocol <sup>59,60</sup>, adapted  
646 for use with mice and FED dispensers. Mice were fasted for 18 hours, FED dispensers were  
647 returned to home cages at dark onset, and behaviour recorded for 40 minutes using infrared  
648 video cameras. Behaviours were subsequently coded offline using BORIS software by trained  
649 observers (Cohen's  $\kappa$  for inter-rater reliability  $> 0.9$ ) blinded to treatment group. Behaviours were  
650 coded as mutually-exclusive categories: eating, drinking, grooming (including scratching),  
651 inactive (resting and sleeping) and active (locomotion and rearing). In pilot experiments, the  
652 duration of water drinking was found to be extremely low and unaffected by our manipulations,  
653 hence was omitted from further analyses. The total duration mice spent exhibiting behaviours in  
654 the remaining 4 categories were calculated for 8 x 5 minute time bins. For qualitative and semi-  
655 quantitative evaluation of the stochastic sequence of satiety behaviours (eating  $\rightarrow$  grooming  $\rightarrow$   
656 inactive), the mean durations of these 3 categories were plotted across all time bins separately  
657 for saline control and CNO activated conditions. To aid visualization of neuronal activation-  
658 induced acceleration of the sequence, horizontal dotted lines were added denoting the time bin  
659 during which the (probabilistic) transition from feeding to resting occurs, which is typically  
660 considered the satiation point / onset of satiety. Data were also presented and analysed to  
661 quantitatively test the effect of chemogenetic activation over time in each behaviour category.

662

### 663 **Indirect Calorimetry**

664 We measured respiratory exchange ratio and energy expenditure concurrently with food intake  
665 from PPG<sup>NTS</sup> ablated and *Glp1r*<sup>Nodose</sup>-hM3Dq mice, using the indirect calorimetry functionality  
666 integrated into the Phenomaster and Promethion systems. Mice were habituated to test cages  
667 for  $\geq 3$  days before testing, and metabolic data were collected for 24 hours for between-subjects  
668 analysis (PPG<sup>NTS</sup>-DTA ablated vs PPG<sup>NTS</sup>-mCherry controls), or during two 24 hour test  
669 sessions (*Glp1r*<sup>Nodose</sup>-hM3Dq, counterbalanced for CNO administration), separated by  $\geq 48$  hour  
670 washout periods during which mice remained in test cages. Respiratory exchange ratio (RER)  
671 was obtained from measurement of mice's O<sub>2</sub> consumption (ml/kg/hr) and CO<sub>2</sub> production  
672 (ml/kg/hr), using the equation:  $RER = VCO_2 / VO_2$ . Energy expenditure (EE) was calculated  
673 using the Weir equation:  $EE = 3.941 \times VO_2 + 1.106 \times VCO_2$ . Raw data from both systems were  
674 used to generate standardized output files, which were imported into the CalR analysis tool<sup>61</sup>  
675 for production and analysis of intake and metabolic data over light and dark phases and total  
676 circadian cycle. As now recommended for analysis of calorimetry data from these systems,  
677 energy expenditure was not normalized to bodyweight.

678

### 679 **Conditioned Flavour Preference**

680 Whether optogenetic activation of *Glp1r* vagal afferent neurons conditioned a preference for (or  
681 avoidance of) a flavour was assessed using a previously-validated protocol<sup>55</sup>. Experiments  
682 were conducted within sound-attenuated cubicles, using behavioural chambers equipped with  
683 two sipper tubes connected to contact-based licking detection devices, allowing high resolution  
684 measurement of licking responses (Med-PC V / Med Associates Inc.). Following recovery from  
685 surgeries for nodose ganglia virus injection and optical fibre implantation, individually-housed  
686 mice were placed on a food and water restriction regime, under which they were maintained at  
687 90% of starting bodyweight and were limited to 6 hours of water access per day. Mice were  
688 habituated to behavioural chambers (including being tethered to fibre cables) and trained to lick  
689 for a 0.025% saccharin solution during daily 1 hour habituation sessions, conducted during the  
690 light phase. Mice were considered trained to saccharin licking once they showed  $< 10\%$   
691 between-session variability in the number of licks, a criterion all mice reached within 10  
692 sessions.

693 Once trained, a 'pre'-test was conducted in which mice were given access to two novel Kool-Aid  
694 flavours (cherry or grape, both 0.05% in 0.025% saccharin solution) for 10 minutes, with sipper  
695 bottle positions switched after 5 minutes to avoid position bias. Mice then underwent 3 x 1 hour

696 training sessions for each flavour (alternately over 6 days), in which both bottles contained the  
697 same flavour. One flavour was paired with laser stimulation (CS+), such that licking triggered  
698 blue light laser stimulation via a TTL output signal. Specifically, 10 licks triggered a 20ms light  
699 pulse of ~5mW intensity, with additional licks during the following 10 seconds having no  
700 programmed consequences. Further bouts of  $\geq 10$  licks triggered additional pulses in the same  
701 manner throughout the 1 hour session. During training sessions with the unpaired (CS-) flavour,  
702 mice were tethered but licking did not elicit laser stimulation. Upon completion of these training  
703 sessions, mice underwent a 'post'-test identical to the 'pre'-test, i.e. both flavours were  
704 available, and licking did not elicit laser stimulation. The number of licks for the laser-paired  
705 flavour during 'pre' and 'post' tests was used to calculate preference ratios (CS+ licks / total  
706 licks) for the flavour before and after training, to determine if optogenetic stimulation of *Glp1r*  
707 vagal afferent neurons increased or decreased preference for the paired flavour.

708

## 709 ***Immunohistochemistry & In Situ Hybridization***

### 710 **Tissue Preparation**

711 Mice were deeply anaesthetized then transcardially perfused with ice-cold PB/PBS (0.1M, pH  
712 7.2) then 4% formaldehyde in PB/PBS. Brains and NG (when required) were extracted and  
713 post-fixed in 4% formaldehyde at 4°C overnight ( $\leq 2$  hours for NG), before being cryoprotected in  
714 20-30% sucrose solution for  $\geq 24$  hours at 4°C. Brains were sectioned into 30-35 $\mu$ m coronal  
715 sections, collected free-floating and stored at 4°C until processing for immunofluorescent  
716 labelling as detailed below. NG were sectioned into 10 $\mu$ m sections, collected on Superfrost Plus  
717 microscope slides and stored at -20°C until processing for *in situ* hybridization as detailed  
718 below.

719

### 720 **Immunofluorescent labelling**

721 Brain sections were processed for amplification of fluorescent reporter signals by  
722 immunofluorescent labelling of tdRFP, mCherry, eYFP, eGFP and/or GCaMP3 using previously-  
723 validated protocols<sup>7</sup>. For all fluorescent protein antigens, sections were incubated free-floating  
724 with primary antibodies (see Methods Table 1 for antibody details) overnight at 4°C in PBS with  
725 2% normal goat/donkey serum and 1% BSA, followed by 2 hours at room temperature with  
726 secondary antibodies conjugated to fluorophores appropriate for the native fluorescent reporter

727 being amplified (i.e. Alexa Fluor 488 for eYFP/eGFP/GCaMP3 and Alexa Fluor 568 for  
728 tdRFP/mCherry; all 1:500).

729

### 730 **RNAscope *In situ* Hybridization (Nodose Ganglia)**

731 Sections from nodose ganglia of mice previously injected with viruses for monosynaptic  
732 retrograde rabies tracing were processed for *in situ* hybridization of *Glp1r* and *Oxtr* mRNA using  
733 a previously-optimised modification of the RNAscope assay<sup>62</sup>. Sections were cut at 10µm on a  
734 cryostat and collected on Superfrost Plus slides, then allowed air-dry at room temperature for  
735 one hour. Slides were then dipped in molecular grade ethanol and further air-dried overnight at  
736 room-temperature. RNAscope *in situ* hybridization was performed on these sections using the  
737 RNAscope Multiplex Fluorescent Kit v2 (Advanced Cell Diagnostics) as per the manufacturer's  
738 instructions, with a modification to the pre-treatment procedure (Protease IV incubation  
739 conducted for 20 min at room temperature) that allows for preservation of the fluorescent  
740 reporter signal while also providing optimal signal from the target mRNAs. Probes for *Glp1r*,  
741 *Oxtr* and appropriate positive (*Ubc*) and negative (*DapB*) controls (detailed in Methods Table 1)  
742 were hybridized and after completion of the procedure slides were immediately cover slipped  
743 using Prolong Antifade medium.

744

### 745 **RNAscope *In situ* Hybridization (Brainstem)**

746 Brainstem sections containing the area postrema were pre-treated with hydrogen peroxide for  
747 30 minutes at room temperature, slide-mounted in dH<sub>2</sub>O and air dried overnight. Sections were  
748 subsequently processed for *in situ* hybridization of *Glp1r* mRNA using the same reagents and  
749 protocol as nodose ganglia sections, followed by additional processing for immunofluorescent  
750 labelling of GFP and tyrosine hydroxylase (TH). Incubation with primary antibodies against GFP  
751 and TH (see Methods Table 1 for antibody details; both 1:1000) was performed concurrently  
752 overnight at room temperature, with the remaining protocol conducted as described above for  
753 labelling of fluorescent reporters. Sections were then dehydrated in increasing concentrations of  
754 ethanol, cleared in xylene and cover slipped using Cytoseal 60.

755

### 756 **cFos Immunohistochemistry and Quantification**

757 For immunohistochemical validation of chemogenetic PPG<sup>NTS</sup> neuron activation, brains from  
758 PPG<sup>NTS</sup>-hM3Dq mice were processed for immunofluorescent labelling of cFos. For validation of  
759 chemogenetic and optogenetic activation of *G11pr* VANs, 35µm free-floating sections were  
760 incubated overnight with anti-cFos rabbit primary antibody (#2250, Cell Signalling Technology;  
761 1:1000) followed by 2 hours in donkey anti-rabbit Alexa-Fluor 647 secondary antibody (1:500).  
762 For quantification of semaglutide-induced cFos expression, mice expressing eYFP in PPG  
763 neurons were habituated to handling and the standard *ad libitum* eating behaviour paradigm,  
764 including vehicle injection 30 minutes prior to dark onset. Food intake was manually quantified  
765 after 3 hours during habituation sessions and on the day semaglutide was administered,  
766 allowing a within-subjects quality control for the effect of semaglutide in this experiment. On the  
767 test day, mice were injected with vehicle or semaglutide (0.06 mg/kg as per behavioural studies)  
768 and transcardially perfused 4 hours later. Coronal brain sections were prepared as above, then  
769 processed for immunoperoxidase labelling of cFos with DAB-Ni followed by immunofluorescent  
770 amplification of eYFP using a previously-optimised protocol<sup>29</sup>. Free-floating sections were first  
771 pre-treated with sodium borohydride solution (0.5% w/v; 20 mins at room temperature) followed  
772 by hydrogen peroxide (0.15% v/v; 15 mins at room temperature) then incubated with anti-cFos  
773 rabbit primary antibody (#2250, Cell Signalling Technology; 1:10,000) overnight at room  
774 temperature. The following day, sections were incubated for 1 hour with biotinylated donkey α-  
775 rabbit antibody (1:500), followed by 2 hours with AB solution (ABC Peroxidase Kit, Vectastain).  
776 Sections were incubated with 2 changes of sodium acetate solution (0.1M, 5 mins) then with  
777 DAB-Ni in sodium acetate solution for 10 mins, before addition of hydrogen peroxide to allow a  
778 chromogenic reaction for ~5 minutes. Sections were subsequently processed for  
779 immunofluorescent labelling of eYFP as described above, dehydrated in increasing  
780 concentrations of ethanol, cleared in xylene, and cover slipped using Cytoseal 60.

781

## 782 **Imaging**

783 Brain sections labelled for fluorescent reporters and/or cFos expression were imaged using an  
784 upright epifluorescence and brightfield microscope (Leica) with a Retiga 3000 CCD camera  
785 (QImaging). For co-localization of DAB-Ni labelled cFos and PPG-eYFP neurons, brightfield and  
786 fluorescence images were sequentially captured in the same focal plane. Quantification of cFos  
787 expression and co-localization was conducted using merged native brightfield (DAB) and  
788 fluorescent (PPG-eYFP) images. For clarity of presentation, brightfield DAB images were  
789 inverted and pseudocolored prior to merging with fluorescent channels. Nodose ganglia and

790 brainstem sections processed for *in situ* hybridization and/or fluorescent reporters were imaged  
791 with a Keyence BZ-x700 at 20x or 40x in 0.6µm optical sections, or a Leica TCS SP8 confocal  
792 microscope at 20x. For imaging of sections processed for *in situ* hybridization, sections  
793 hybridized with positive and negative control probes were used to determine exposure time and  
794 image processing parameters necessary for optimal visualization of mRNA signals and control  
795 for possible degradation. Generation of montages from individual images, brightness and  
796 contrast adjustment, and quantification of cFos expression using the Cell Counter plugin were  
797 all performed using Fiji open source biological image analysis software<sup>63</sup>.

798

## 799 ***Brain Slice Ca<sup>2+</sup> Imaging***

### 800 **Imaging Data Capture**

801 Coronal brainstem slices (200µm) were obtained from PPG-Cre:GCaMP3 mice and used to  
802 assess the effects of bath-applied oxytocin on PPG<sup>NTS</sup> neuron calcium dynamics using a  
803 previously-optimised protocol<sup>43</sup>. Oxytocin was dissolved in aCSF (3mM KCl, 118mM NaCl,  
804 25mM NaHCO<sub>3</sub>, 5mM glucose, 1mM MgCl<sub>2</sub>, 2mM CaCl<sub>2</sub>; pH 7.4) to give a bath concentration of  
805 100nM, based on reports that this concentration elicits robust activation of vagal afferent  
806 neurons under *ex vivo* conditions<sup>44</sup>. Slices were superfused with aCSF for ≥10 minutes, with  
807 the final 5 minute period prior to oxytocin application used to determine baseline fluorescence  
808 intensity. Slices were then superfused with oxytocin solution for 3-5 minutes, washed with aCSF  
809 for ≥10 minutes, then finally superfused with 100µM glutamate for 1 minute as a positive control  
810 to confirm imaged neurons were healthy and responsive to glutamatergic input. GCaMP3  
811 fluorescence was excited at 460 ± 25 nm using an LED light source, for 250ms every 5  
812 seconds. Imaging was conducted using a widefield microscope (Zeiss) with 40x water  
813 immersion lens and captured at 12-bit on a CCD camera (QClick, QImaging). Data were  
814 obtained from 8 experiments (i.e. recordings from single slices) from 3 mice.

815

### 816 **Imaging Data Analysis**

817 Time-lapse image recordings were imported into FIJI software, with the StackReg plugin used to  
818 correct for XY drift. Regions of interest (ROIs) were manually drawn around all PPG<sup>NTS</sup> somata  
819 in the field of view, with additional ROIs used to determine background intensity for each  
820 experiment. Background intensity was subtracted from ROIs and a cubic polynomial function

821 was used to adjust for bleaching. Data are presented as  $\Delta F/F_0$ , where  $F_0$  is the mean  
822 fluorescence intensity over the 5 minute baseline period, and  $\Delta F$  is the intensity at each  
823 timepoint with  $F_0$  subtracted. Response magnitudes were determined using the area under the  
824 curve (AUC) over 4 minutes from first application of oxytocin. To ensure artifactual fluctuations  
825 were not included in analyses, only fluorescence changes for which the magnitude was greater  
826 (or less) than 3 standard deviations of the baseline period AUC were considered to be  
827 'responders'. As the noise level (i.e. variability in baseline AUC) differs between slice  
828 recordings, this threshold is not absolute, hence there is some degree of overlap between the  
829 AUC of 'non-responsive' ROIs from noisier recordings and 'responsive' ROIs from less noisy  
830 recordings. As a further quality control, oxytocin-responsive ROIs were only included for  
831 analysis if they subsequently were responsive to glutamate.

832

### 833 ***Quantification and statistical methods***

834 Data are presented as mean  $\pm$  SEM, and were analysed for statistical significance as detailed in  
835 figure legends using Student's *t*-test, one-way within-subjects or two-way within-subjects/mixed-  
836 model ANOVA (with the Greenhouse-Geisser correction applied where appropriate). Where  
837 data were not normally distributed, non-parametric equivalents were used as detailed.  
838 Significant one-way ANOVA tests were followed by pairwise comparisons with Tukey's  
839 correction for multiple comparisons. For two-way ANOVA, either simple main effects were  
840 reported, or significant interactions were reported and followed by pairwise comparisons with  
841 Sidak's correction for multiple comparisons. The threshold for statistical significance was  
842 considered  $<0.05$ , and significant comparisons are reported in all figures as: \*  $p<0.05$ , \*\*  
843  $p<0.01$ , \*\*\*  $p<0.001$ , \*\*\*\*  $p<0.0001$ . For transparency, all comparisons in which  $p<0.1$  (but  
844  $\geq 0.05$ ) are additionally reported with exact *p* values shown. Statistical analyses were conducted  
845 using Microsoft Excel, GraphPad Prism or IBM SPSS Statistics.

846

### 847 ***Data availability***

848 There are no publicly available datasets for this manuscript. All data necessary to interpret,  
849 replicate and build on the methods or findings reported here are contained within the manuscript  
850 and extended data figures. Primary data from ex vivo calcium recordings, food intake, metabolic  
851 and behavioural analyses, videos for behavioural satiety sequence coding, and

852 photomicrographs for ISH and IHC analyses are available in native format upon request from  
853 the corresponding authors. Access to stored tissue samples used for ISH and IHC is available  
854 upon request from the corresponding authors. All mouse lines, plasmids and reagents used in  
855 this study have been previously published and/or are commercially available, and are detailed in  
856 the Reporting Summary. Further information and requests for resources and reagents should be  
857 directed to and will be fulfilled by Prof. Stefan Trapp ([s.trapp@ucl.ac.uk](mailto:s.trapp@ucl.ac.uk)).

858

859

860

861

862

863

<b>Table 1. Reagents and Resources</b>		
<b>Antibodies &amp; Viruses</b>		
$\alpha$ -DsRed rabbit pAb (1:500 IF)	Takara Bio	Cat #632496, RRID:AB_10013483
$\alpha$ -mCherry rabbit pAb (1:500 IF)	Abcam	Cat# ab167453, RRID:AB_2571870
$\alpha$ -GFP chicken pAb (1:1000 IF)	Abcam	Cat #13970, RRID:AB_300798
$\alpha$ -cFos (9F6) rabbit mAb (1:1000 IF / 1:10,000 IHC)	Cell Signaling Technology	Cat# 2250, RRID:AB_2247211
$\alpha$ -cFos rabbit pAb (1:500 IF)	Millipore	Cat# ABE457, RRID:AB_2631318
$\alpha$ -tyrosine hydroxylase rabbit pAb (1:1000 IF)	Millipore	Cat# AB152, RRID:AB_390204
$\alpha$ -rabbit IgG biotinylated goat pAb (1:500 IHC)	Vector Laboratories	Cat# BA-1000, RRID:AB_2313606
Alexa Fluor 488 goat $\alpha$ -chicken (1:500 IF)	Thermo Fisher Scientific	Cat# A-11039, RRID:AB_2534096
Alexa Fluor 488 goat $\alpha$ -rabbit (1:500 IF)	Thermo Fisher Scientific	Cat# A-11008, RRID:AB_143165
Alexa Fluor 568 donkey $\alpha$ -rabbit (1:500 IF)	Thermo Fisher Scientific	Cat# A-10042, RRID:AB_2534017
Alexa Fluor 647 donkey $\alpha$ -rabbit (1:500 IF)	Thermo Fisher Scientific	Cat# A-31573, RRID:AB_2536183
AAV8-EF1a-mCherry-DIO-DTA ( $3.3 \times 10^{12}$ )	UNC Vector Core, NC	Gift from Naoshige Uchida, RRID:Addgene_58536 <sup>64</sup>
AAV8-hSyn1-DIO-mCherry ( $9.0 \times 10^{12}$ )	Viral Vector Facility, ETH Zurich	Cat# v116-8, Gift from Bryan Roth, RRID:Addgene_50459
AAV8-hSyn1-DIO-eGFP ( $6.3 \times 10^{12}$ )	Viral Vector Facility, ETH Zurich	Cat# v115-8, Gift from Bryan Roth, RRID:Addgene_50457
AAV2-hSyn1-DIO-hM4Di:mCherry ( $6.4 \times 10^{12}$ )	UNC Vector Core, NC	Lot AV4500F
AAV8- hSyn1-DIO-hM3Dq:mCherry ( $4.5 \times 10^{12}$ )	Viral Vector Facility, ETH Zurich	Cat# v89-8, Gift from Bryan Roth, RRID:Addgene_44361 <sup>65</sup>
AAV5- hSyn1-DIO-hM3Dq:mCherry ( $\geq 7 \times 10^{12}$ )	Addgene Viral Service	Cat# 44361-AAV5, Gift from Bryan Roth, RRID:Addgene_44361 <sup>65</sup>
AAV9- hSyn1-DIO-hM3Dq:mCherry ( $\geq 7 \times 10^{12}$ )	Addgene Viral Service	Cat# 44361-AAV9, Gift from Bryan Roth, RRID:Addgene_44361 <sup>65</sup>
AAV5-EF1a-DIO-hChr2(H134R):mCherry ( $5.7 \times 10^{12}$ )	UNC Vector Core, NC	Gift from Karl Deisseroth, RRID:Addgene_20297
AAV9-EF1a-DIO-hChr2(H134R):eYFP ( $\geq 1 \times 10^{13}$ )	Addgene Viral Service	Cat# 20298-AAV9, Gift from Karl Deisseroth, RRID:Addgene_20297
AAV-PHP.S-CAG-DIO-tdTomato ( $\geq 1 \times 10^{13}$ )	Addgene Viral Service	Cat# 28306-PHP.S, Gift from Edward Boyden, RRID:Addgene_28306
AAV5-EF1a-FLEX-TVA:mCherry ( $5.6 \times 10^8$ )	Stanford Gene Vector and Virus Core	Cat# GVC-AAV-67, Gift from Karl Deisseroth <sup>66</sup>
AAV8/733-CAG-FLEX-RabiesG ( $2.13 \times 10^{12}$ )	Stanford Gene Vector and Virus Core	Cat# GVC-AAV-59 <sup>66</sup>
(EnvA)-RV- $\Delta$ G-GFP ( $2 \times 10^8$ )	Kevin Beier, UC Irvine	<sup>67</sup>
<b>Drugs, Chemicals &amp; Assays</b>		
Clozapine <i>N</i> -Oxide (CNO)	Hello Bio	Cat# HB1807
Clozapine <i>N</i> -Oxide (CNO)	Enzo Life Sciences	Cat# BML-NS105
Oxytocin	Tocris	Cat# 1910
Liraglutide	Novo Nordisk A/S	Batch GP52108, Gift from Lotte Bjerre Knudsen
Semaglutide	Novo Nordisk A/S	Batch GV40057, Gift from Lotte Bjerre Knudsen
Ensure Plus (vanilla)	Abbott	Cat# ENS100V
Purified dustless precision pellets (20mg)	Bio-Serv	Cat# F0071
Vectastain Elite ABC-Peroxidase Kit	Vector Laboratories	Cat# PK-7100, RRID:AB_2336827
RNAscope Multiplex Fluorescent Kit v2	Advanced Cell Diagnostics	Cat# 323100
RNAscope target probe for mouse <i>Glp1r</i>	Advanced Cell Diagnostics	Cat# 418851-C2
RNAscope target probe for mouse <i>Oxtr</i>	Advanced Cell Diagnostics	Cat# 402651-C3
RNAscope positive control probe (mouse <i>Ubc</i> )	Advanced Cell Diagnostics	Cat# 310771-C2/3
RNAscope negative control probe (mouse <i>DapB</i> )	Advanced Cell Diagnostics	Cat# 310043-C2/3
<b>Mice</b>		
<i>mGlu-Cre/tdRFP</i> (referred to here as PPG-Cre:tdRFP)	Frank Reimann, University of Cambridge	<sup>53</sup>
<i>mGlu-Cre/GCaMP3</i> (referred to here as PPG-Cre:GCaMP3)	Frank Reimann, University of Cambridge	<sup>42</sup>
<i>mGlu-YFP</i> (referred to here as PPG-YFP)	Frank Reimann, University of Cambridge	<sup>52</sup>
<i>Glp1r-Cre/tdRFP</i> (referred to here as GLP-1R-Cre:tdRFP)	Frank Reimann, University of Cambridge	<sup>54</sup>

864

865

866 **References:**

- 867 1. Knudsen, L. B. & Lau, J. The discovery and development of liraglutide and semaglutide.  
868 *Front. Endocrinol. (Lausanne)*. **10**, 155 (2019).
- 869 2. Turton, M. D. *et al.* A role for glucagon-like peptide-1 in the central regulation of feeding.  
870 *Nature* **379**, 69–72 (1996).
- 871 3. Trapp, S. & Richards, J. E. The gut hormone glucagon-like peptide-1 produced in brain: is  
872 this physiologically relevant? *Curr. Opin. Pharmacol.* **13**, 964–969 (2013).
- 873 4. Müller, T. D. *et al.* Glucagon-Like Peptide 1 (GLP-1). *Mol. Metab.* **30**, 72–130 (2019).
- 874 5. Gaykema, R. P. *et al.* Activation of murine pre-proglucagon-producing neurons reduces  
875 food intake and body weight. *J. Clin. Invest.* **127**, 1031–1045 (2017).
- 876 6. Liu, J. *et al.* Enhanced AMPA Receptor Trafficking Mediates the Anorexigenic Effect of  
877 Endogenous Glucagon-like Peptide-1 in the Paraventricular Hypothalamus. *Neuron* **96**,  
878 897-909.e5 (2017).
- 879 7. Holt, M. K. *et al.* Preproglucagon neurons in the nucleus of the solitary tract are the main  
880 source of brain GLP-1, mediate stress-induced hypophagia, and limit unusually large  
881 intakes of food. *Diabetes* **68**, 21–33 (2019).
- 882 8. Zheng, H., Stornetta, R. L., Agassandian, K. & Rinaman, L. Glutamatergic phenotype of  
883 glucagon-like peptide 1 neurons in the caudal nucleus of the solitary tract in rats. *Brain*  
884 *Struct. Funct.* **220**, 3011–3022 (2015).
- 885 9. Trapp, S. *et al.* PPG neurons of the lower brain stem and their role in brain GLP-1  
886 receptor activation. *Am. J. Physiol. Regul. Integr. Comp. Physiol.* **309**, R795-804 (2015).
- 887 10. Cheng, W. *et al.* Leptin receptor-expressing nucleus tractus solitarius neurons suppress  
888 food intake independently of GLP1 in mice. *JCI Insight* **5**, e134359 (2020).
- 889 11. Merchenthaler, I., Lane, M. & Shughrue, P. Distribution of pre-pro-glucagon and  
890 glucagon-like peptide-1 receptor messenger RNAs in the rat central nervous system. *J.*  
891 *Comp. Neurol.* **403**, 261–80 (1999).

- 892 12. Cork, S. C. *et al.* Distribution and characterisation of Glucagon-like peptide-1 receptor  
893 expressing cells in the mouse brain. *Mol. Metab.* **4**, 718–731 (2015).
- 894 13. Card, J. P. *et al.* GLP-1 neurons form a local synaptic circuit within the rodent nucleus of  
895 the solitary tract. *J. Comp. Neurol.* **526**, 2149–2164 (2018).
- 896 14. Hisadome, K., Reimann, F., Gribble, F. M. & Trapp, S. Leptin directly depolarizes  
897 preproglucagon neurons in the nucleus tractus solitarius: Electrical properties of  
898 glucagon-like peptide 1 neurons. *Diabetes* **59**, 1890–1898 (2010).
- 899 15. Drucker, D. J. Mechanisms of Action and Therapeutic Application of Glucagon-like  
900 Peptide-1. *Cell Metab.* **27**, 740–756 (2018).
- 901 16. Krieger, J. P. Intestinal glucagon-like peptide-1 effects on food intake: Physiological  
902 relevance and emerging mechanisms. *Peptides* **131**, 170342 (2020).
- 903 17. Grill, H. J. A role for GLP-1 in treating hyperphagia and obesity. *Endocrinology* bqaa093  
904 (2020) doi:10.1210/endo/bqaa093.
- 905 18. Holt, M. K. *et al.* PPG neurons in the nucleus of the solitary tract modulate heart rate but  
906 do not mediate GLP-1 receptor agonist-induced tachycardia in mice. *Mol. Metab.* 101024  
907 (2020) doi:10.1016/j.molmet.2020.101024.
- 908 19. Secher, A. *et al.* The arcuate nucleus mediates GLP-1 receptor agonist liraglutide-  
909 dependent weight loss. *J. Clin. Invest.* **124**, 4473–88 (2014).
- 910 20. Gabery, S. *et al.* Semaglutide lowers body weight in rodents via distributed neural  
911 pathways. *JCI Insight* **5**, e133429 (2020).
- 912 21. Varin, E. M. *et al.* Distinct Neural Sites of GLP-1R Expression Mediate Physiological  
913 versus Pharmacological Control of Incretin Action. *Cell Rep.* **27**, 3371–3384.e3 (2019).
- 914 22. Kanoski, S. E., Fortin, S. M., Arnold, M., Grill, H. J. & Hayes, M. R. Peripheral and central  
915 GLP-1 receptor populations mediate the anorectic effects of peripherally administered  
916 GLP-1 receptor agonists, liraglutide and exendin-4. *Endocrinology* **152**, 3103–3112  
917 (2011).
- 918 23. Punjabi, M. *et al.* Circulating Glucagon-like Peptide-1 (GLP-1) Inhibits Eating in Male Rats  
919 by Acting in the Hindbrain and Without Inducing Avoidance. *Endocrinology* **155**, 1690–  
920 1699 (2014).

- 921 24. Ast, J. *et al.* Super-resolution microscopy compatible fluorescent probes reveal  
922 endogenous glucagon-like peptide-1 receptor distribution and dynamics. *Nat. Commun.*  
923 **11**, 1–18 (2020).
- 924 25. Krieger, J. P. *et al.* Knockdown of GLP-1 receptors in vagal afferents affects normal food  
925 intake and glycemia. *Diabetes* **65**, 34–43 (2016).
- 926 26. Kim, K. S., Seeley, R. J. & Sandoval, D. A. Signalling from the periphery to the brain that  
927 regulates energy homeostasis. *Nature Reviews Neuroscience* vol. 19 185–196 (2018).
- 928 27. Williams, E. K. K. *et al.* Sensory Neurons that Detect Stretch and Nutrients in the  
929 Digestive System. *Cell* **166**, 209–221 (2016).
- 930 28. Bai, L. *et al.* Genetic Identification of Vagal Sensory Neurons That Control Feeding. *Cell*  
931 **179**, 1129-1143.e23 (2019).
- 932 29. Holt, M. K. *et al.* Synaptic Inputs to the Mouse Dorsal Vagal Complex and Its Resident  
933 Preproglucagon Neurons. *J. Neurosci.* **39**, 9767–9781 (2019).
- 934 30. Kreisler, A. D., Davis, E. A. & Rinaman, L. Differential activation of chemically identified  
935 neurons in the caudal nucleus of the solitary tract in non-entrained rats after intake of  
936 satiating vs. non-satiating meals. *Physiol. Behav.* **136**, 47–54 (2014).
- 937 31. Nguyen, K. P., O’Neal, T. J., Bolonduro, O. A., White, E. & Kravitz, A. V. Feeding  
938 Experimentation Device (FED): A flexible open-source device for measuring feeding  
939 behavior. *J. Neurosci. Methods* **267**, 108–114 (2016).
- 940 32. Kreisler, A. D. & Rinaman, L. Hindbrain glucagon-like peptide-1 neurons track intake  
941 volume and contribute to injection stress-induced hypophagia in meal-entrained rats. *Am.*  
942 *J. Physiol. - Regul. Integr. Comp. Physiol.* **310**, R906–R916 (2016).
- 943 33. Terrill, S. J. *et al.* Endogenous GLP-1 in lateral septum promotes satiety and suppresses  
944 motivation for food in mice. *Physiol. Behav.* **206**, 191–199 (2019).
- 945 34. Ishii, Y. *et al.* Differential effects of the selective orexin-1 receptor antagonist SB-334867  
946 and lithium chloride on the behavioural satiety sequence in rats. *Physiol. Behav.* **81**, 129–  
947 140 (2004).
- 948 35. Wright, F. L. & Rodgers, R. J. Behavioural profile of exendin-4/naltrexone dose  
949 combinations in male rats during tests of palatable food consumption.

- 950 *Psychopharmacology (Berl)*. **231**, 3729–3744 (2014).
- 951 36. Vrang, N., Phifer, C. B., Corkern, M. M. & Berthoud, H.-R. Gastric distension induces c-  
952 Fos in medullary GLP-1/2-containing neurons. *Am. J. Physiol. Integr. Comp. Physiol.* **285**,  
953 R470–R478 (2003).
- 954 37. Schwartz, G. J. & Moran, T. H. Sub-diaphragmatic vagal afferent integration of meal-  
955 related gastrointestinal signals. *Neurosci. Biobehav. Rev.* **20**, 47–56 (1996).
- 956 38. Al Helaili, A., Park, S. J. & Beyak, M. J. Chronic high fat diet impairs glucagon like  
957 peptide-1 sensitivity in vagal afferents. *Biochem. Biophys. Res. Commun.* **533**, 110–117  
958 (2020).
- 959 39. Kanoski, S. E., Hayes, M. R. & Skibicka, K. P. GLP-1 and weight loss: unraveling the  
960 diverse neural circuitry. *Am. J. Physiol. - Regul. Integr. Comp. Physiol.* **310**, R885–R895  
961 (2016).
- 962 40. Yamaguchi, E., Yasoshima, Y. & Shimura, T. Systemic administration of anorexic gut  
963 peptide hormones impairs hedonic-driven sucrose consumption in mice. *Physiol. Behav.*  
964 **171**, 158–164 (2017).
- 965 41. Hayes, M. R. & Schmidt, H. D. GLP-influences food and drug reward. *Current Opinion in*  
966 *Behavioral Sciences* vol. 9 66–70 (2016).
- 967 42. Anesten, F. *et al.* Preproglucagon neurons in the hindbrain have IL-6 receptor- $\alpha$  and  
968 show Ca<sup>2+</sup> influx in response to IL-6. *Am. J. Physiol. - Regul. Integr. Comp. Physiol.* **311**,  
969 R115–R123 (2016).
- 970 43. Holt, M. K., Llewellyn-Smith, I. J., Reimann, F., Gribble, F. M. & Trapp, S. Serotonergic  
971 modulation of the activity of GLP-1 producing neurons in the nucleus of the solitary tract  
972 in mouse. *Mol. Metab.* **6**, 909–921 (2017).
- 973 44. Iwasaki, Y. *et al.* Peripheral oxytocin activates vagal afferent neurons to suppress feeding  
974 in normal and leptin-resistant mice: a route for ameliorating hyperphagia and obesity. *Am.*  
975 *J. Physiol. - Regul. Integr. Comp. Physiol.* **308**, R360–R369 (2015).
- 976 45. Iwasaki, Y. *et al.* Relay of peripheral oxytocin to central oxytocin neurons via vagal  
977 afferents for regulating feeding. *Biochem. Biophys. Res. Commun.* **519**, 553–558 (2019).
- 978 46. Kawatani, M., Yamada, Y. & Kawatani, M. Glucagon-like peptide-1 (GLP-1) action in the

- 979 mouse area postrema neurons. *Peptides* **107**, 68–74 (2018).
- 980 47. Yamamoto, H. *et al.* Glucagon-like peptide-1-responsive catecholamine neurons in the  
981 area postrema link peripheral glucagon-like peptide-1 with central autonomic control  
982 sites. *J. Neurosci.* **23**, 2939–2946 (2003).
- 983 48. Hisadome, K., Reimann, F., Gribble, F. M. & Trapp, S. CCK stimulation of GLP-1 neurons  
984 involves  $\alpha$  1-adrenoceptor- mediated increase in glutamatergic synaptic inputs. *Diabetes*  
985 **60**, 2701–2709 (2011).
- 986 49. Adams, J. M. *et al.* Liraglutide modulates appetite and body weight through glucagon-like  
987 peptide 1 receptor-expressing glutamatergic neurons. *Diabetes* **67**, 1538–1548 (2018).
- 988 50. Fortin, S. M. *et al.* GABA neurons in the nucleus tractus solitarius express GLP-1  
989 receptors and mediate anorectic effects of liraglutide in rats. *Sci. Transl. Med.* **12**,  
990 eaay8071 (2020).
- 991 51. Llewellyn-Smith, I. J., Reimann, F., Gribble, F. M. & Trapp, S. Preproglucagon neurons  
992 project widely to autonomic control areas in the mouse brain. *Neuroscience* **180**, 111–  
993 121 (2011).
- 994 52. Reimann, F. *et al.* Glucose Sensing in L Cells: A Primary Cell Study. *Cell Metab.* **8**, 532–  
995 539 (2008).
- 996 53. Parker, H. E. *et al.* Predominant role of active versus facilitative glucose transport for  
997 glucagon-like peptide-1 secretion. *Diabetologia* **55**, 2445–2455 (2012).
- 998 54. Richards, P. *et al.* Identification and characterization of GLP-1 receptor-expressing cells  
999 using a new transgenic mouse model. *Diabetes* **63**, 1224–33 (2014).
- 1000 55. Han, W. *et al.* A Neural Circuit for Gut-Induced Reward. *Cell* **175**, 665–678 (2018).
- 1001 56. Rakipovski, G. *et al.* The GLP-1 Analogs Liraglutide and Semaglutide Reduce  
1002 Atherosclerosis in ApoE  $-/-$  and LDLr  $-/-$  Mice by a Mechanism That Includes  
1003 Inflammatory Pathways. *JACC Basic to Transl. Sci.* **3**, 844–857 (2018).
- 1004 57. de Lartigue, G., Ronveaux, C. C. & Raybould, H. E. Deletion of leptin signaling in vagal  
1005 afferent neurons results in hyperphagia and obesity. *Mol. Metab.* **3**, 595–607 (2014).
- 1006 58. Friard, O. & Gamba, M. BORIS: a free, versatile open-source event-logging software for  
1007 video/audio coding and live observations. *Methods Ecol. Evol.* **7**, 1325–1330 (2016).

- 1008 59. Halford, J. C., Wanninayake, S. C. & Blundell, J. E. Behavioral satiety sequence (BSS)  
1009 for the diagnosis of drug action on food intake. *Pharmacol. Biochem. Behav.* **61**, 159–68  
1010 (1998).
- 1011 60. Rodgers, R. J., Holch, P. & Tallett, A. J. Behavioural satiety sequence (BSS): separating  
1012 wheat from chaff in the behavioural pharmacology of appetite. *Pharmacol. Biochem.*  
1013 *Behav.* **97**, 3–14 (2010).
- 1014 61. Mina, A. I. *et al.* CalR: A Web-Based Analysis Tool for Indirect Calorimetry Experiments.  
1015 *Cell Metab.* **28**, 656–666.e1 (2018).
- 1016 62. de Kloet, A. D. *et al.* Reporter mouse strain provides a novel look at angiotensin type-2  
1017 receptor distribution in the central nervous system. *Brain Struct. Funct.* **221**, 891–912  
1018 (2016).
- 1019 63. Schindelin, J. *et al.* Fiji: An open-source platform for biological-image analysis. *Nature*  
1020 *Methods* vol. 9 676–682 (2012).
- 1021 64. Wu, Z., Autry, A. E., Bergan, J. F., Watabe-Uchida, M. & Dulac, C. G. Galanin neurons in  
1022 the medial preoptic area govern parental behaviour. *Nature* **509**, 325–30 (2014).
- 1023 65. Krashes, M. J. *et al.* Rapid, reversible activation of AgRP neurons drives feeding behavior  
1024 in mice. *J. Clin. Invest.* **121**, 1424–8 (2011).
- 1025 66. Watabe-Uchida, M., Zhu, L., Ogawa, S. K., Vamanrao, A. & Uchida, N. Whole-Brain  
1026 Mapping of Direct Inputs to Midbrain Dopamine Neurons. *Neuron* **74**, 858–873 (2012).
- 1027 67. Wickersham, I. R. *et al.* Monosynaptic Restriction of Transsynaptic Tracing from Single,  
1028 Genetically Targeted Neurons. *Neuron* **53**, 639–647 (2007).
- 1029
- 1030

1031 **Figure Legends:**

1032

1033 **Figure 1. PPG<sup>NTS</sup> neurons selectively encode large meal satiation**

1034 (a) Experimental model and paradigm for meal pattern analysis of post-fast refeeding in  
1035 PPG<sup>NTS</sup>-hM4Di mice using FED system. n=6 animals for analyses presented in b-f.

1036 (b) 4h dark phase food intake, 2-way within-subjects ANOVA: Drug x Time  $F_{(3,15)}=3.664$ ,  
1037  $p=0.0367$ .

1038 (c) Raster plot of chow pellet retrievals over 1h dark phase. Plots from the same mouse after  
1039 saline and CNO injections presented adjacently.

1040 (d) 1h intake by sex, 2-way mixed-model ANOVA: Drug  $F_{(1,4)}=29.09$ ,  $p=0.0057$ .

1041 (e-f) Meal pattern parameters during 1h refeed, paired 2-tailed t-test or Wilcoxon matched-pairs  
1042 test: E)  $t_{(5)}=2.757$ ,  $p=0.040$ ; F)  $W=-3$ ,  $p=0.500$ .

1043 (g) Experimental model and paradigm for temporal analysis of Ensure intake in PPG<sup>NTS</sup>-hM4Di  
1044 mice. n=7 animals for analyses presented in h-k.

1045 (h) 1h Ensure intake, paired 2-tailed t-test:  $t_{(6)}=2.859$ ,  $p=0.0288$ . Ensure intake was sex-  
1046 independent, 2-way mixed-model ANOVA: Sex x Drug  $F_{(1,5)}=2.553$ ,  $p=0.171$ .

1047 (i) Raster plot of Ensure drinking bouts over 1h dark phase. Plots from the same mouse after  
1048 saline and CNO injections presented adjacently.

1049 (j-k) Temporal parameters of Ensure drinking, paired 2-tailed t-test: J)  $t_{(6)}=6.55$ ,  $p=0.0006$ ; K)  
1050  $t_{(6)}=1.263$ ,  $p=0.254$ ; M)  $t_{(6)}=4.784$ ,  $p=0.0031$ .

1051 All data presented as mean  $\pm$  SEM.

1052

1053

1054 **Figure 2. PPG<sup>NTS</sup> neurons suppress eating without behavioural disruption**

1055 (a) Experimental model and paradigm for *ad libitum* pellet eating from FED in PPG<sup>NTS</sup>- hM3Dq  
1056 mice. n=7 animals for analyses presented in b-d.

1057 (b) Daily food intake during 48h test, 2-way within-subjects ANOVA: Drug x Day  $F_{(1,6)}=14.52$ ,  
1058  $p=0.0089$ .

1059 (c) Cumulative hourly food intake over two days, 2-way within-subjects ANOVA: Drug x Time  
1060  $F_{(48,288)}=6.481$ ,  $p<0.0001$ .

1061 (d) 24h and 48h bodyweight change, 2-way within-subjects ANOVA: Drug  $F_{(1,6)}=10.41$ ,  $p=0.018$ .

1062 (e) Experimental model and paradigm for BSS analysis in 18h fasted PPG<sup>NTS</sup>-hM3Dq mice. n=7  
1063 animals for analyses presented in f-k.

1064 (f-g) Behavioural satiety sequences following saline and CNO injections. Satiation point/satiety  
1065 onset (when duration inactive exceeds eating) shown by dotted lines.

1066 (h-k) Quantitative analysis of hM3Dq effect on BSS behaviours, 2-way with-subjects ANOVA: h)  
1067 Drug x Time  $F_{(7,42)}=5.673$ ,  $p=0.0001$ ; i) Drug  $F_{(1,6)}=5.261$ ,  $p=0.0616$ ; j) Drug  $F_{(1,6)}=12.48$ ,  
1068  $p=0.0123$ ; k) Drug  $F_{(1,6)}=4.028$ ,  $p=0.0915$ .

1069 All data presented as mean  $\pm$  SEM.

1070

1071

### 1072 **Figure 3. *Glp1r*-expressing VANs suppress eating and condition flavour avoidance**

1073 (a) Experimental model and paradigm for food intake and metabolic analysis of *ad libitum* eating  
1074 GLP-1R<sup>Nodose</sup>-hM3Dq mice. n=7 animals for analyses presented in b-e.

1075 (b) Cumulative hourly dark phase food intake, 2-way within-subjects ANOVA: Drug x Time  
1076  $F_{(12,144)}=2.078$ ,  $p=0.0218$ .

1077 (c-e) Dark phase metabolic parameters and 24h bodyweight change, paired 2-tailed t-test: c)  
1078  $t_{(6)}=1.642$ ,  $p=0.152$ ; d)  $t_{(6)}=0.543$ ,  $p=0.607$ ; e)  $t_{(6)}=2.323$ ,  $p=0.0296$ .

1079 (f) Experimental model and paradigm for optogenetically-evoked conditioned flavour preference  
1080 and intake analysis in GLP-1R<sup>Nodose</sup>-ChR2 mice. n=5 animals for analyses presented in h-i; n=5  
1081 (Ctrl) / 4 (ChR2) for analyses presented in k-l.

1082 (g) Z-projection photomicrograph of ChR2-mCherry expression in nodose ganglia  
1083 (representative of 7 independent experiments). Scale=100 $\mu$ m.

1084 (h-i) Conditioned stimulus (CS+) preference and 0.5h food intake, paired 2-tailed t-test: h)  
1085  $t_{(4)}=3.216, p=0.0324$ ; i)  $t_{(4)}=3.976, p=0.0165$ .

1086 (j) Photomicrographs of cFos immunoreactivity (cFos-ir) in coronal NTS sections from GLP-1R-  
1087 Cre x PPG-YFP mice bilaterally injected in nodose ganglia with control virus (Control) or AAV9-  
1088 DIO-ChR2-eYFP (ChR2) and exposed to blue light (photomicrographs representative of  
1089 independent experiments from 4/5 animals). Distance in mm posterior to Bregma in bottom left,  
1090 cc: central canal. Scale=100 $\mu$ m.

1091 (k) Total cFos immunoreactive cells in the NTS of control and ChR2 mice, unpaired 2-tailed t-  
1092 test:  $t_{(7)}=4.122, p=0.0044$ .

1093 (l) PPG<sup>NTS</sup> neurons co-localised with cFos immunoreactivity in the NTS. Mann-Whitney 2-tailed  
1094 U-test:  $U=6, p=0.4127$ .

1095 All data presented as mean  $\pm$  SEM.

1096

1097

1098 **Figure 4. *Oxtr* rather than *Glp1r* VANs are the major vagal input to PPG<sup>NTS</sup> neurons**

1099 (a) Experimental model for viral-mediated mapping of left and right *Glp1r* vagal afferent  
1100 projections to the NTS, and photomicrographs of tdTomato expression in virus-injected nodose  
1101 ganglia (NG) and non-injected contralateral NG (photomicrographs in a-c representative of  
1102 independent experiments from 3 animals per injection side). Scale=100 $\mu$ m.

1103 (b-c) Photomicrographs of tdTomato-expressing terminal fields of L and R branch *Glp1r* vagal  
1104 afferents along the rostro-caudal extent of the NTS (mm posterior to Bregma in bottom left) in  
1105 PPG-YFP mice, cc: central canal. Scale=100 $\mu$ m.

1106 (d) Experimental model for rabies virus (RABV)-mediated monosynaptic retrograde tracing of  
1107 vagal inputs to PPG<sup>NTS</sup> neurons combined with RNAscope fluorescence *in situ* hybridization for  
1108 GLP-1R (*Glp1r*) and oxytocin receptor (*Oxtr*) transcripts (photomicrographs in e-i representative  
1109 of independent experiments from 8 animals).

1110 (e) Photomicrograph of nodose ganglion showing rabies virus GFP expression (RABV) and  
1111 *Glp1r* FISH. RABV+*Glp1r* co-localization shown by white arrows, RABV+*Glp1r*+*Oxtr* by white-  
1112 edged green arrow. Scale=100 $\mu$ m.

1113 (f) RABV and *Glp1r* co-localization as proportions of all RABV+ cells and all *Glp1r*+ cells, from  
1114 903 RABV+, 1188 *Glp1r*+ and 1460 *Oxtr*+ cells from L and R NG.

1115 (g) Photomicrograph of nodose ganglion showing RABV expression and *Oxtr* FISH.  
1116 Scale=100 $\mu$ m.

1117 (h) RABV and *Oxtr* co-localization as proportions of all RABV+ cells and all *Oxtr*+ cells.  
1118 RABV+*Oxtr* co-localization shown by green arrows, RABV+*Glp1r*+*Oxtr* by white-edged green  
1119 arrow.

1120 (i) High magnification Z-projection of RABV, *Glp1r* and *Oxtr* cells in NG. Scale=20 $\mu$ m.

1121 All data presented as mean  $\pm$  SEM.

1122

1123

1124 **Figure 5. PPG<sup>NTS</sup> neurons are necessary for oxytocin-induced eating suppression**

1125 (a) Experimental model for imaging of oxytocin-induced neuronal calcium dynamics in *ex vivo*  
1126 brainstem slices from mice expressing GCaMP3 in PPG neurons. n=75 cells from 3 animals  
1127 examined over 8 independent experiments for analyses in b-e.

1128 (b) Representative  $\Delta F/F_0$  traces from individual neurons and mean response (purple line) during  
1129 bath application of oxytocin and glutamate.

1130 (c) Representative images of PPG<sup>NTS</sup>:GCaMP3 neurons pseudocolored for fluorescence  
1131 intensity under baseline conditions (aCSF) and responding to oxytocin (purple arrows) and  
1132 glutamate (grey arrows).

1133 (d) Oxytocin-responsive PPG<sup>NTS</sup>:GCaMP3 neurons as a proportion of all glutamate-responsive  
1134 PPG<sup>NTS</sup> neurons (i.e. healthy neurons with functional GCaMP3 expression).

1135 (e) Median AUC during exposure to oxytocin in oxytocin unresponsive and responsive  
1136 PPG<sup>NTS</sup>:GCaMP3 neurons, Mann-Whitney 2-tailed U-test: U=48,  $p < 0.0001$ .

1137 (f) Experimental model and paradigm for oxytocin-induced eating suppression in PPG<sup>NTS</sup>-DTA  
1138 ablated mice or eGFP-transduced controls. n=5 (DTA) / 7 (eGFP) animals for analyses  
1139 presented in g-i.

1140 (g-h) Cumulative 4h dark phase food intake in eGFP and DTA mice administered oxytocin (0.4  
1141 mg/kg, i.p.), 2-way within-subjects ANOVA: g) Drug x Time  $F_{(2,12)}=6.133$ ,  $p=0.0146$ ; h) Drug  
1142  $F_{(1,4)}=0.0117$ ,  $p=0.919$ .

1143 (i) 4h food intake by virus, 2-way mixed-model ANOVA: Drug x Virus  $F_{(1,10)}=8.472$ ,  $p=0.0155$ .

1144 All data presented as mean  $\pm$  SEM except box plot in e, in which the box is centred on the  
1145 median and bound at 25 and 75%, with whiskers at 5 and 95% and blue cross at the mean.

1146

1147

1148 **Figure 6. PPG<sup>NTS</sup> neurons are not a major target of area postrema *Glp1r* neurons**

1149 (a) Experimental model for rabies virus-mediated monosynaptic retrograde tracing of area  
1150 postrema inputs to PPG<sup>NTS</sup> neurons combined with FISH for *Glp1r* (photomicrographs in b-d  
1151 representative of independent experiments from 4 animals).

1152 (b) Photomicrographs of coronal NTS section showing RABV expression and *Glp1r* FISH.  
1153 RABV+*Glp1r* co-localization shown by white arrows. Scale=100 $\mu$ m (inset 20 $\mu$ m).

1154 (c) RABV and *Glp1r* co-localization as proportions of all RABV+ cells and all *Glp1r*+ cells, from  
1155 53 RABV+ and 549 *Glp1r*+ cells.

1156 (d) Photomicrographs of coronal NTS section showing RABV expression and TH-ir. Examples  
1157 of RABV+TH-ir co-localization shown by green arrows. Scale=100 $\mu$ m (inset 20 $\mu$ m).

1158 (e) Quantification of RABV and TH-ir co-localization as proportions of all RABV+ cells and all  
1159 TH-ir cells, from a total of 53 RABV+ and 341 TH-ir cells.

1160 All data presented as mean  $\pm$  SEM.

1161

1162

1163 **Figure 7. Liraglutide and semaglutide suppress eating independently of PPG<sup>NTS</sup> neurons**

1164 (a) Experimental model and paradigm for GLP-1RA-induced eating suppression in PPG<sup>NTS</sup>-DTA  
1165 ablated mice or eGFP-transduced controls. n=8 (DTA) / 7 (eGFP) animals for analyses  
1166 presented in b-g.

1167 (b-d) Cumulative food intake and bodyweight change over 1 day in eGFP and DTA mice  
1168 administered liraglutide (200 µg/kg, s.c.), 2-way within-subjects or mixed-model ANOVA: b)  
1169 Drug x Time  $F_{(5,30)}=35.35$ ,  $p<0.0001$ ; c) Drug x Time  $F_{(5,35)}=74.95$ ,  $p<0.000$ ; d) Drug  
1170  $F_{(1,13)}=33.17$ ,  $p=0<0.0001$ , Virus  $F_{(1,13)}=1.198$ ,  $p=0.294$ .

1171 (e-g) Cumulative food intake and bodyweight change over 1 day in eGFP and DTA mice  
1172 administered semaglutide (60 µg/kg, s.c.), 2-way within-subjects or mixed-model ANOVA: e)  
1173 Drug x Time  $F_{(5,30)}=51.83$ ,  $p<0.0001$ ; f) Drug x Time  $F_{(5,35)}=54.28$ ,  $p<0.0001$ ; g) Drug  
1174  $F_{(1,13)}=122.6$ ,  $p=0<0.0001$ , Virus  $F_{(1,13)}=0.224$ ,  $p=0.644$ .

1175 (h) Photomicrographs of cFos immunoreactivity (cFos-ir) in coronal NTS sections (mm posterior  
1176 to Bregma in bottom left) from PPG-YFP mice perfused 4h after vehicle (VEH) or semaglutide  
1177 (SEMA; 60 µg/kg, s.c.) administration (photomicrographs representative of independent  
1178 experiments from 3/4 animals). n=3 (VEH) / 4 (SEMA) animals for analyses presented in i-k, cc:  
1179 central canal. Scale=100µm.

1180 (i-j) Total cFos in NTS and AP of mice administered vehicle or semaglutide, unpaired 1-tailed t-  
1181 tests: i)  $t_{(5)}=4.59$ ,  $p=0.0029$ ; j)  $t_{(5)}=2.66$ ,  $p=0.0225$ .

1182 (k) PPG<sup>NTS</sup> neurons co-localised with cFos immunoreactivity in NTS. Mann-Whitney 2-tailed U-  
1183 test: U=0,  $p=0.0571$ .

1184 All data presented as mean ± SEM.

1185

1186

1187 **Figure 8. PPG<sup>NTS</sup> neuron activation augments semaglutide-induced eating suppression**

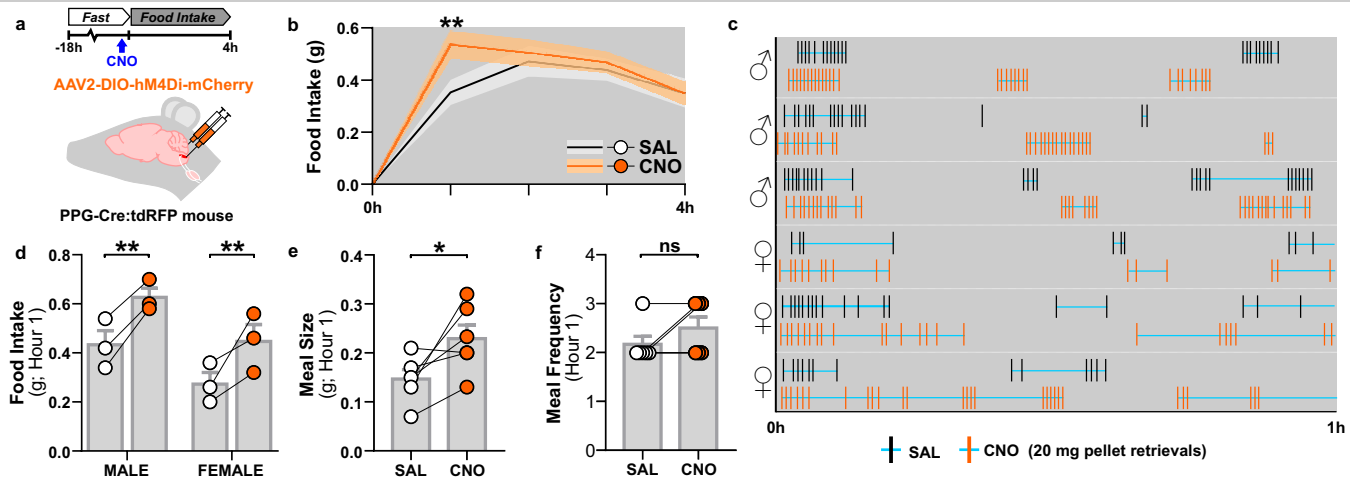
1188 (a) Experimental model and paradigm for semaglutide-induced eating suppression in PPG<sup>NTS</sup>-  
1189 hM3Dq mice and administered semaglutide (60 µg/kg, s.c.) and CNO (2 mg/kg, i.p.). n=6  
1190 animals for analyses presented in b-f.

1191 (b-f) Cumulative food intake at 1, 2, 4, 6 and 24 hours, 1-way within-subjects ANOVA: b) Drug  
1192  $F_{(1,6,8,0)}=11.94$ ,  $p=0.0050$ ; c) Drug  $F_{(1,5,7,7)}=22.12$ ,  $p=0.0009$ ; d) Drug  $F_{(1,3,6,3)}=35.35$ ,  $p=0.0006$ ; e)  
1193 Drug  $F_{(1,2,6,0)}=40.72$ ,  $p=0.0005$ ; f) Drug  $F_{(1,6,8,2)}=125.8$ ,  $p<0.0001$ .

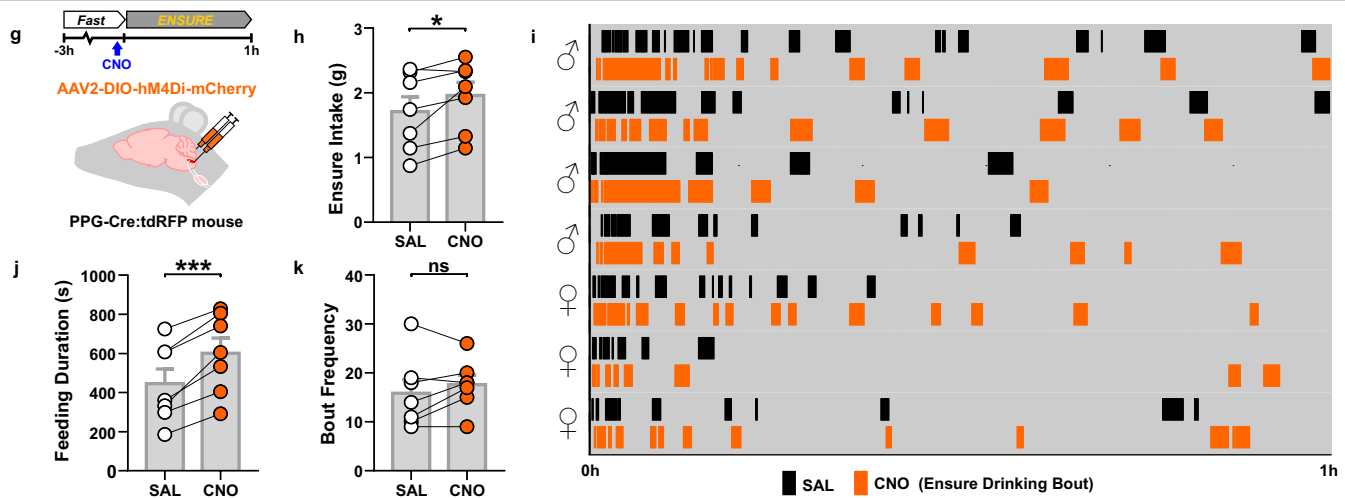
1194 (g) Graphical representation of the core findings of this study and proposed model of central and  
1195 peripheral GLP-1 system gut-brain satiation circuit architecture in the brainstem.

1196 All data presented as mean ± SEM.

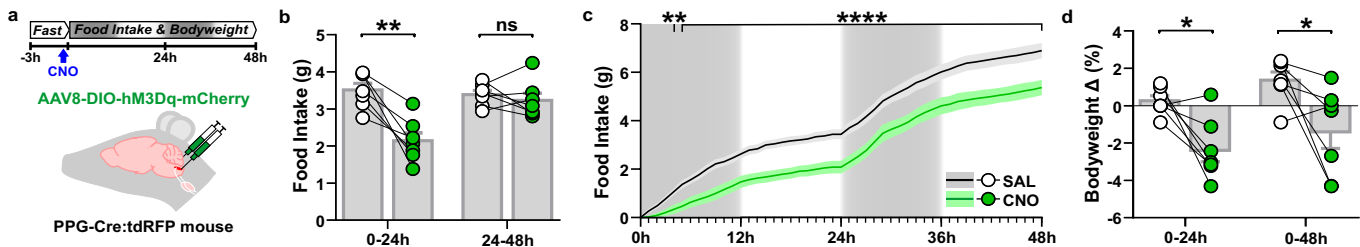
### Refeeding in fasted $PPG^{NTS}$ -hM4Di mice



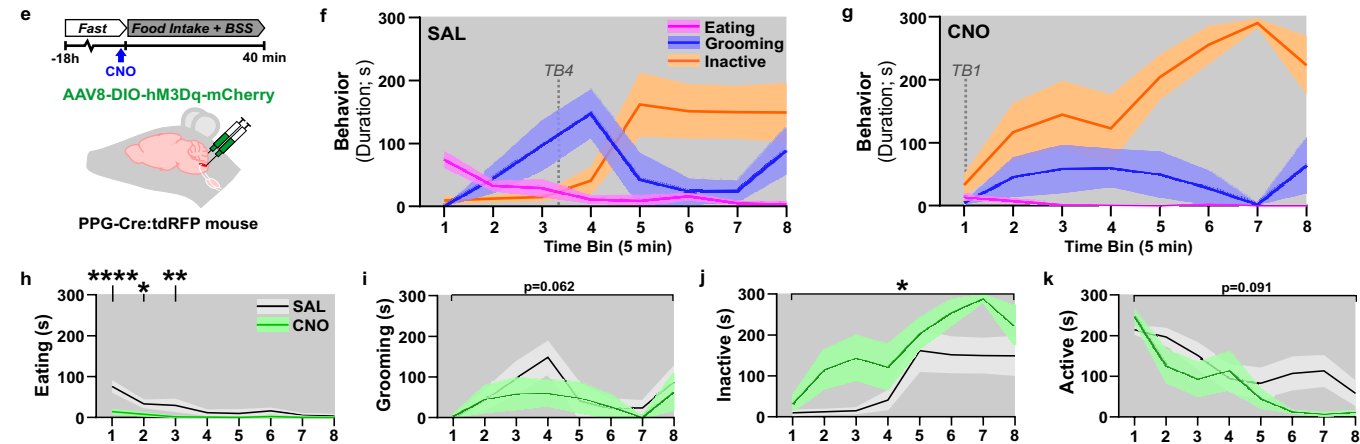
### Ensure liquid diet intake in ad libitum eating $PPG^{NTS}$ -hM4Di mice



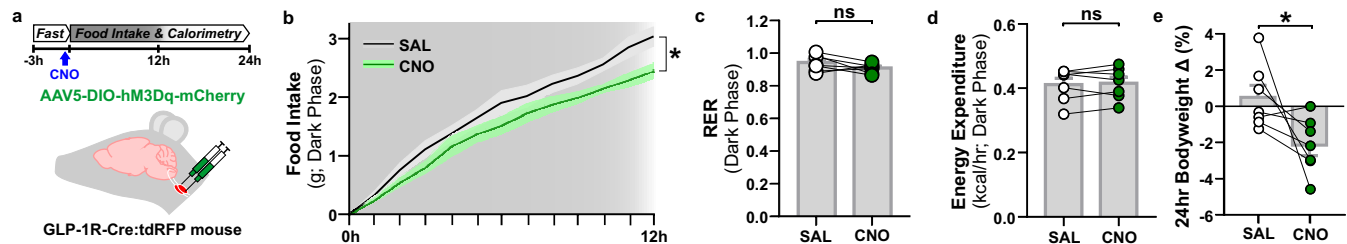
### Ad libitum eating in PPG<sup>NTS</sup>-hM3Dq mice



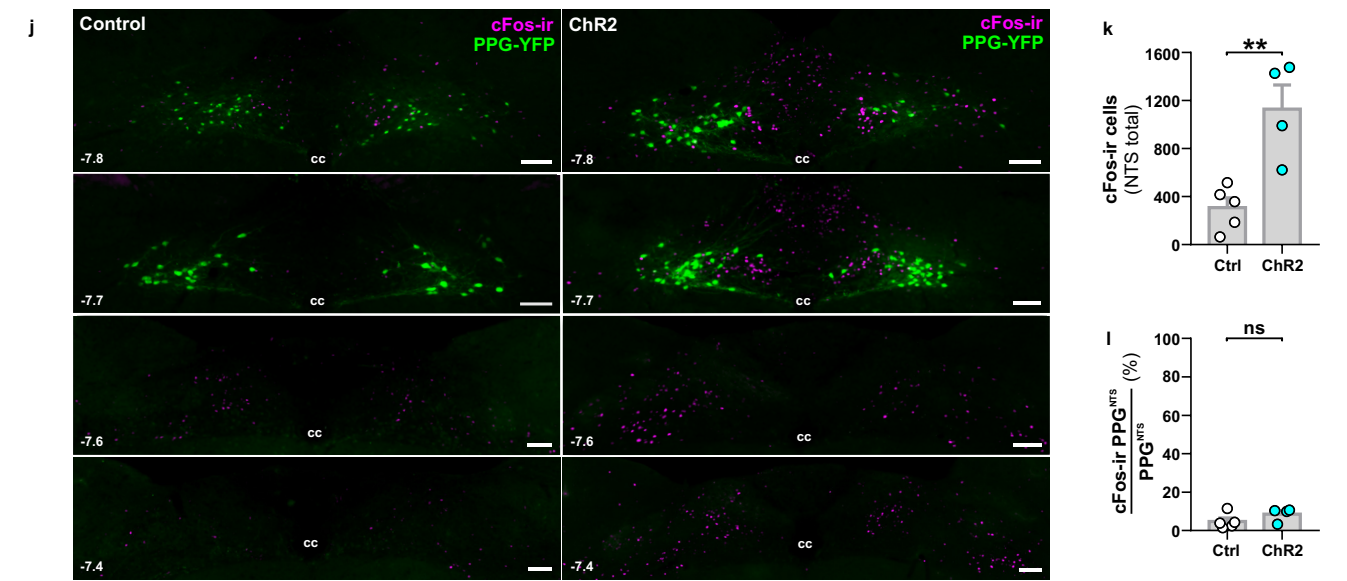
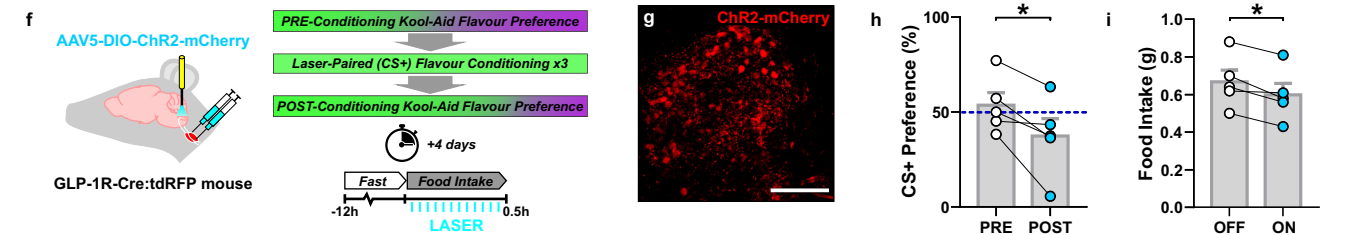
### Behavioural satiety sequence in fasted PPG<sup>NTS</sup>-hM3Dq mice



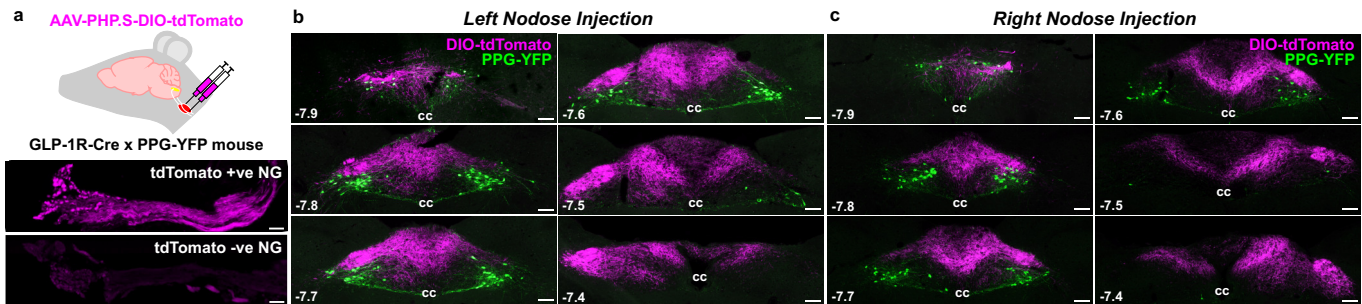
### Ad libitum eating in $GLP-1R^{Nodose}$ -hM3Dq mice



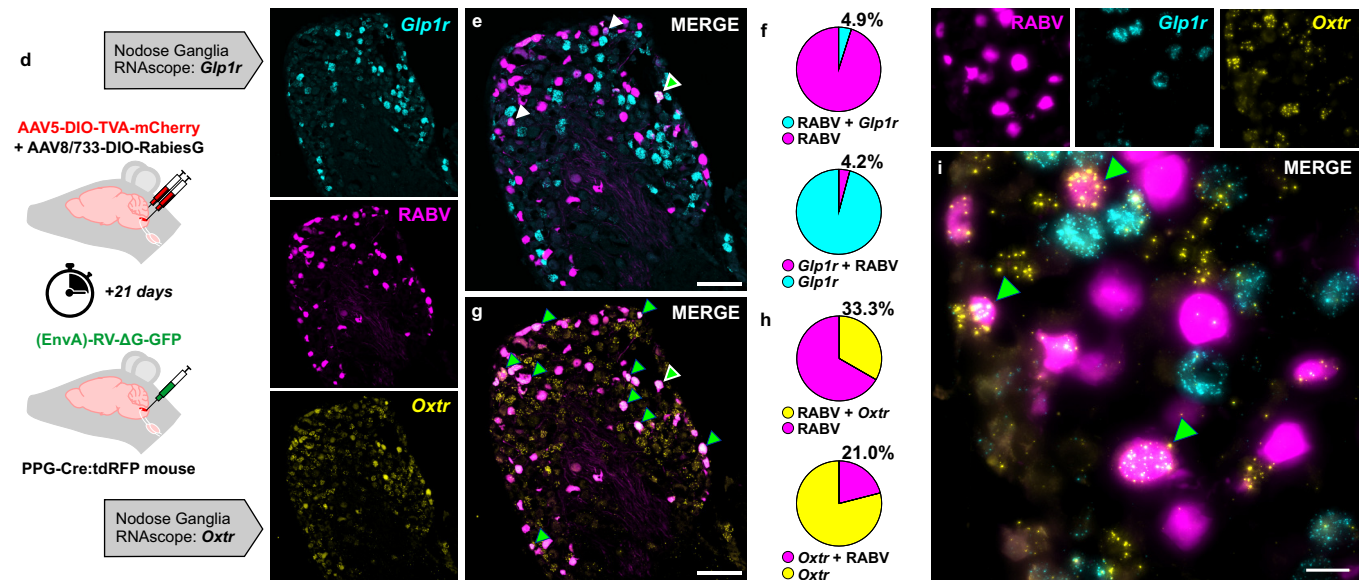
### Conditioned flavour preference and ad libitum eating in $GLP-1R^{Nodose}$ -ChR2 mice



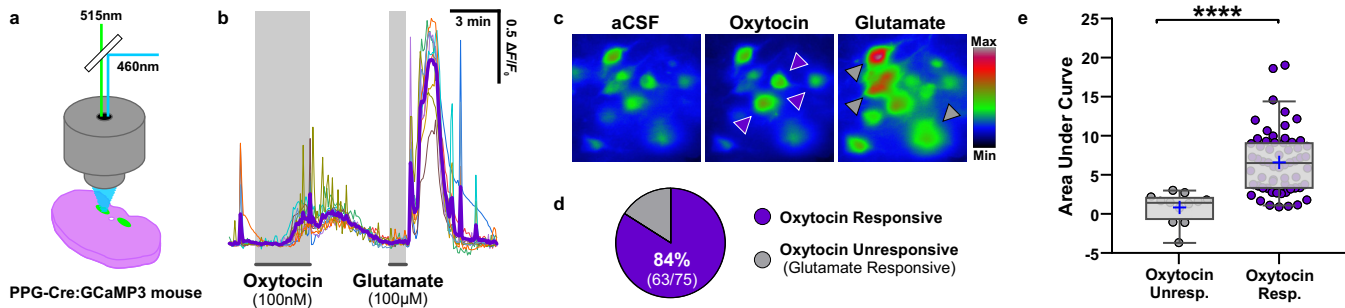
Neuroanatomical circuit mapping of *Glp1r* vagal projections to the NTS



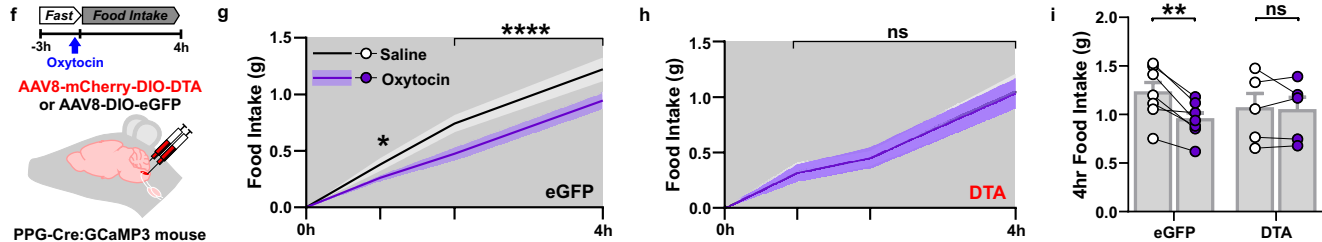
Monosynaptic retrograde rabies virus tracing of vagal inputs to PPG<sup>NTS</sup> neurons



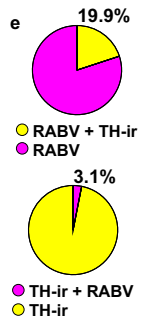
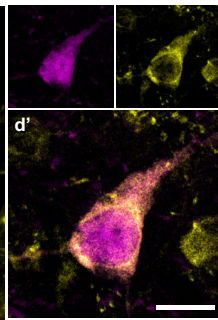
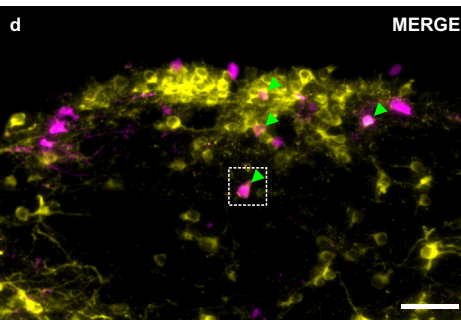
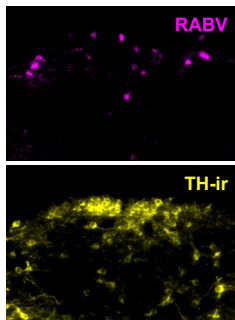
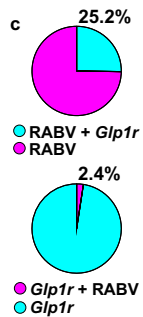
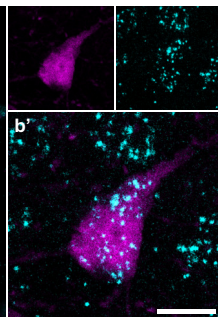
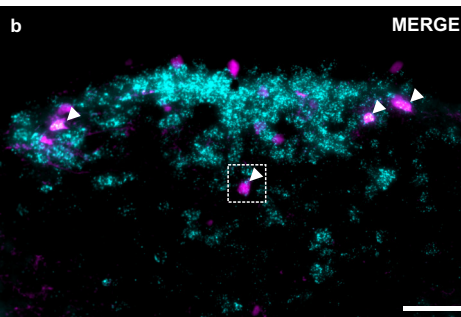
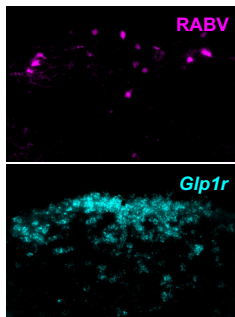
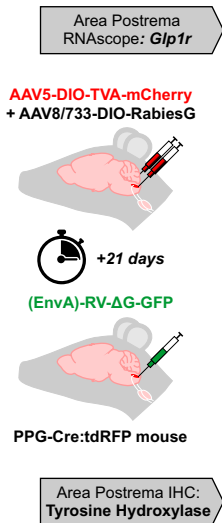
## Ex vivo $Ca^{2+}$ imaging of oxytocin-induced PPG<sup>NTS</sup> neuronal activation



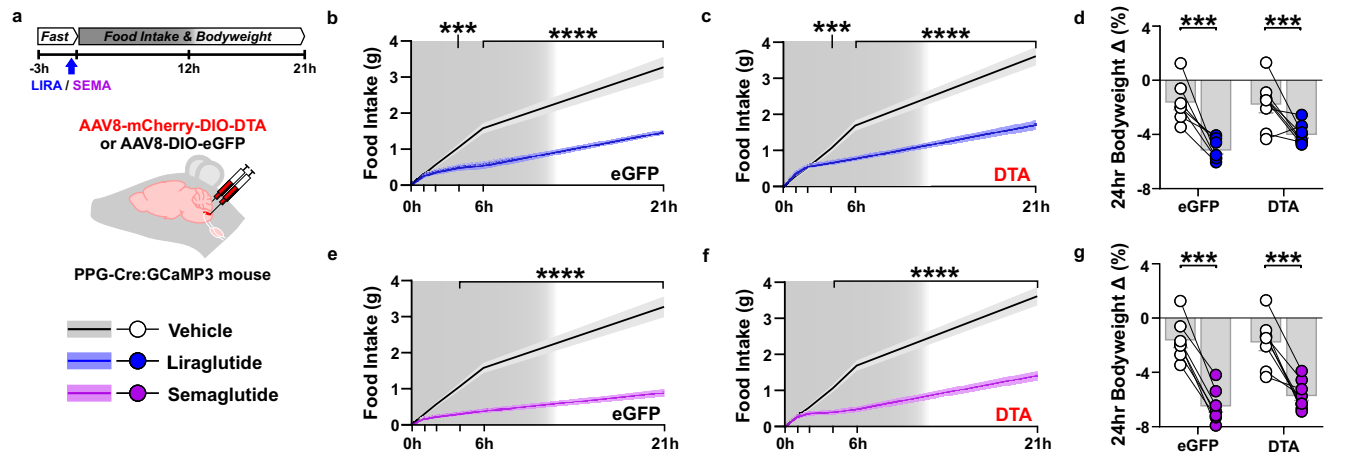
## Oxytocin-induced eating suppression in ad libitum eating PPG<sup>NTS</sup>-DTA mice



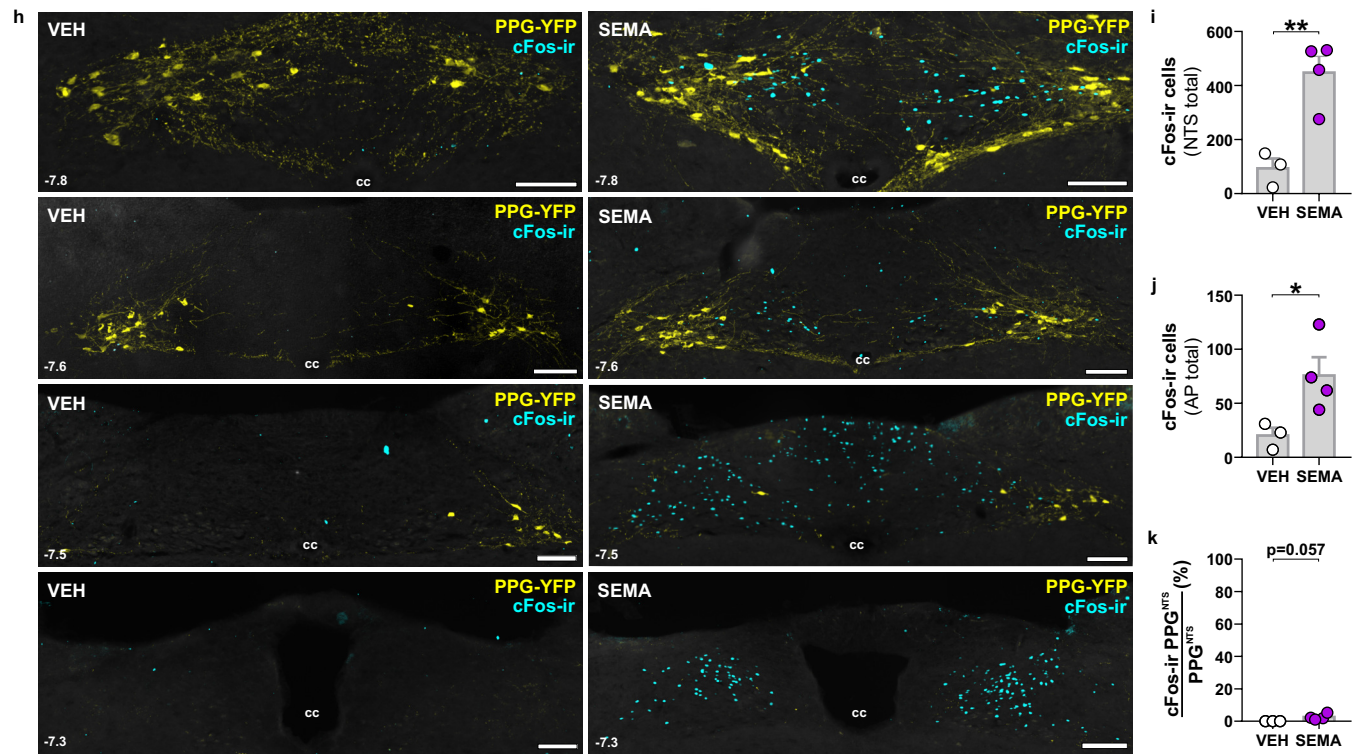
a



GLP-1RA-induced eating suppression in *ad libitum* eating PPG<sup>NTS</sup>-DTA mice

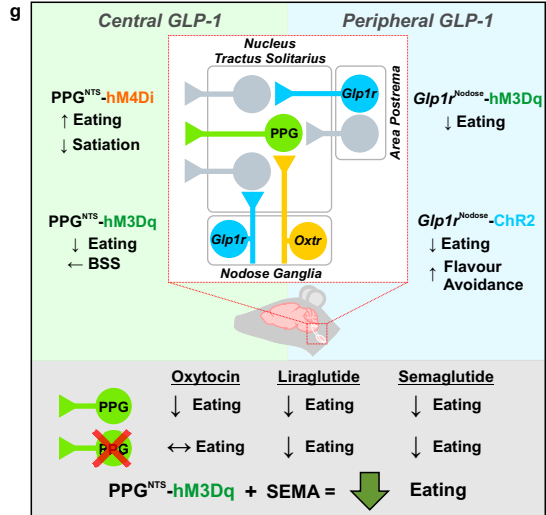
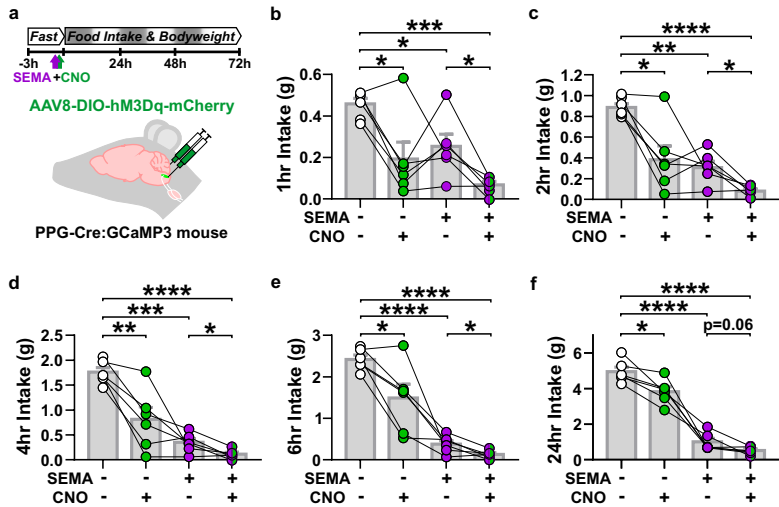


Semaglutide-induced neuronal activation in the dorsal vagal complex

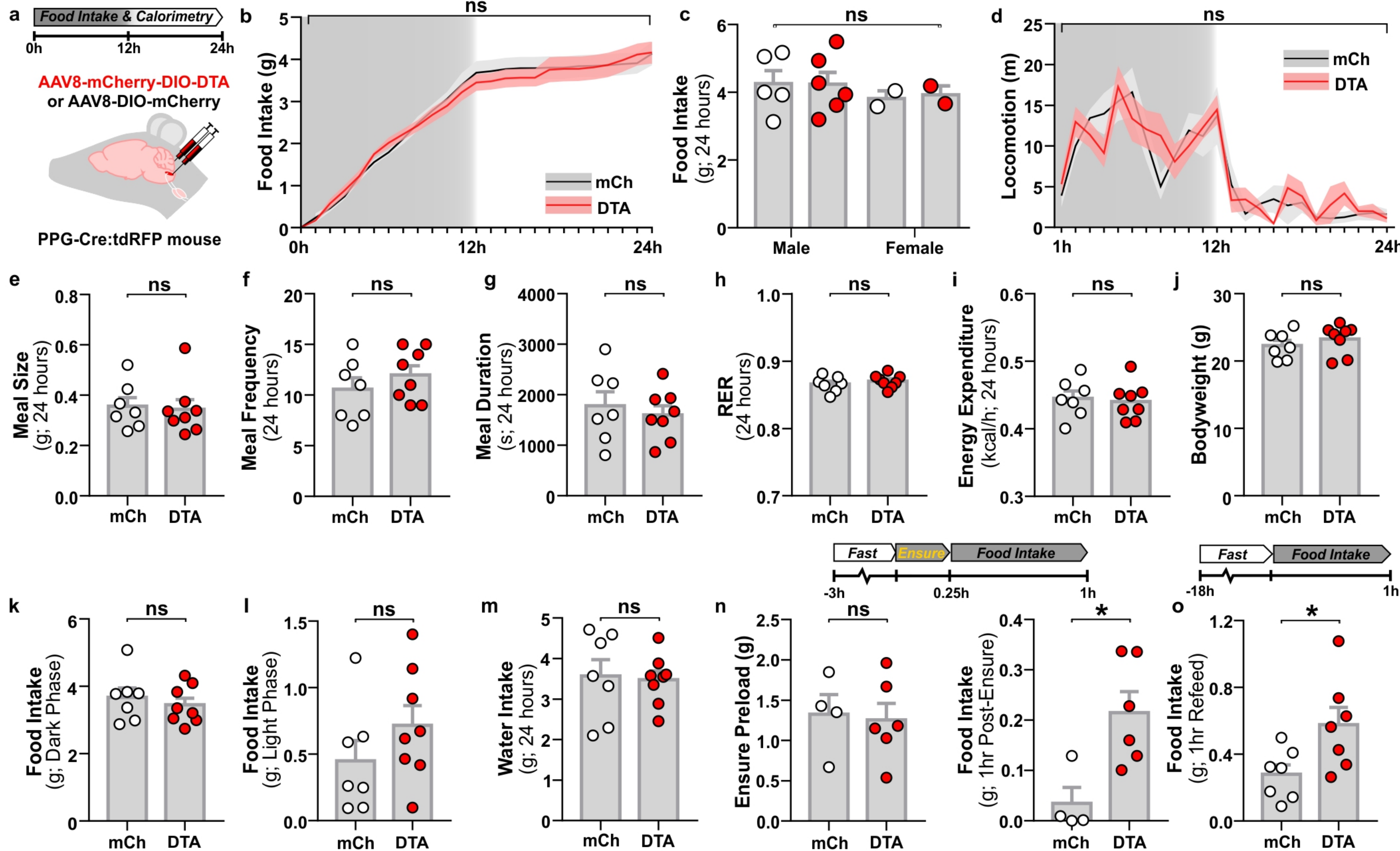


# Semaglutide-induced eating suppression in $PPG^{NTS}$ -hM3Dq mice

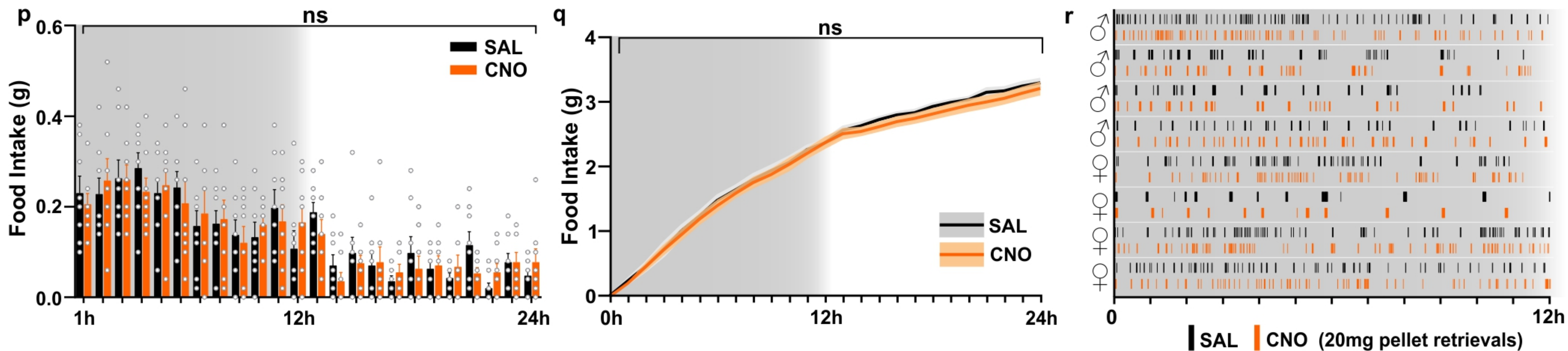
# Results summary and model schematic



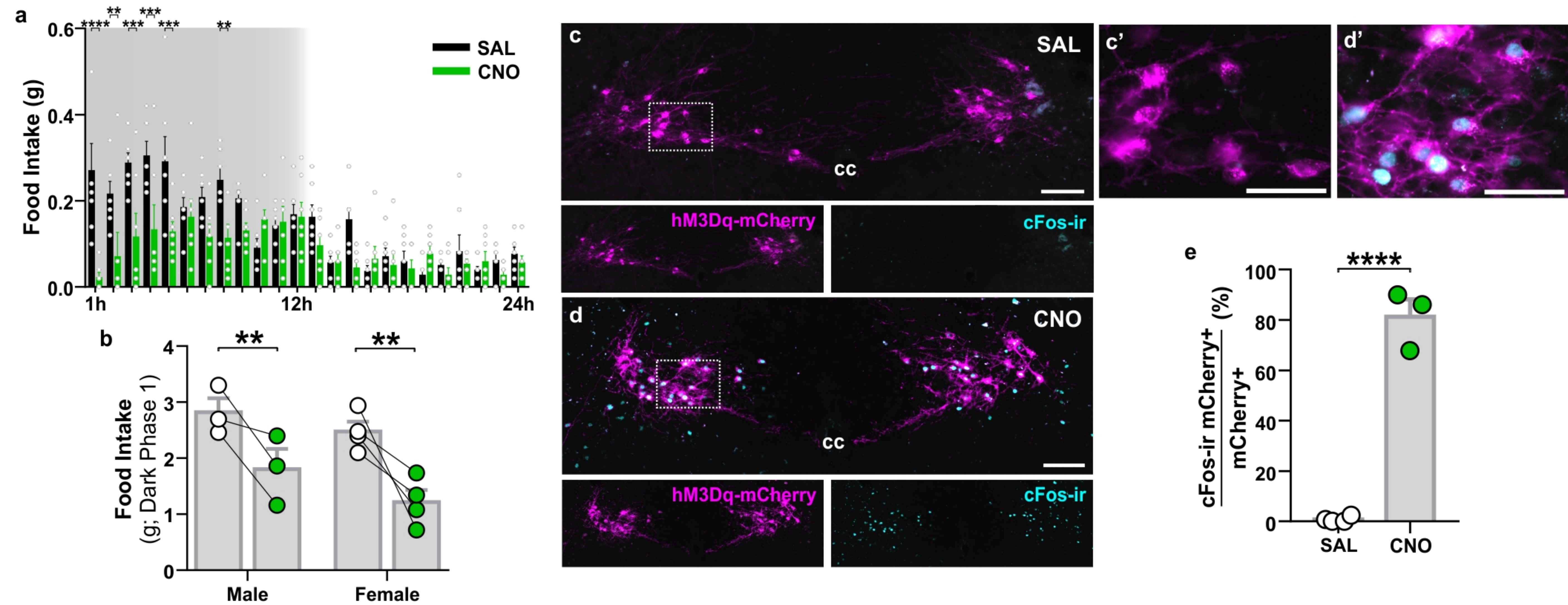
Metabolic phenotyping of ad libitum eating  $PPG^{NTS}$ -DTA mice



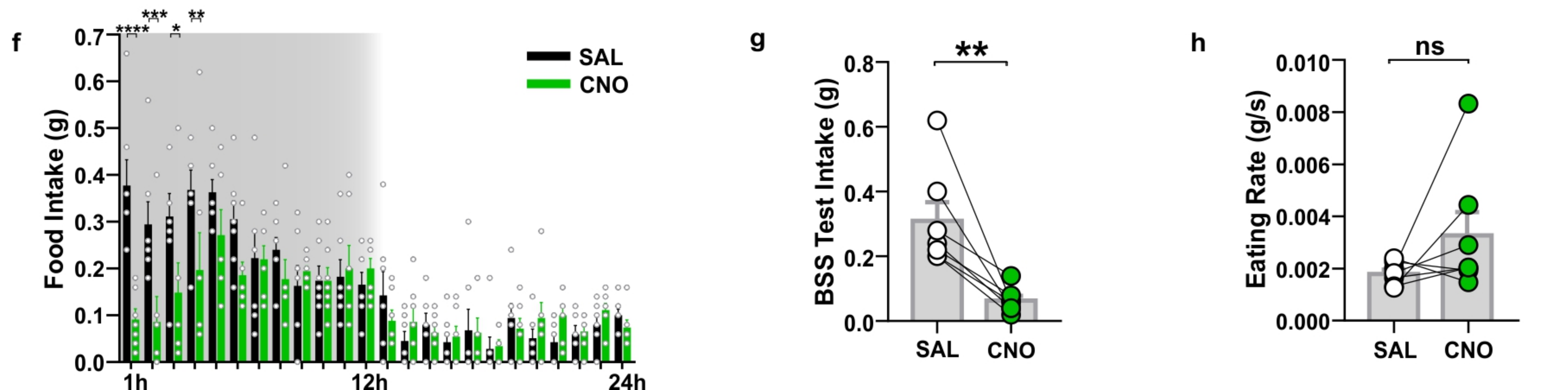
Ad libitum eating in  $PPG^{NTS}$ -hM4Di mice



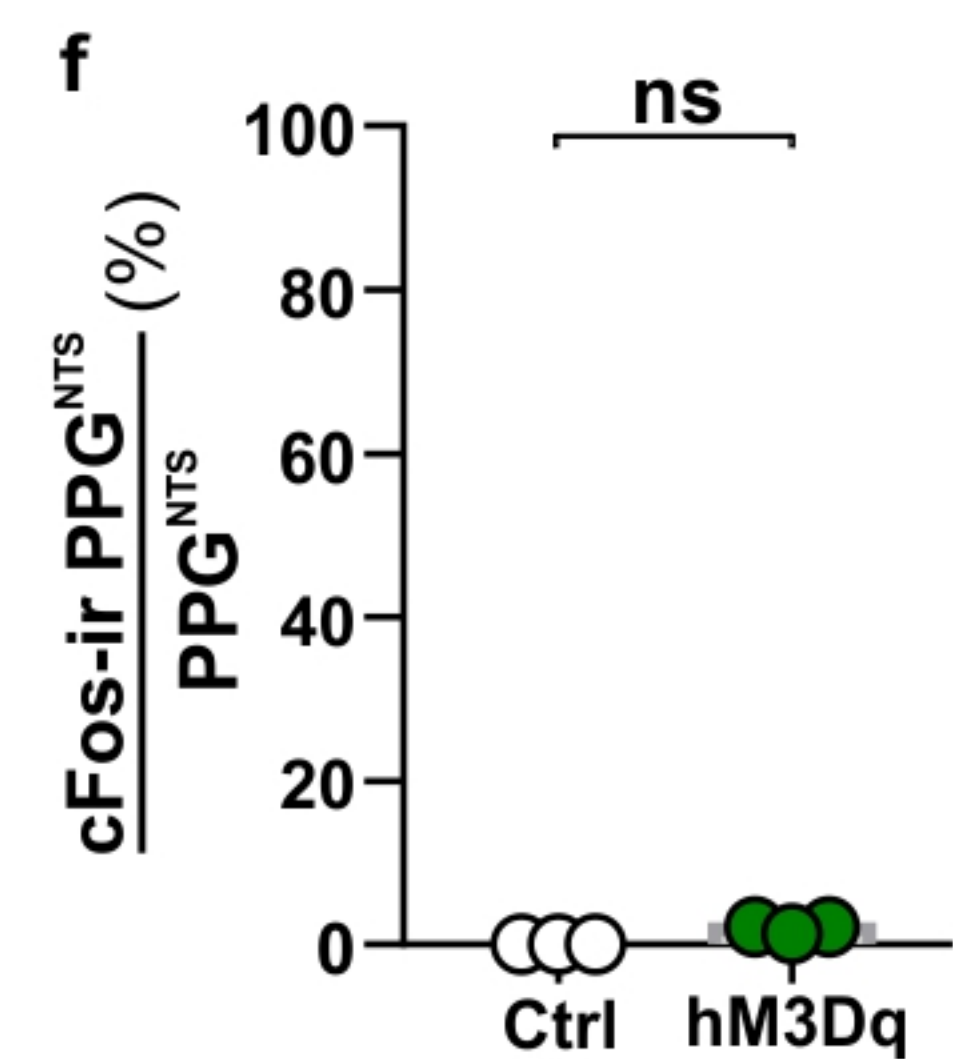
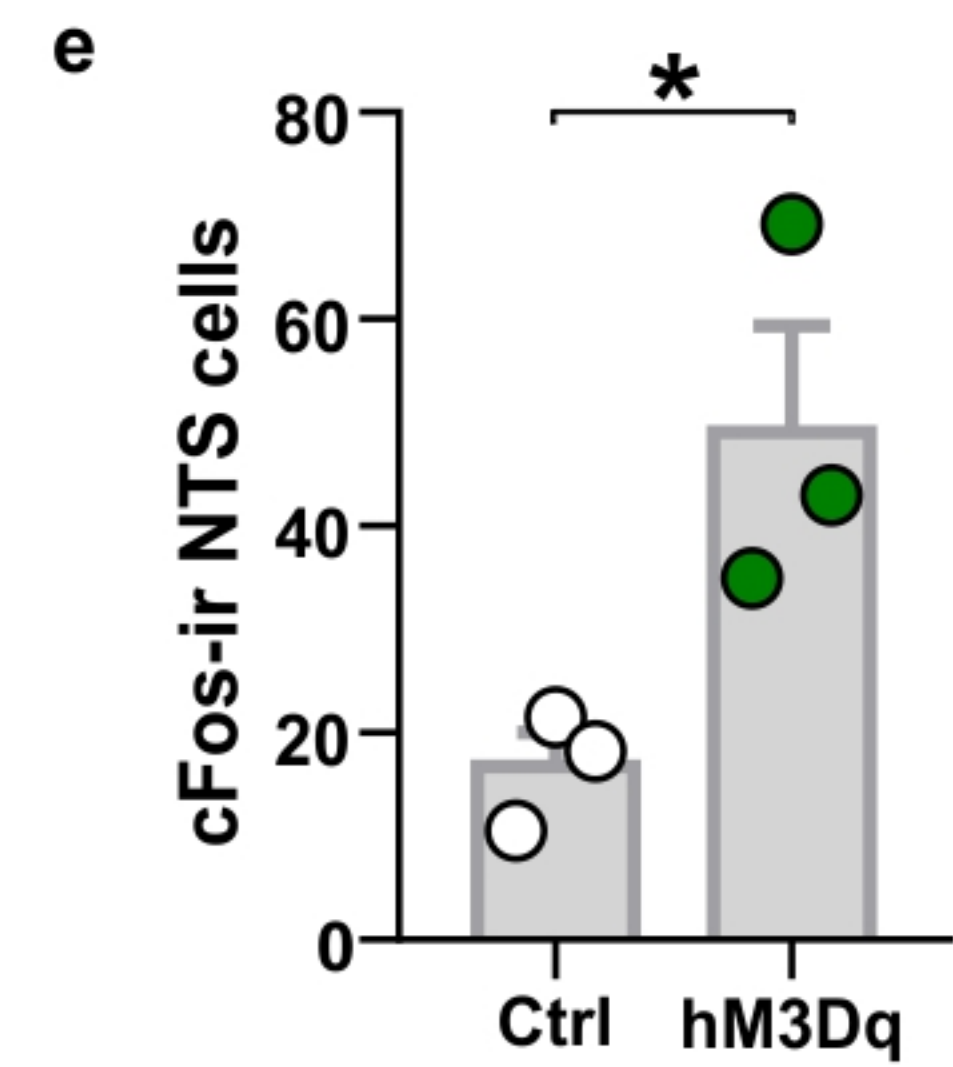
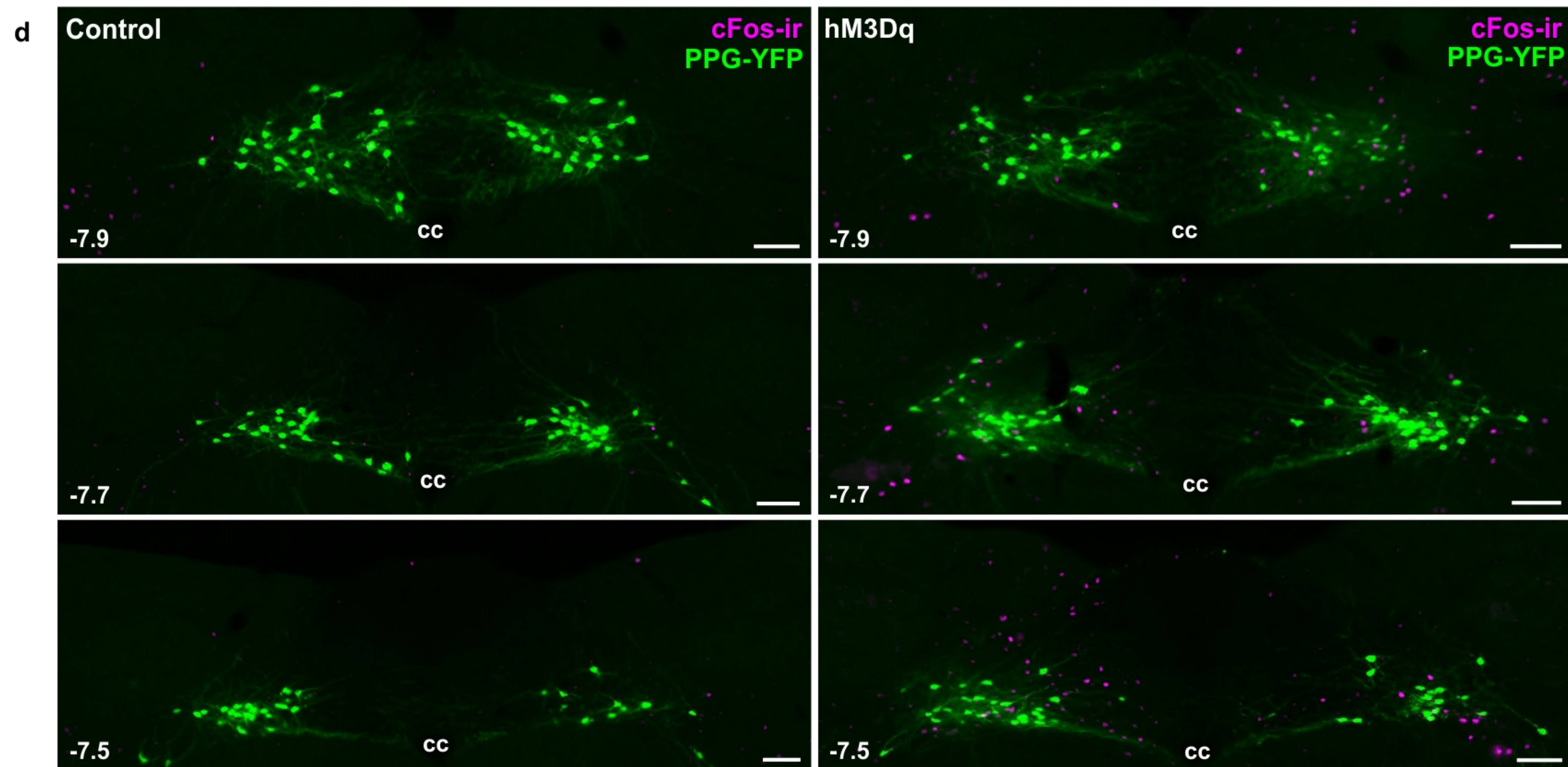
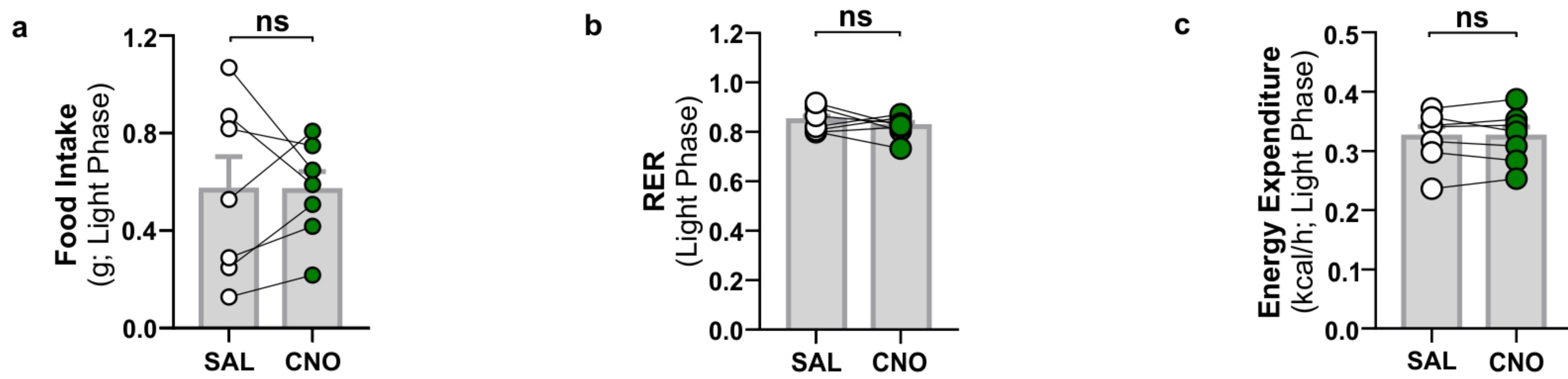
Ad libitum eating in  $PPG^{NTS}$ -hM3Dq mice



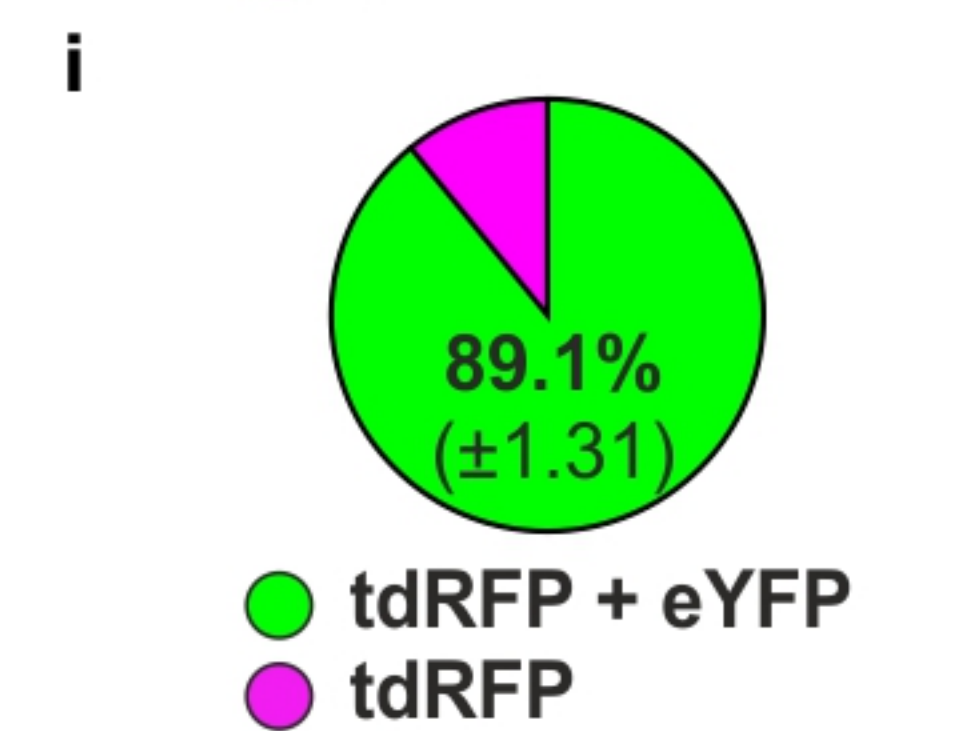
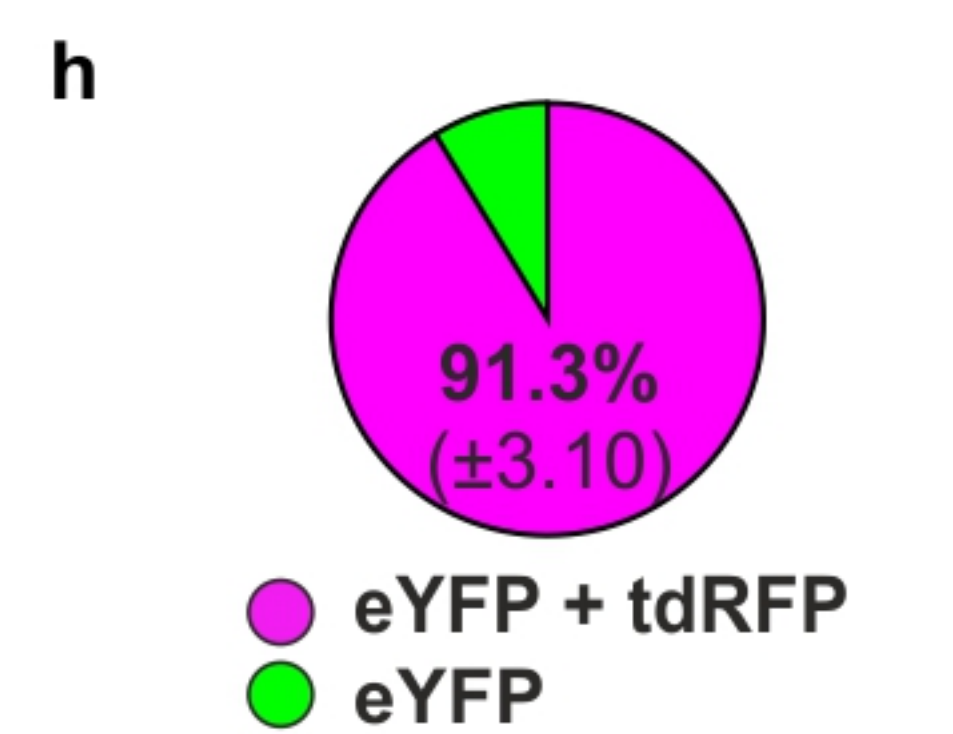
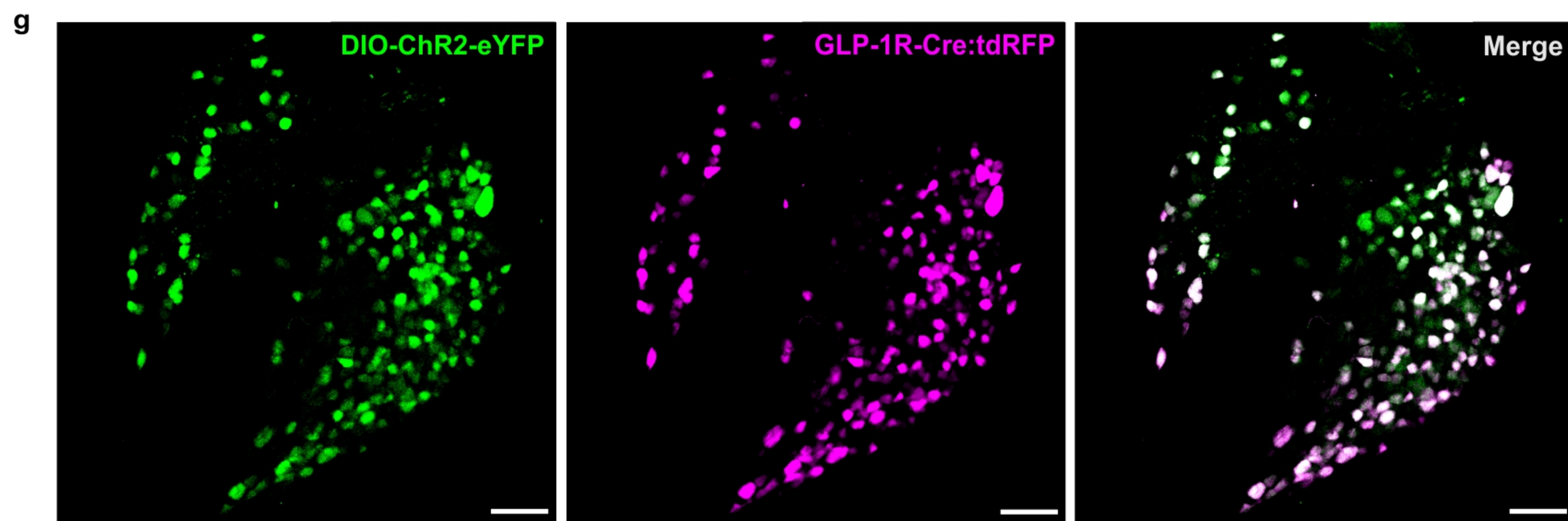
Behavioural satiety sequence in fasted  $PPG^{NTS}$ -hM3Dq mice



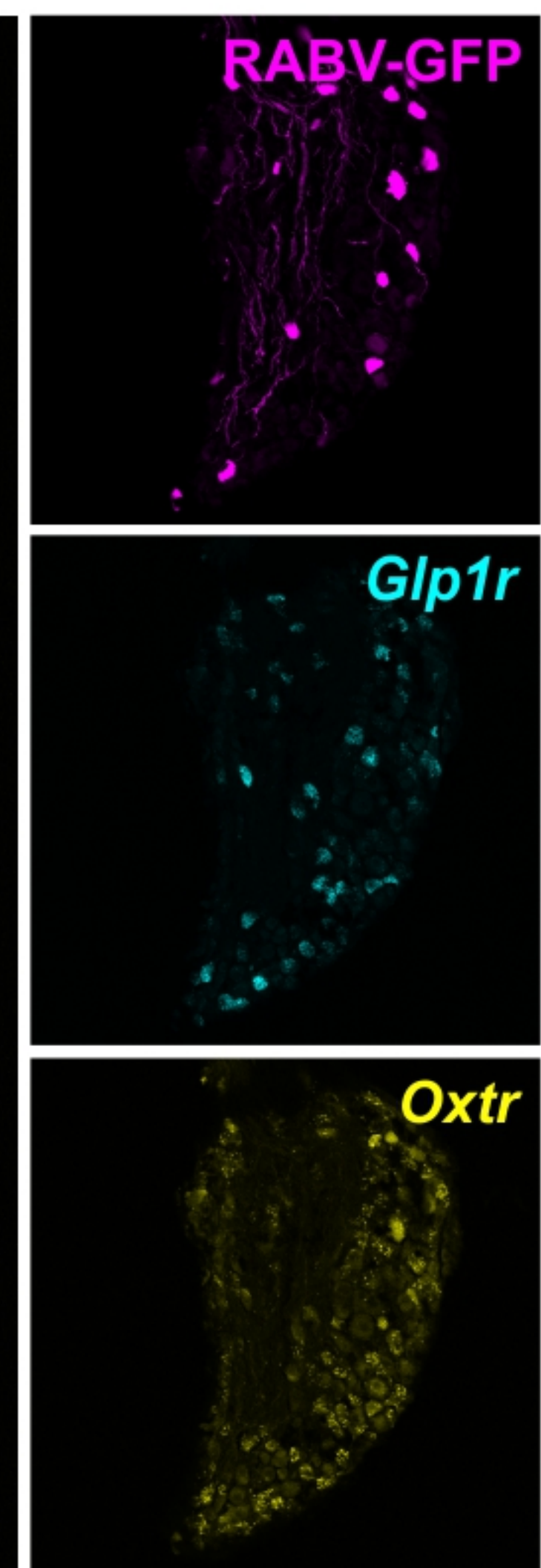
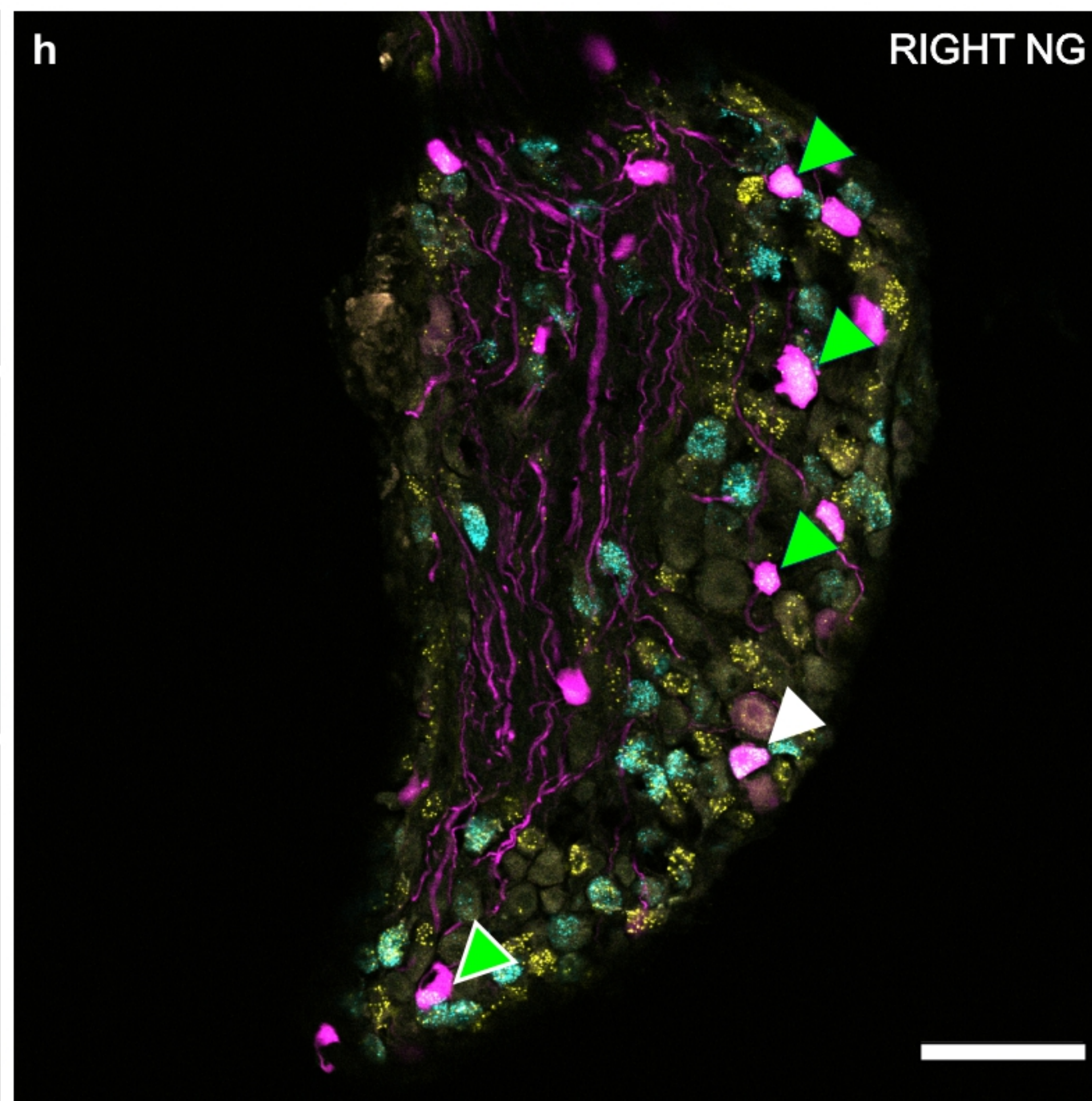
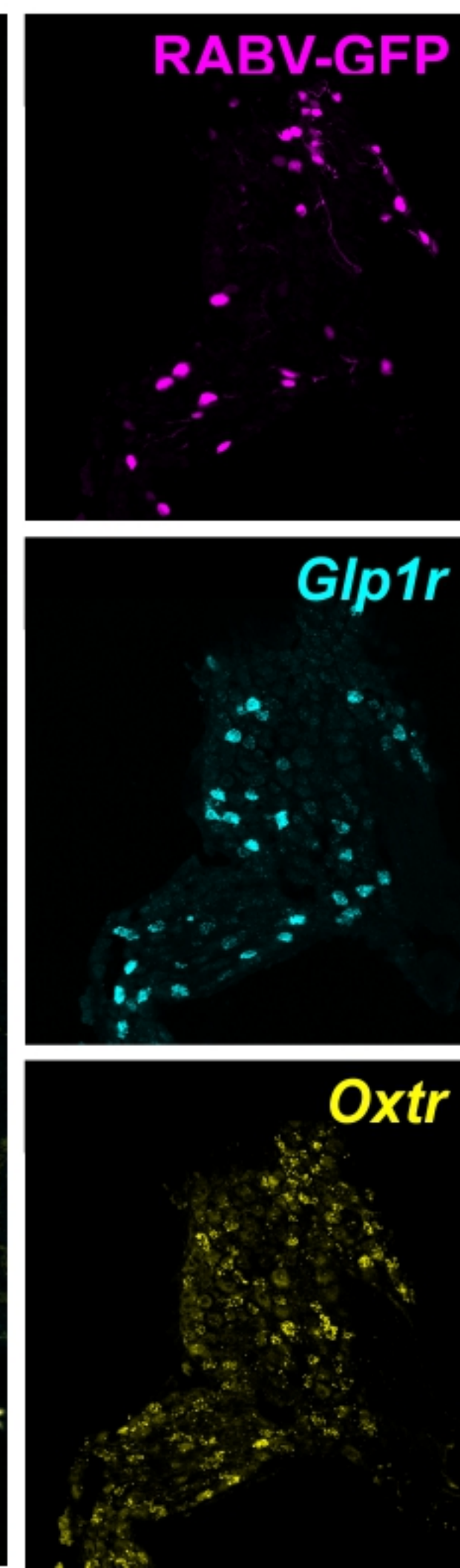
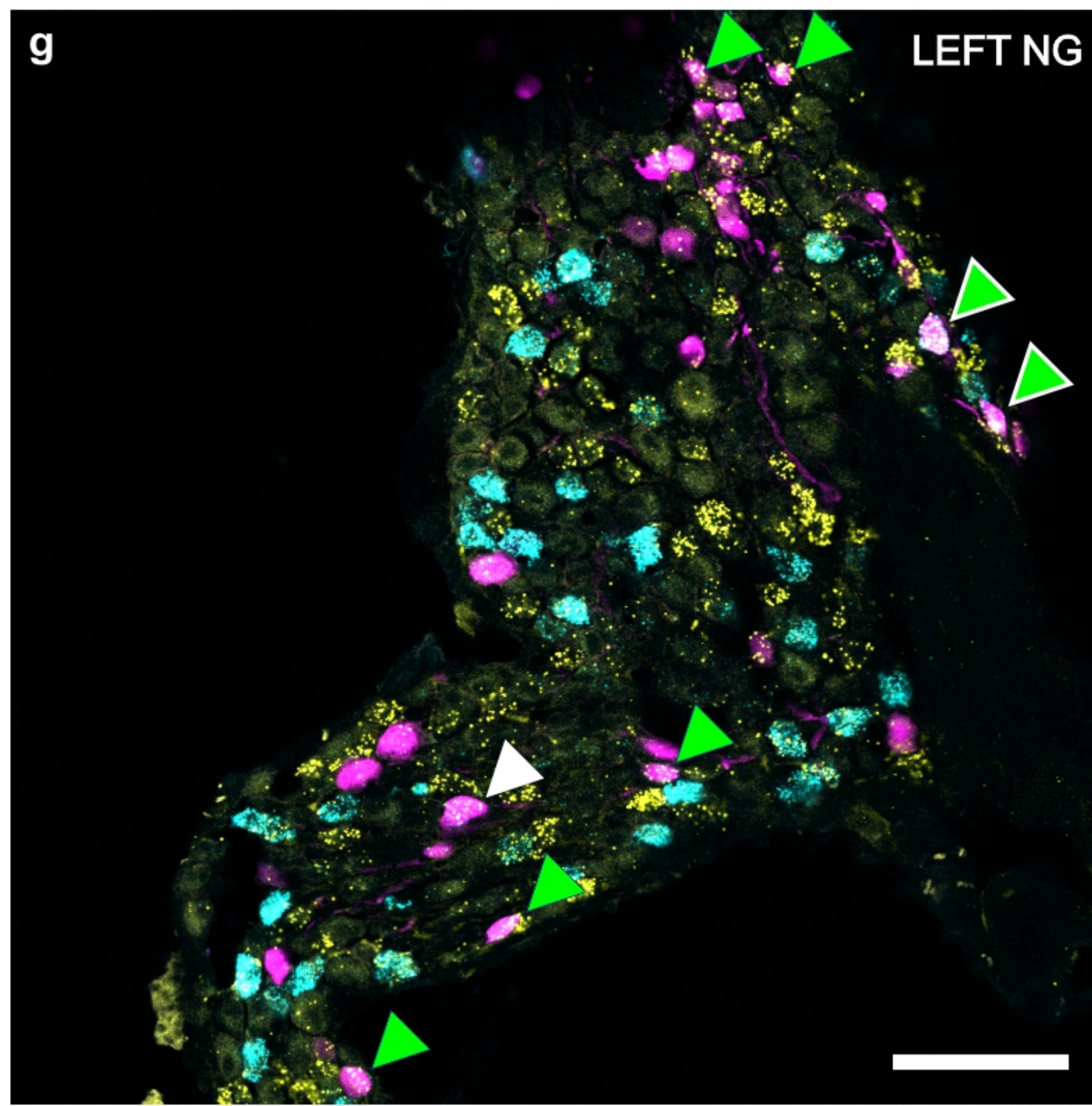
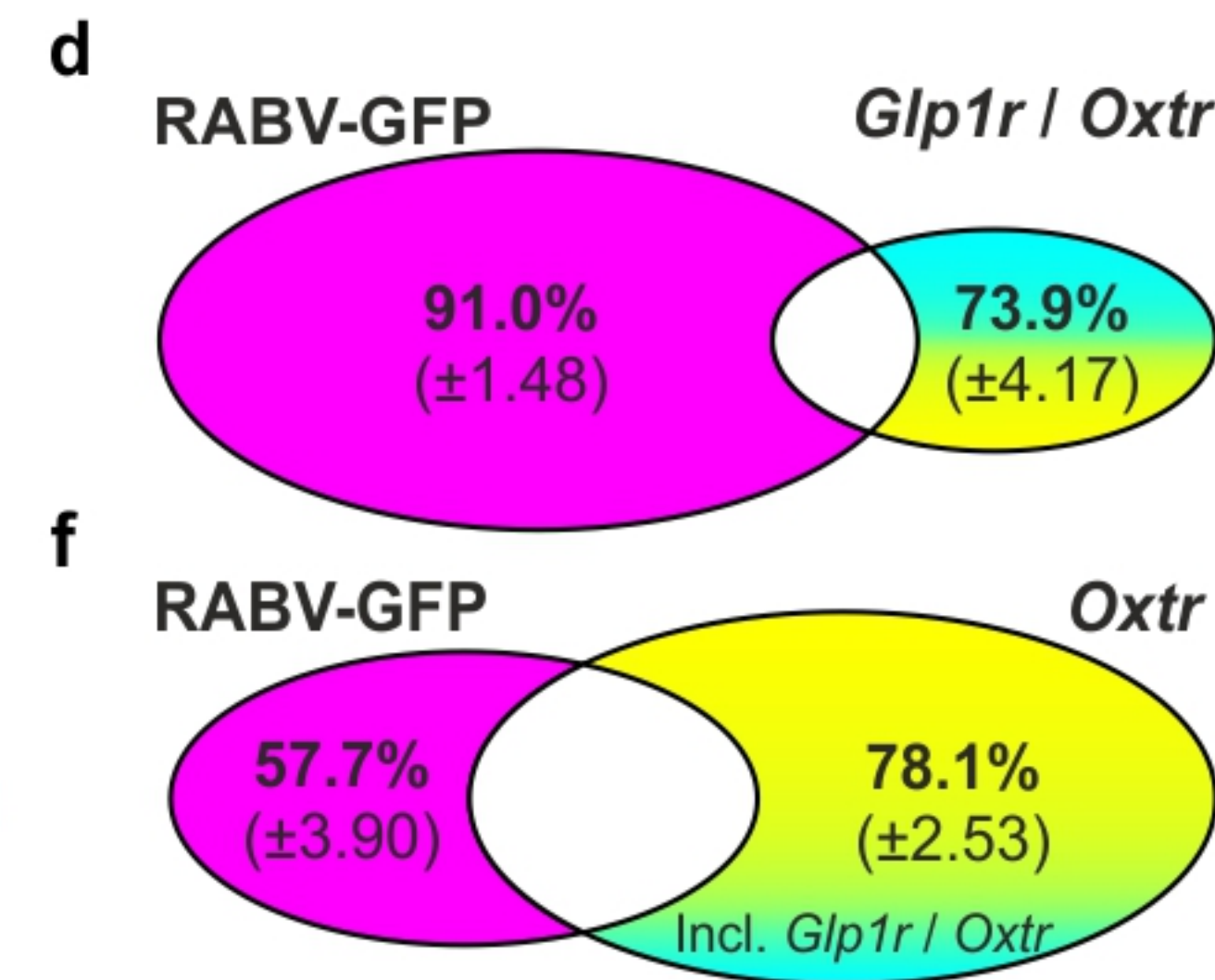
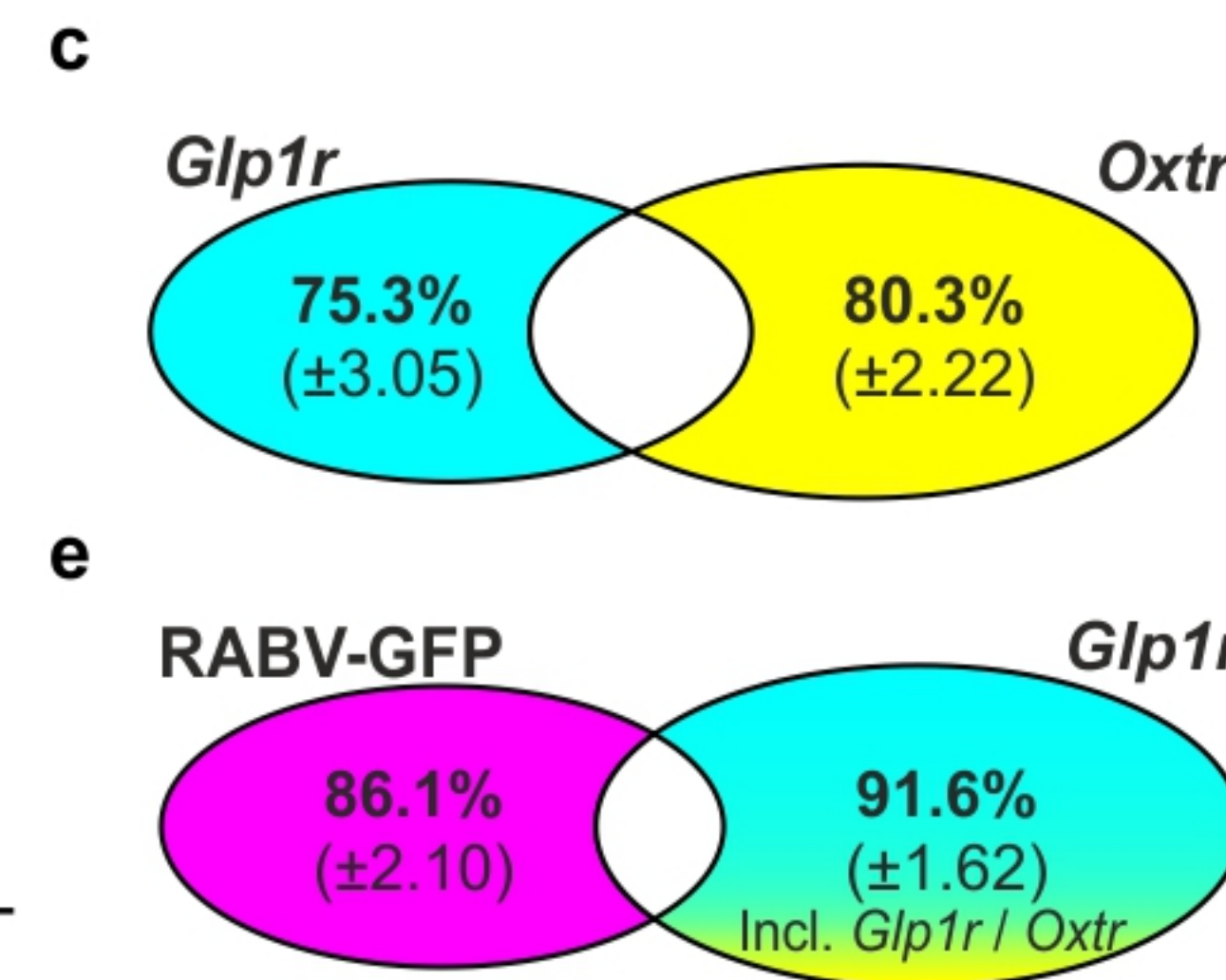
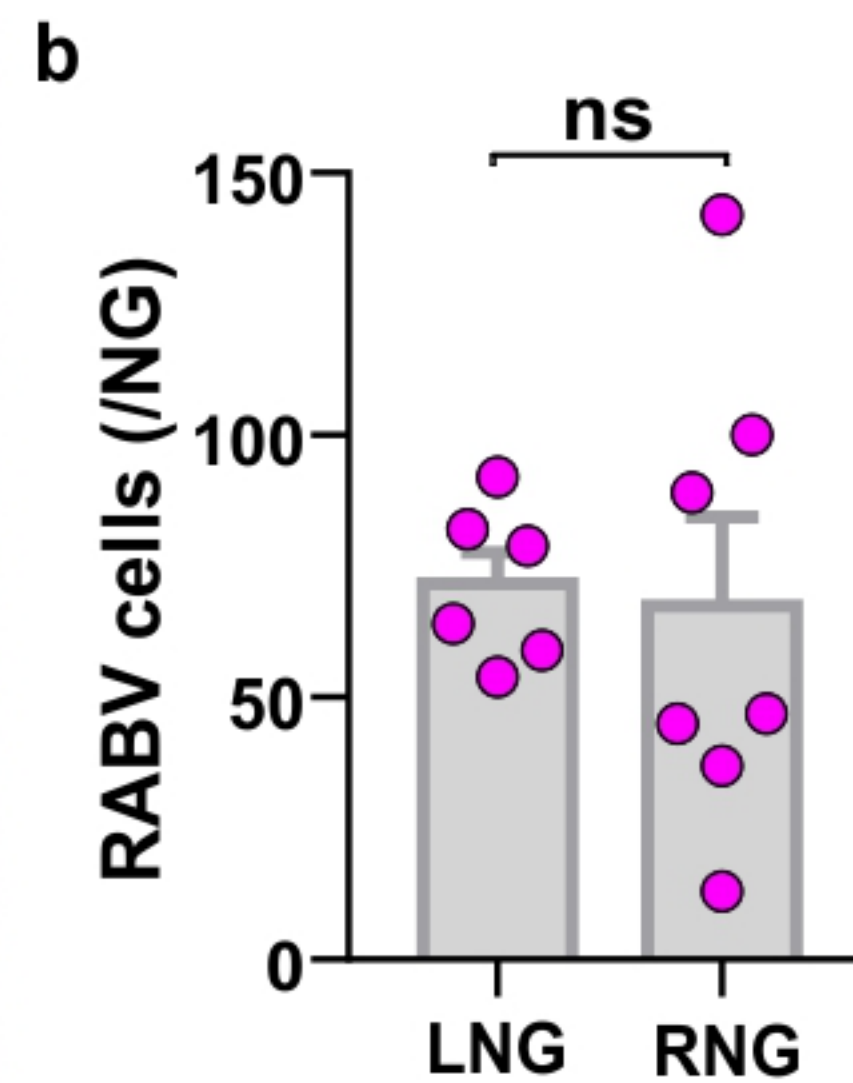
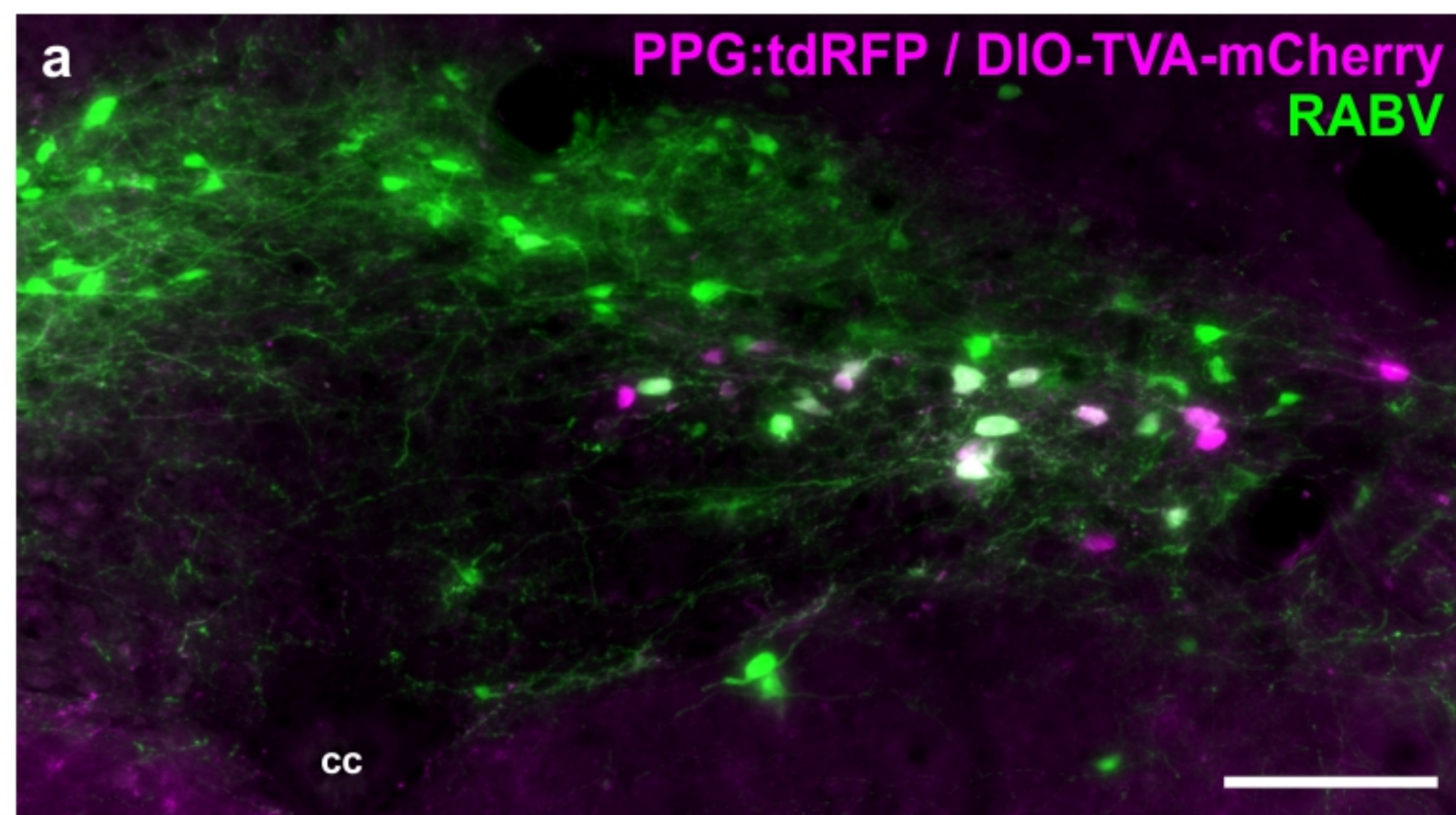
Ad libitum eating in  $GLP-1R^{Nodose}$ -hM3Dq mice



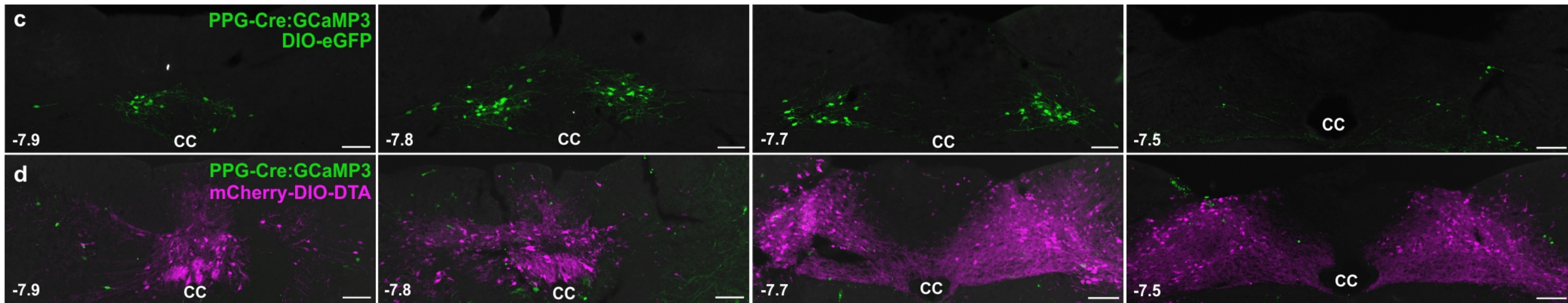
Conditioned flavour preference and ad libitum eating in  $GLP-1R^{Nodose}$ -ChR2 mice



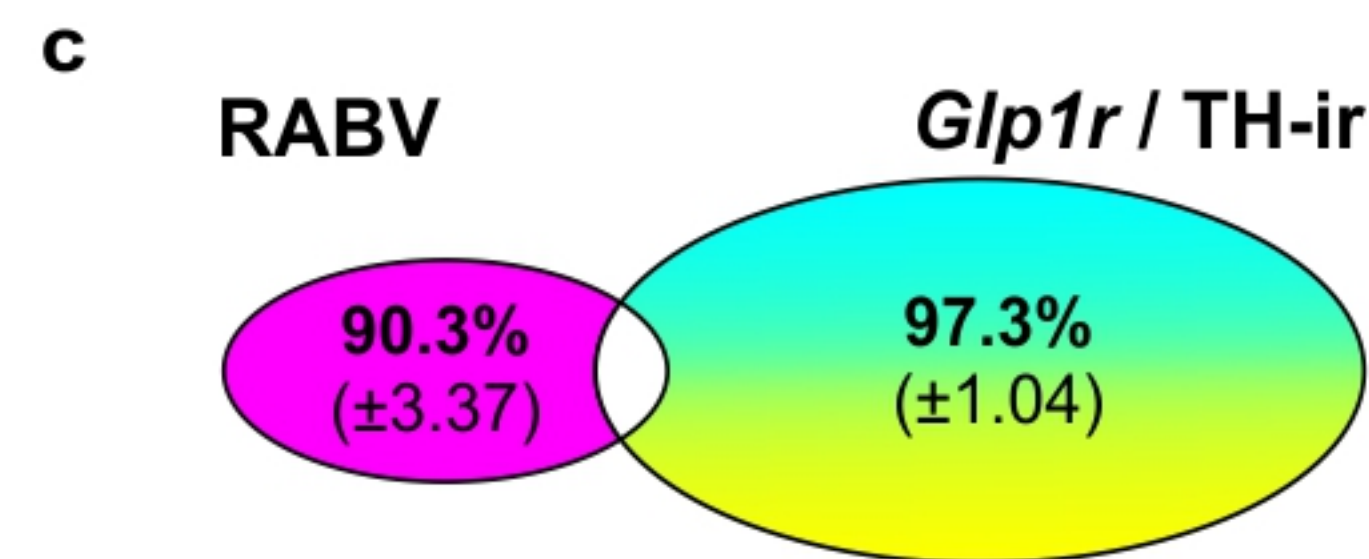
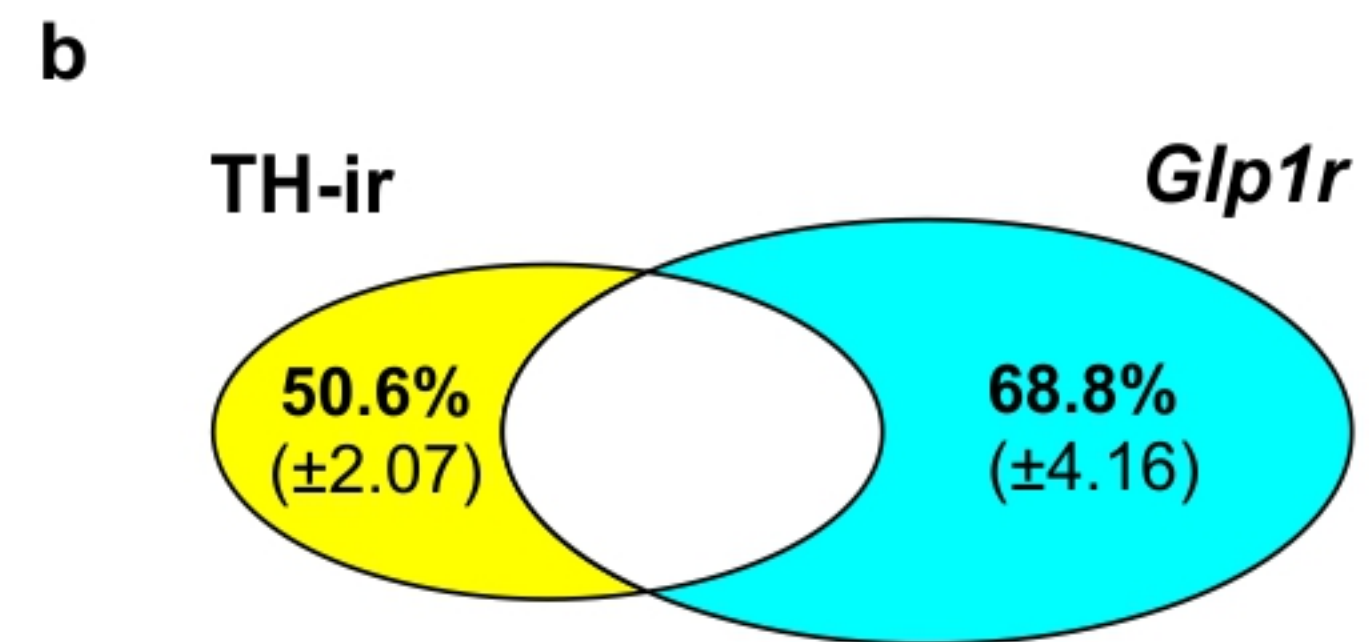
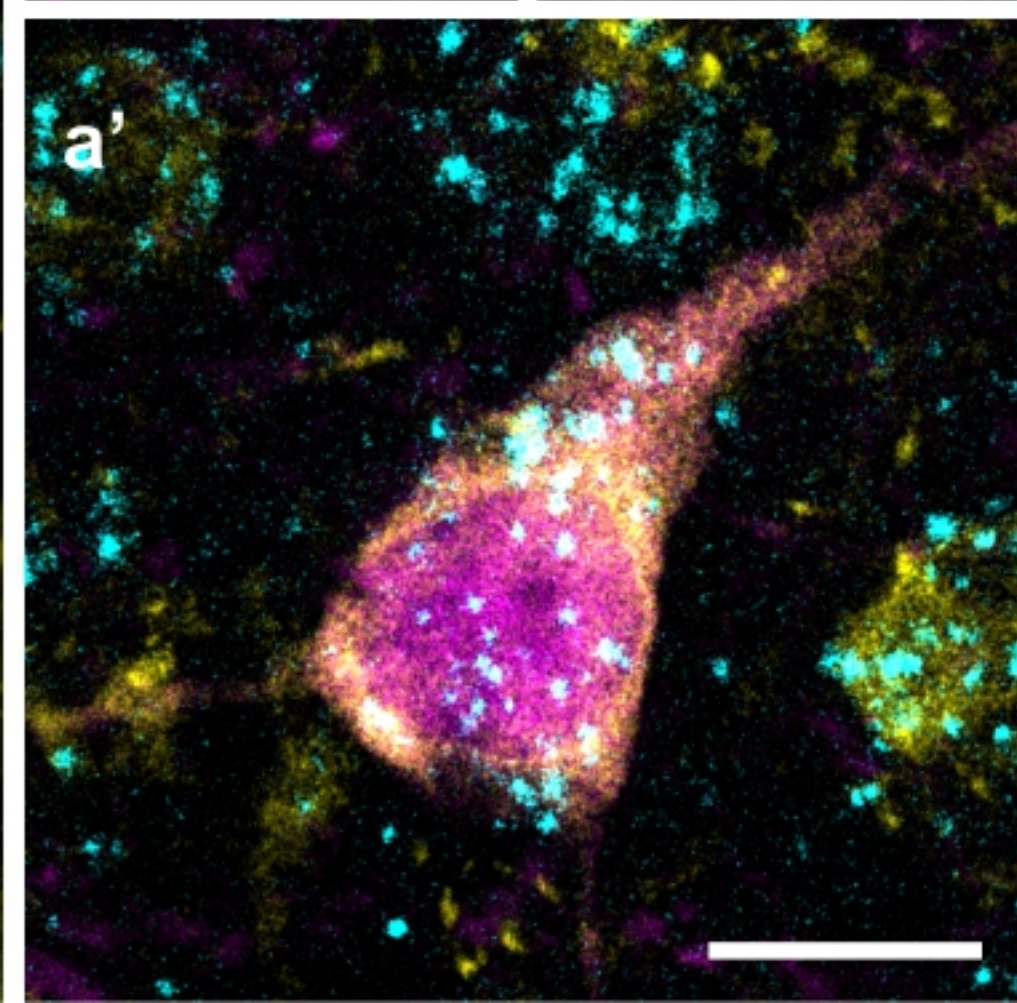
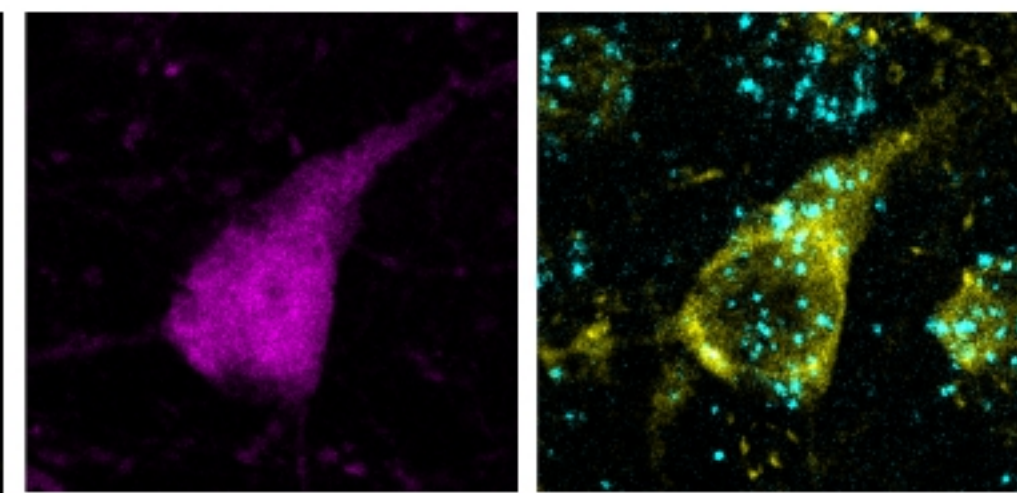
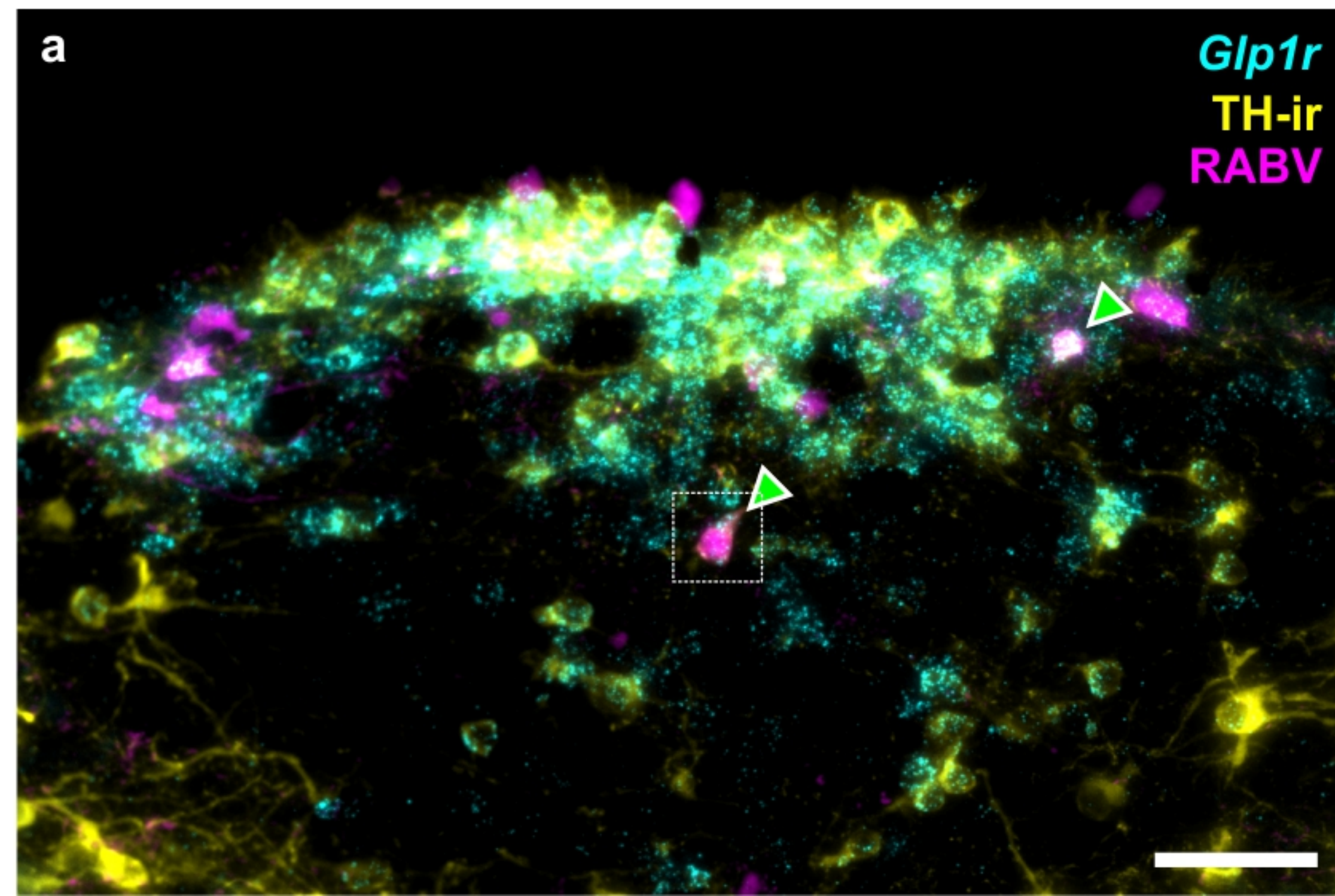
Monosynaptic retrograde rabies virus tracing of vagal inputs to PPG<sup>NTS</sup> neurons



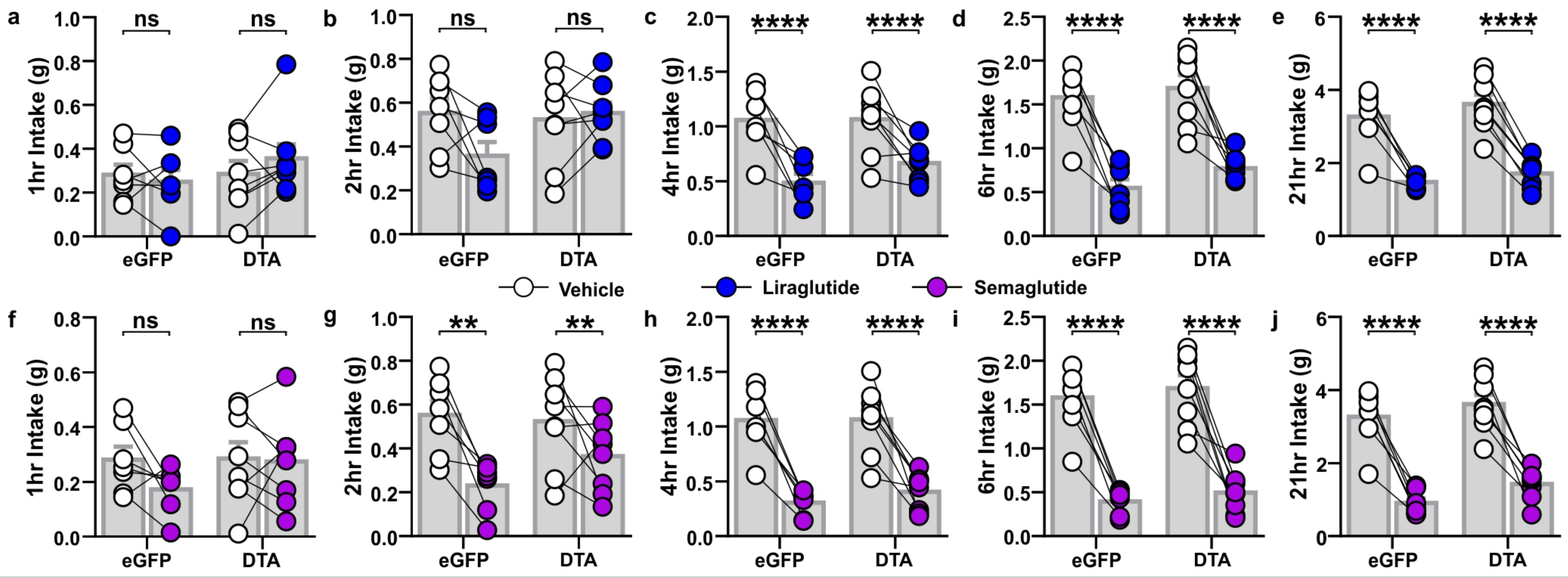
Oxytocin-induced eating suppression in ad libitum eating  $PPG^{NTS}$ -DTA mice



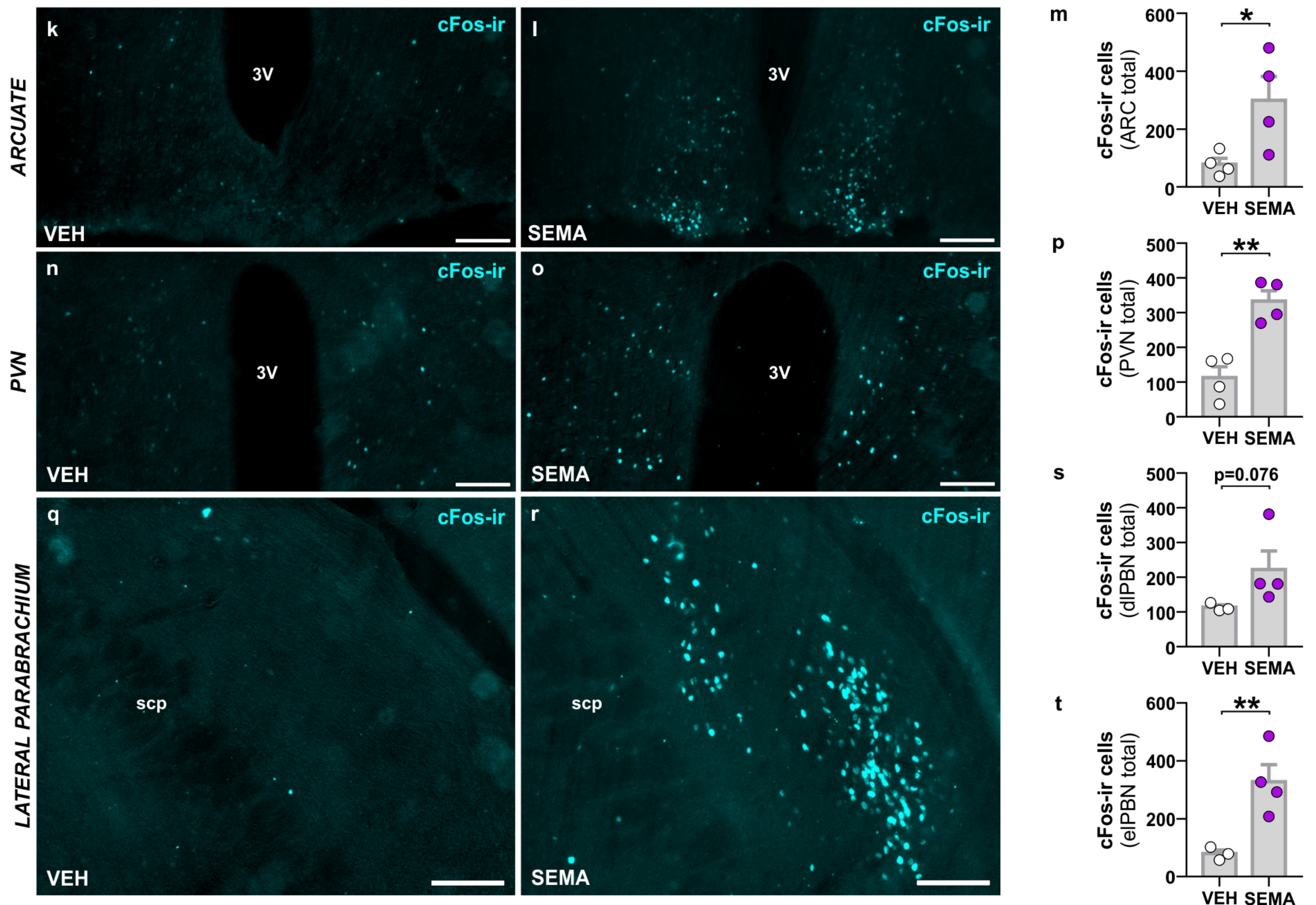
Monosynaptic retrograde rabies virus tracing of area postrema inputs to  $PPG^{NTS}$  neurons



GLP-1RA-induced eating suppression in ad libitum eating PPG<sup>NTS</sup>-DTA mice



Semaglutide-induced neuronal activation in hypothalamus and lateral parabrachium



Semaglutide-induced eating suppression in ad libitum eating PPG<sup>NTS</sup>-hM3Dq mice

